1. General methods

Unless otherwise stated, all commercial reagents and solvents were used as commercially purchased without additional purification. The ^{1}H NMR, ^{13}C NMR, ^{1}H-^{1}H COSY, DOSY, HSQC spectra were recorded on Bruker AVANCE III 400 (400 MHz). IR spectra were measured on a Nicolet/Nexus-670 FT-IR spectrometer with KBr pellets in the range 4000–400 cm^{-1}. HR-ESI-MS spectra were tested on Bruker Maxis 4G and data analyses were processed on Bruker Data Analysis software. UV-vis absorption spectra were measured using a Shimadzu/UV-250PC spectrophotometer. Photoluminescence spectra were measured on an EDINBURGH FLS980 fluorescence spectrophotometer. Ring closing and opening experiments for the ligand and cages were carried out using standard hand-held UV lamp irradiation (365 nm), and 150 W halogen source (Philips 13629 EKE), which was passed through a Y48 (> 455 nm) cutoff filter to eliminate higher energy light, respectively.

Single-crystal diffraction data for *o*-PADTE (CCDC 1917233), *c*-PADTE (CCDC 1919654), *o*-$A^{1}_{2}L_{3}Zn_{2}$ cage (CCDC 1917232), *c*-$A^{1}_{2}L_{3}Zn_{2}$ cage (CCDC 1917235), *o*-$A^{2}_{2}L_{3}Cd_{2}$ cage (CCDC 1917234), *c*-$A^{2}_{2}L_{3}Cd_{2}$ cage (CCDC 1917798), and *o*-R-$A^{1}_{2}L_{3}$ cage (CCDC 1922928) were collected on an Agilent Gemini S Ultra diffractometer with the Enhanced X-ray Source of Cu-Kα radiation (λ = 1.54178 Å). Empirical absorption correction was applied using spherical harmonics implemented in SCALE3 ABSPACK scaling algorithm. Structural solution and refinement against F^{2} were carried out using the SHELXL programs. All the non-hydrogen atoms were refined with anisotropic parameters. Crystallographic data and structural refinement information, selected bond lengths and angles are listed in Tables S1-12.

2. Syntheses and characterization

2.1 PADTE ligand

The ligand PADTE was synthesized according to a modified method in literature,[S1] with the procedure as shown in Scheme S1. The hexane solution of *n*BuLi (3.1 mL, 1.6 mmol L^{-1}) was added dropwise at 0 °C under N_2 atmosphere to a solution of 1,2-bis(5-chloro-2-methylthiophen-3-yl)cyclopent-1-ene (0.98 g, 3 mmol) in anhydrous THF (45 mL). After 20 min, 2.4 mL of tributyl borate was added and heated to room temperature. After stirring for 1 h, the resulting reddish solution was used directly for the following procedure. To 50 mL of N_2-degassed DMSO, 15 mL water solution of Na_2CO_3 (2 mol L^{-1}) and 1.5 mL ethylene glycol in a Schlenk system, 5-bromopicolinaldehyde (7 mmol) and $Pd(PPh_3)_4$ (100 mg) were added under the protection of N_2. After that, the reddish THF solution prepared in the above procedure was added into the mixture and reacted at 90 °C for 24 h in dark. Upon reaction completion, 50 mL of toluene and 20 mL water was added, and the extracted organic phase was washed successively with water and brine. Flash column chromatography on silica gel (ethyl acetate/petroleum ether, 1/3) of the concentrated and $MgSO_4$-dried residue afforded 500 mg of

PADTE ligand. Yield, 20%. For single crystal suitable for X-ray diffraction, 4 mg powder product of the PADTE was dissolved in $CHCl_3$ and natural evaporation under room temperature for five days led to block yellow single crystals. ^{1}H NMR data (400 MHz, $CDCl_3$): δ 10.02 (s, 2H), 8.88 (s, 2H), 7.90 (m, 4H), 7.22 (s, 2H), 2.88 (t, J = 7.4 Hz, 4H), 2.15 (m, 2H), 2.08 (s, 6H). ^{13}C NMR data (100 MHz, $CDCl_3$): δ 192.61, 150.89, 146.41, 138.19, 137.44, 134.94, 134.83, 134.18, 132.50, 126.90, 122.05, 99.98. IR (KBr pellets, cm^{-1}): 2946, 2840, 1700, 1578, 1490, 1452, 1370, 1298, 1204, 1122, 1024, 948, 832, 710, 614, 470.

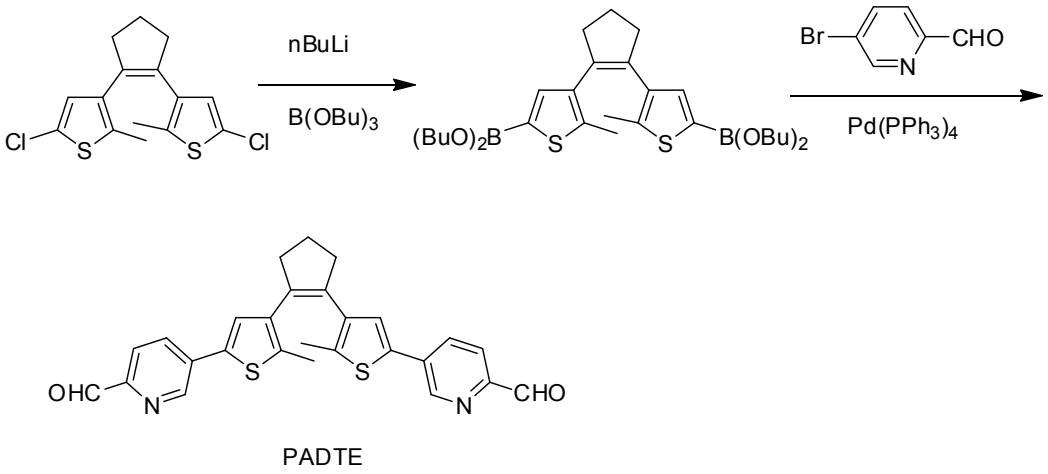

Scheme S1. Synthetic route for ligand PADTE.

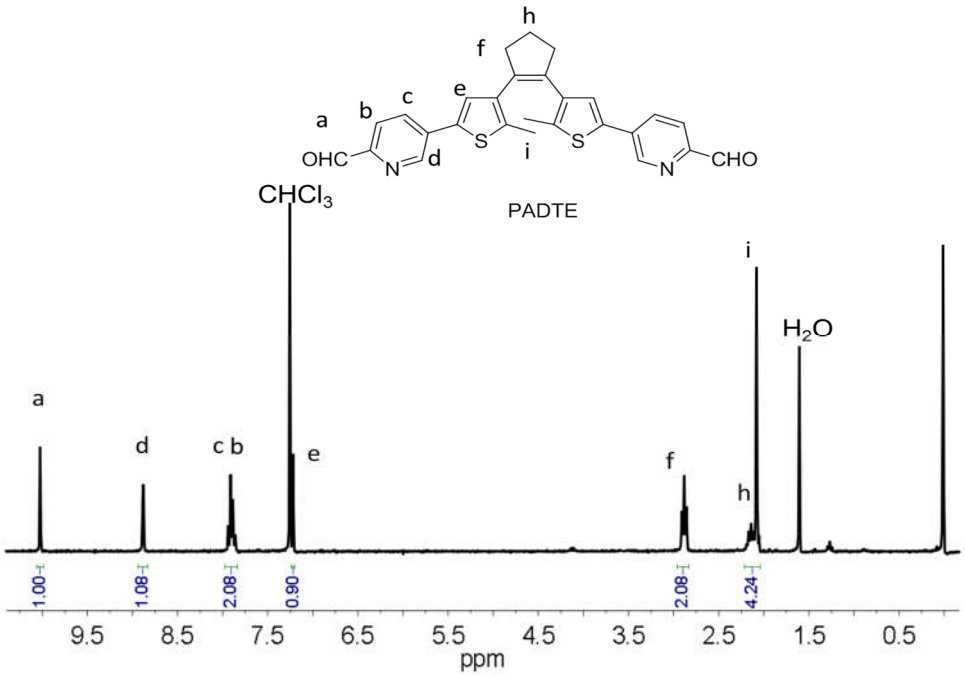

Figure S1. ^{1}H NMR spectrum for ligand PADTE ($CDCl_3$, 25°C).

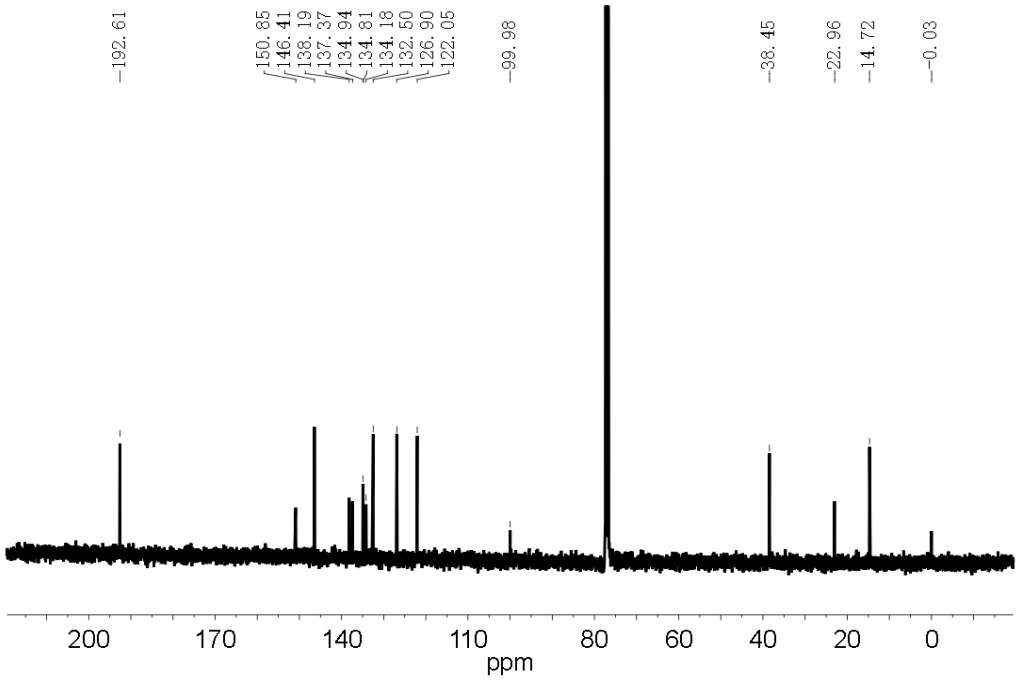

Figure S2. ^{13}C NMR spectrum for ligand PADTE ($CDCl_3$, 25˚C).

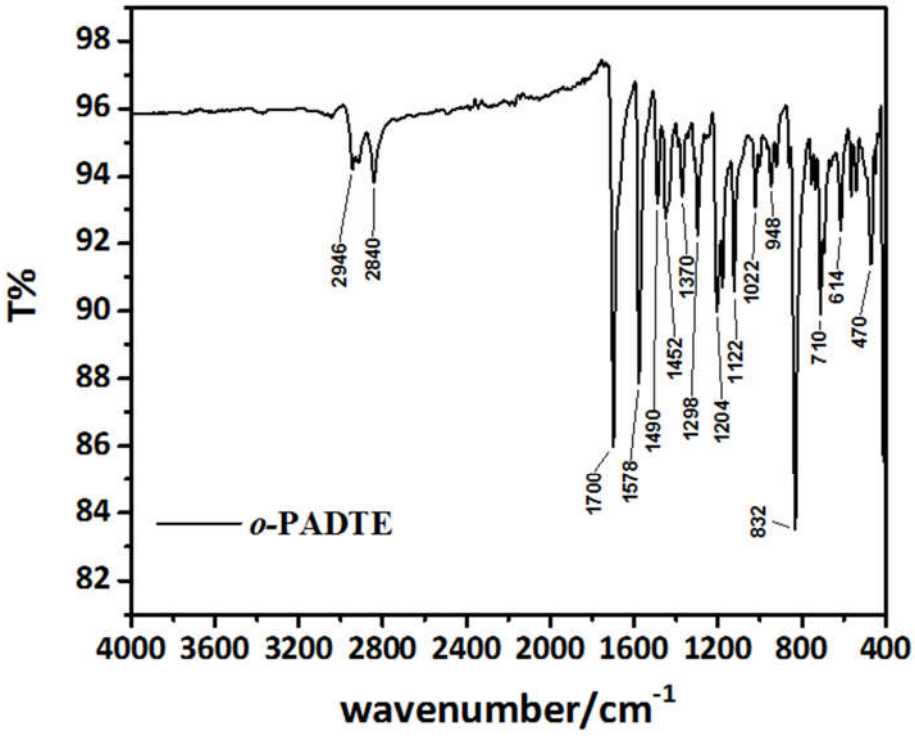

Figure S3. FT-IR spectrum for ligand PADTE.

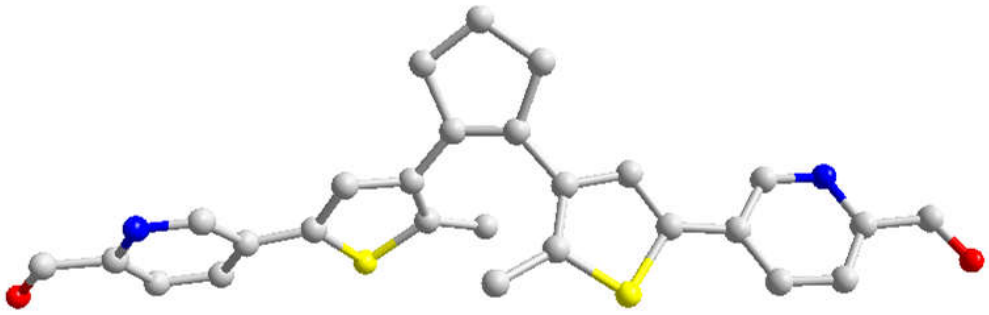

Figure S4. Single-crystal structure of *o*-PADTE (CCDC 1917233, grey for C, blue for N, yellow for S, red for O, H atoms and solvents are omitted for clarity).

2.2 *o*-$A^1_2L_3Zn_2$ cage

PADTE (4.7 mg, 0.01 mmol, 3 equiv) and zinc triflate (2.4 mg, 2 equiv) was added into 0.5 mL CH_3CN and stirred for 10 minutes. Addition of tris(2-aminoethyl)amine (1 μl, 0.0067 mmol, 2 equiv) resulted in large quantity of precipitates. Further addition of 1 mL $CHCl_3$ and heating at 50 °C for 12 hours led to clear yellow solution. Yellow crude product of *o*-$A^1_2L_3Zn_2$ cage was obtained by rotary evaporation of the solvent, which was washed with $CHCl_3$ and water successively and then dissolved again in CH_3CN. 5 mg pure powder product of the cage was obtained by evaporation of the filtrate, yield 65%. For single crystal suitable for X-ray diffraction, 2 mg powder product of the cage was dissolved in CH_3CN, and natural evaporation under room temperature for three days led to block yellowish green single crystals. High resolution ESI-MS (m/z) data: calc. (measured): 1012.1696 (1012.1769) for $[A^1_2L_3Zn_2 + 2CF_3SO_3]^{2+}$; 625.1289 (625.1324) for $[A^1_2L_3Zn_2 + CF_3SO_3]^{3+}$. EA calc. for $C_{97}H_{90}F_{12}N_{14}O_{12}S_{10}Zn_2 \cdot 3CH_3CN \cdot 15H_2O$ ($[A^1_2L_3Zn_2] \cdot 3CH_3CN \cdot 15H_2O$): C, 45.54, H, 4.79, N, 8.77%; Found, C, 45.15, H, 4.47, N, 8.63%. ^{1}H NMR (400 MHz, CD_3CN) δ 8.65 (s, 2H), 8.49 (d, 2H), 8.00 (d, 2H), 7.56 (s, 2H), 7.06 (s, 2H), 3.86 (s, 1H), 3.64 (s, 1H), 3.23 (s, 1H), 2.95 (s, 2H), 2.61 (s, 1H), 2.10 (s, 1H), 1.64 (s, 3H). ^{13}C NMR (100 MHz, CD_3CN) δ 162.56, 145.23, 144.28, 138.05, 137.72, 135.80, 135.15, 134.66, 133.46, 128.77, 128.50, 56.01, 53.96, 38.41, 22.95 – 21.88, 13.88. IR (KBr pellets, cm^{-1}): 3450, 2915, 2852, 1654, 1589, 1562, 1495, 1459, 1380, 1258, 1223, 1162, 1031, 899, 875, 639.

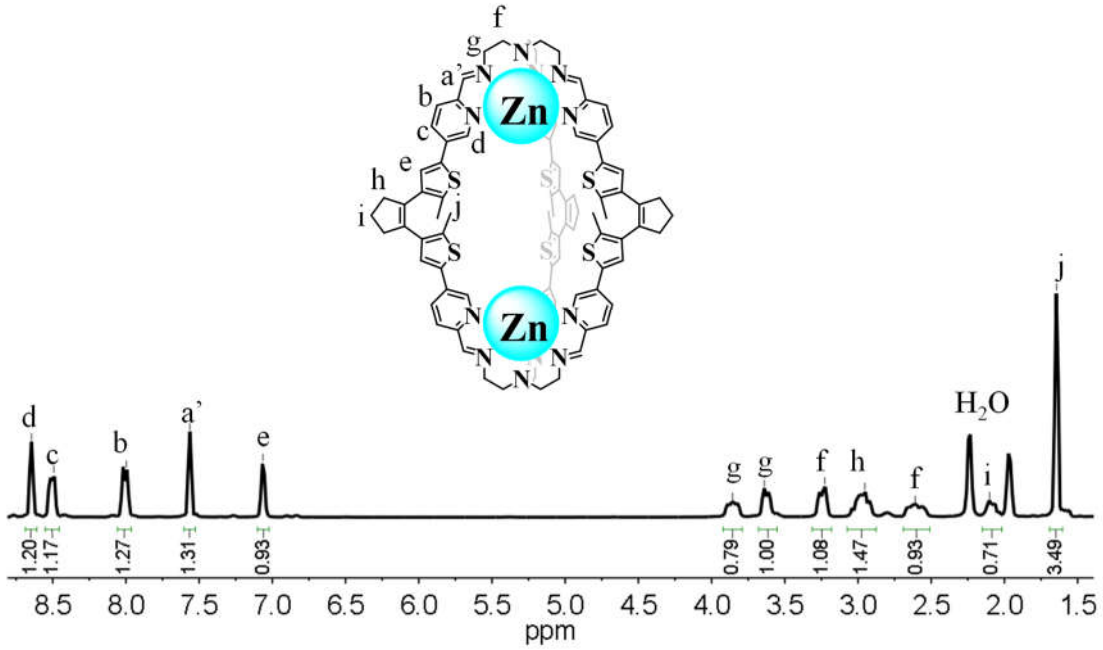

Figure S5. ^{1}H NMR spectrum for *o*-A$^{1}_{2}$L$_{3}$Zn$_{2}$ cage (CD$_{3}$CN, 25˚C).

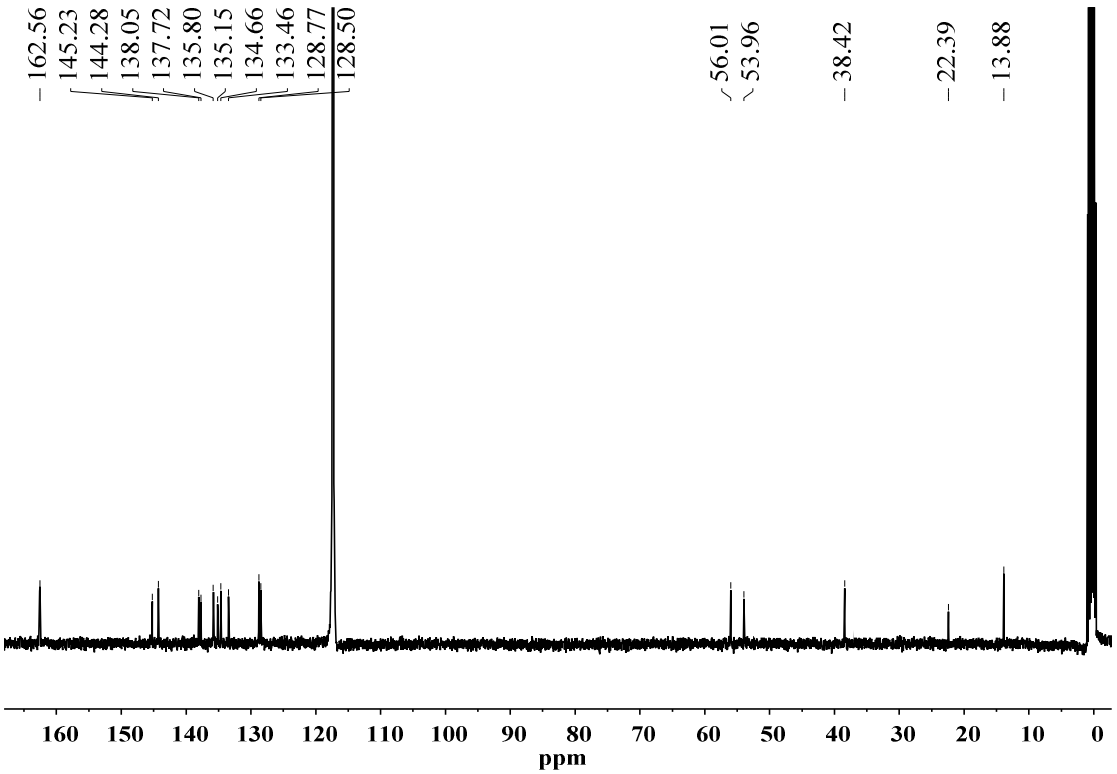

Figure S6. ^{13}C NMR spectrum for *o*-A$^{1}_{2}$L$_{3}$Zn$_{2}$ cage (CD$_{3}$CN, 25˚C).

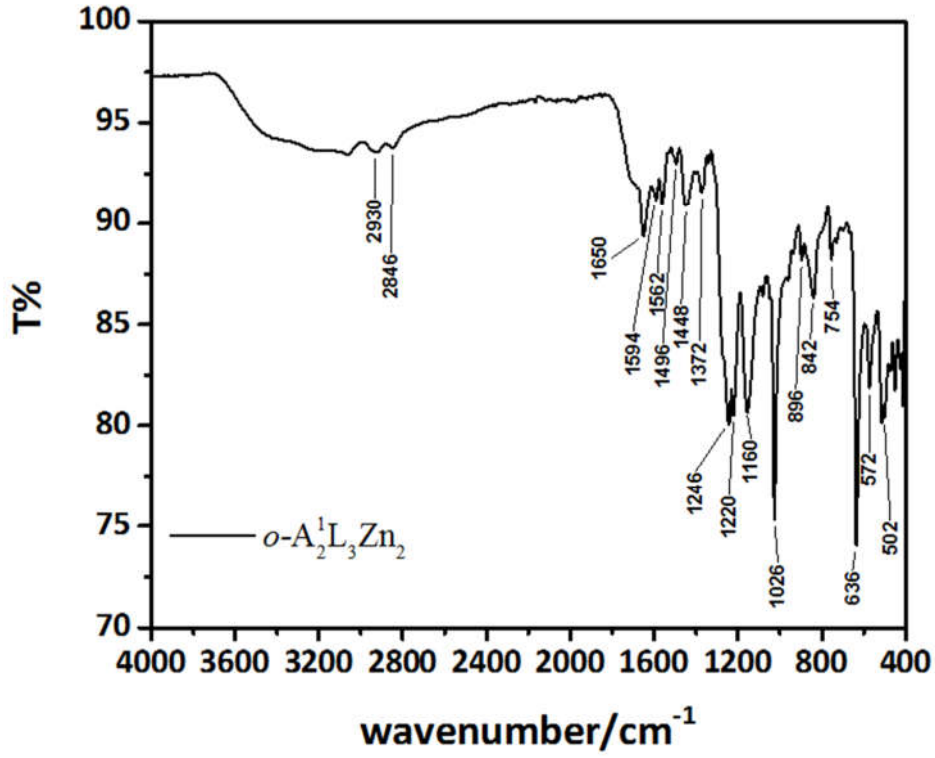

Figure S7. FT-IR spectrum for *o*-$A^1_2L_3Zn_2$ cage.

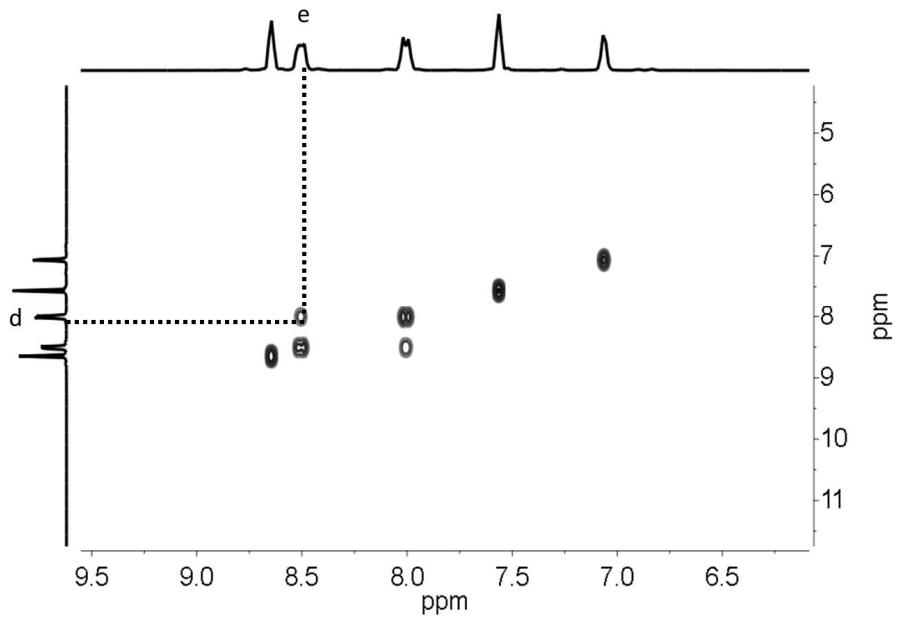

Figure S8. ^{1}H-^{1}H COSY spectrum for *o*-$A^1_2L_3Zn_2$ cage (CD_3CN, 25˚C).

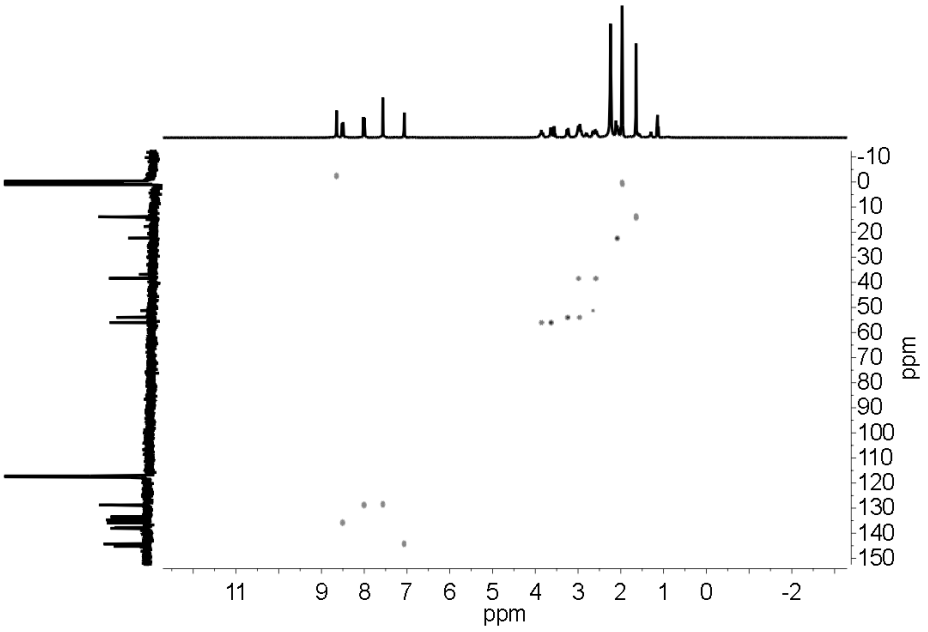

Figure S9. HSQC spectrum for *o*-$A^1{}_2L_3Zn_2$ cage (CD_3CN, 25˚C).

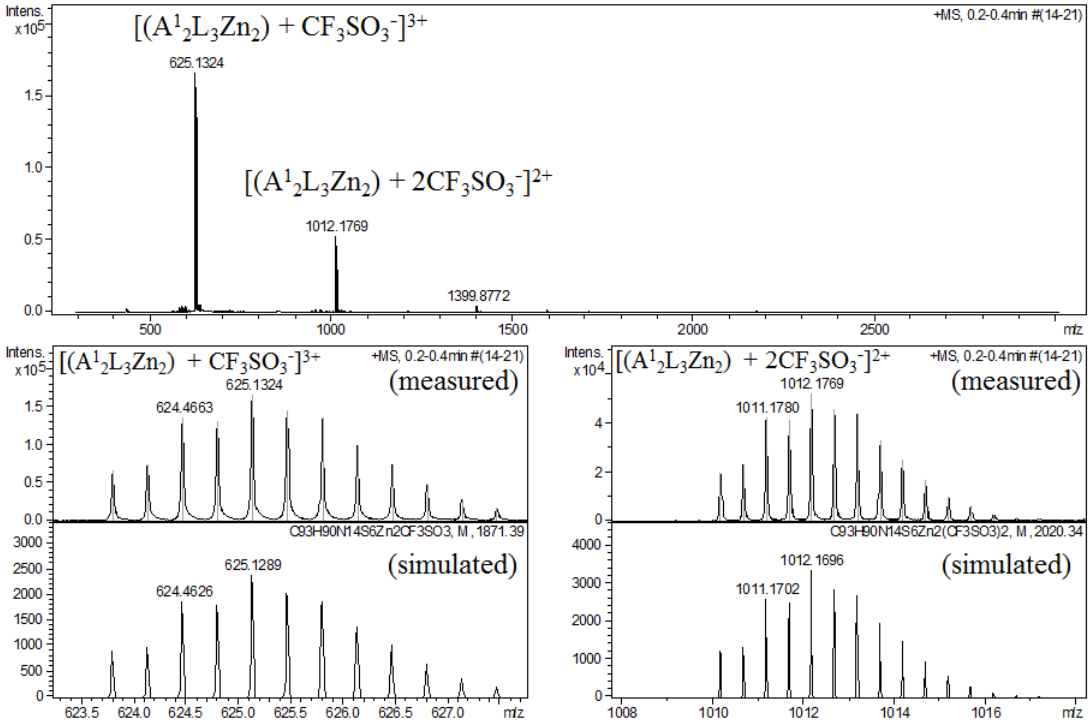

Figure S10. High resolution ESI-MS spectrum for *o*-$A^1{}_2L_3Zn_2$ cage (CH_3CN, 25˚C).

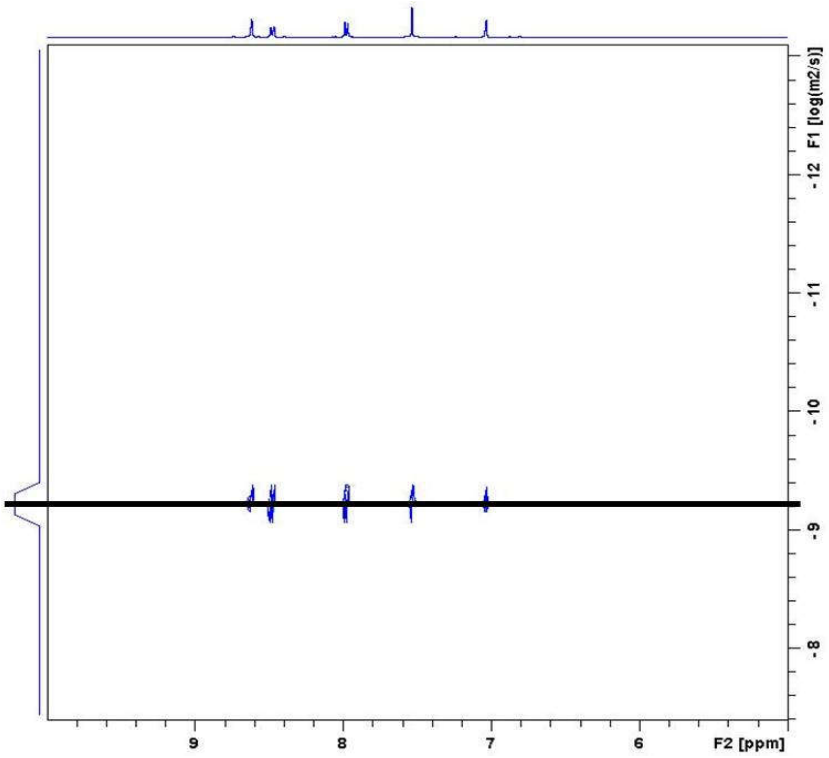

Figure S11. DOSY spectrum for *o*-$A^1{}_2L_3Zn_2$ cage (CD_3CN, 25˚C).

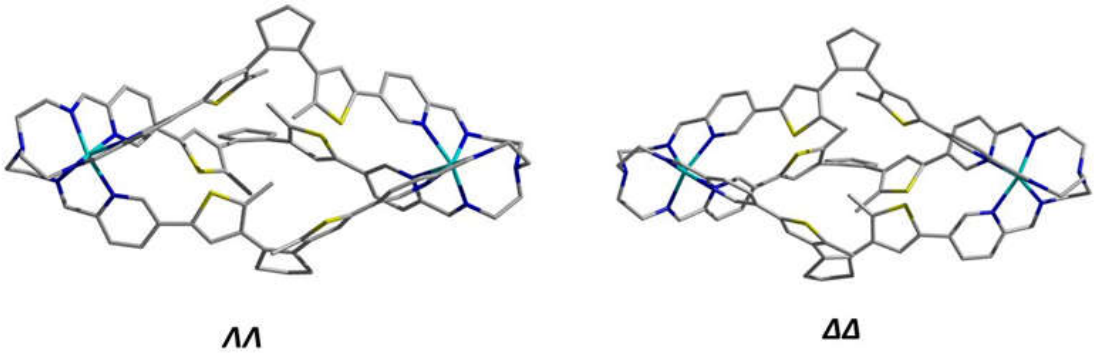

Figure S12. A pair of *ΛΛ*- and *ΔΔ*-enantiomeric cages coexist in the crystal lattice of *o*-$A^1{}_2L_3Zn_2$ cage (grey for C, blue for N, yellow for S, cyan for Zn, H atoms, solvents and counter anions are omitted for clarity).

2.3 *o*-$A^2_2L_3Cd_2$ cage

PADTE (4.7 mg, 0.01 mmol, 3 equiv) and cadmium triflate (2.7 mg, 2 equiv) was added into 0.5 mL CH_3CN and stirred for 10 minutes. Addition of tris(3-aminopropyl)amine (1.3 μl, 0.0067 mmol, 2 equiv) resulted in large quantity of precipitates. Further addition of 1 mL $CHCl_3$ and heating at 50 °C for 12 hours resulted in clear yellow solution. Yellow crude product of *o*-$A^2_2L_3Cd_2$ cage was obtained by rotary evaporation of the solvent, which was washed with $CHCl_3$ and water successively and then dissolved again in CH_3CN. 3 mg pure powder product of the cage was obtained by evaporation of the filtrate, yield 34%. For single crystal suitable for X-ray diffraction, 3 mg powder product of the cage was dissolved in CH_3CN, and then diffusion of ether into the CH_3CN solution under room temperature for one month led to block yellowish green single crystals. High resolution ESI-MS (m/z) data: calc. (measured): 1011.1926 (1011.1926) for $[A^2_2L_3Cd_2 + 2CF_3SO_3]^{2+}$; 684.8131 (684.8111) for $[A^2_2L_3Cd_2 + CF_3SO_3]^{3+}$; 476.1235 (476.1201) for $[A^2_2L_3Cd_2]^{4+}$. ^{1}H NMR (400 MHz, CD_3CN) δ 8.54 (d, *J* = 1.9 Hz, 1H), 8.36 (dd, *J* = 8.1, 2.3 Hz, 1H), 7.89 (d, *J* = 8.2 Hz, 1H), 7.42 (s, 1H), 7.07 (d, *J* = 2.4 Hz, 1H), 3.80 (d, *J* = 12.3 Hz, 1H), 3.47 (q, *J* = 13.6, 13.1 Hz, 2H), 2.89 (dt, *J* = 14.3, 7.3 Hz, 1H), 2.53 (dt, *J* = 14.8, 7.1 Hz, 1H), 2.26 (t, *J* = 13.6 Hz, 1H), 2.06 (q, *J* = 7.7, 7.3 Hz, 1H), 1.93 (s, 2H), 1.62 (s, 3H). ^{13}C NMR (100 MHz, CD_3CN) δ 162.03, 145.58, 144.91, 137.88, 137.62, 135.88, 135.10, 135.06, 133.84, 128.54, 127.70, 61.89, 58.26, 38.38, 25.43, 22.45, 13.41. IR (KBr pellets, cm^{-1}): 3482, 2924, 2844, 1648, 1584, 1558, 1498, 1444, 1358, 1252, 1220, 1152, 1028, 838, 740, 636, 572, 514.

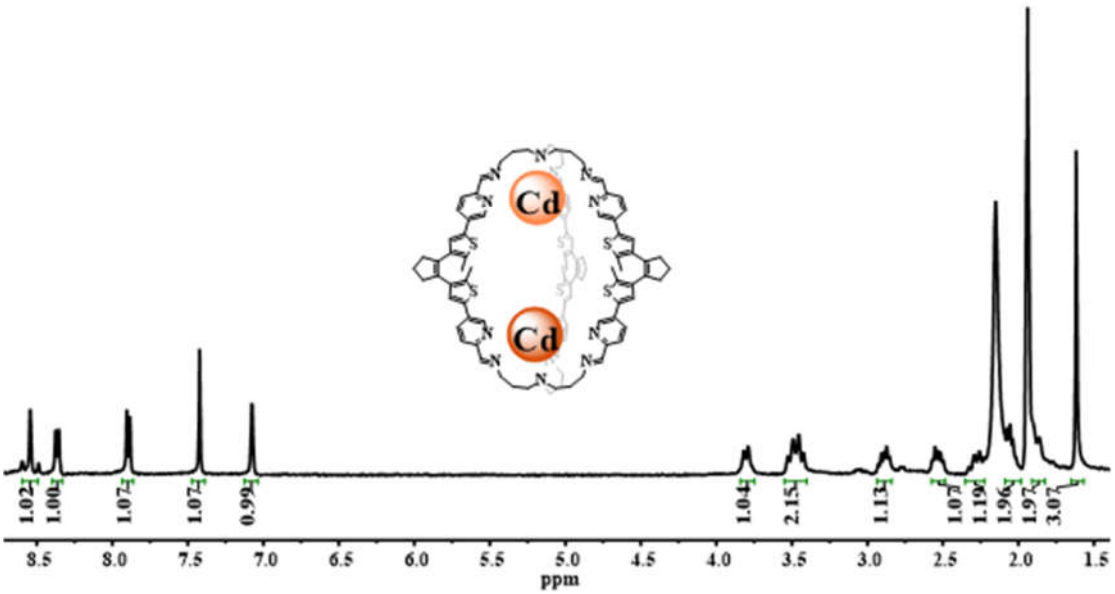

Figure S13. ^{1}H NMR spectrum for *o*-$A^2_2L_3Cd_2$ cage (CD_3CN, 25°C).

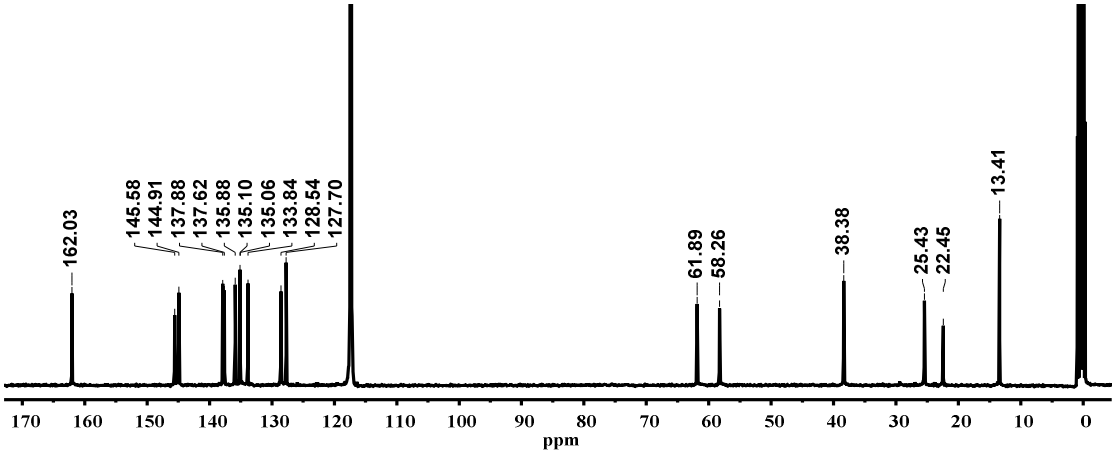

Figure S14. ^{13}C NMR spectrum for *o*-$A^2_2L_3Cd_2$ cage (CD_3CN, 25˚C).

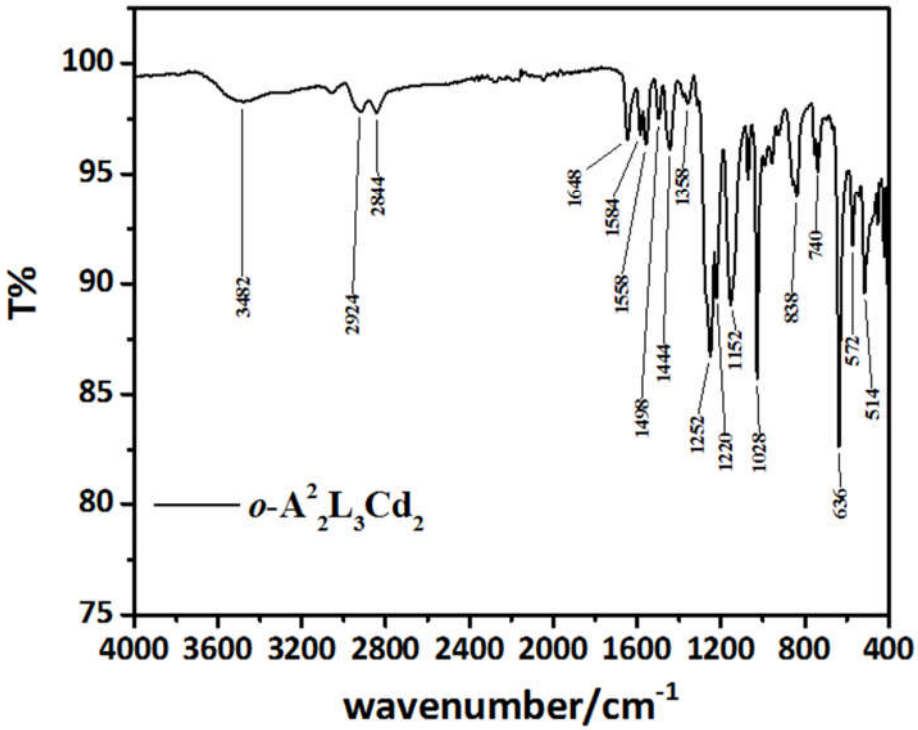

Figure S15. FT-IR spectrum for *o*-$A^2_2L_3Cd_2$ cage.

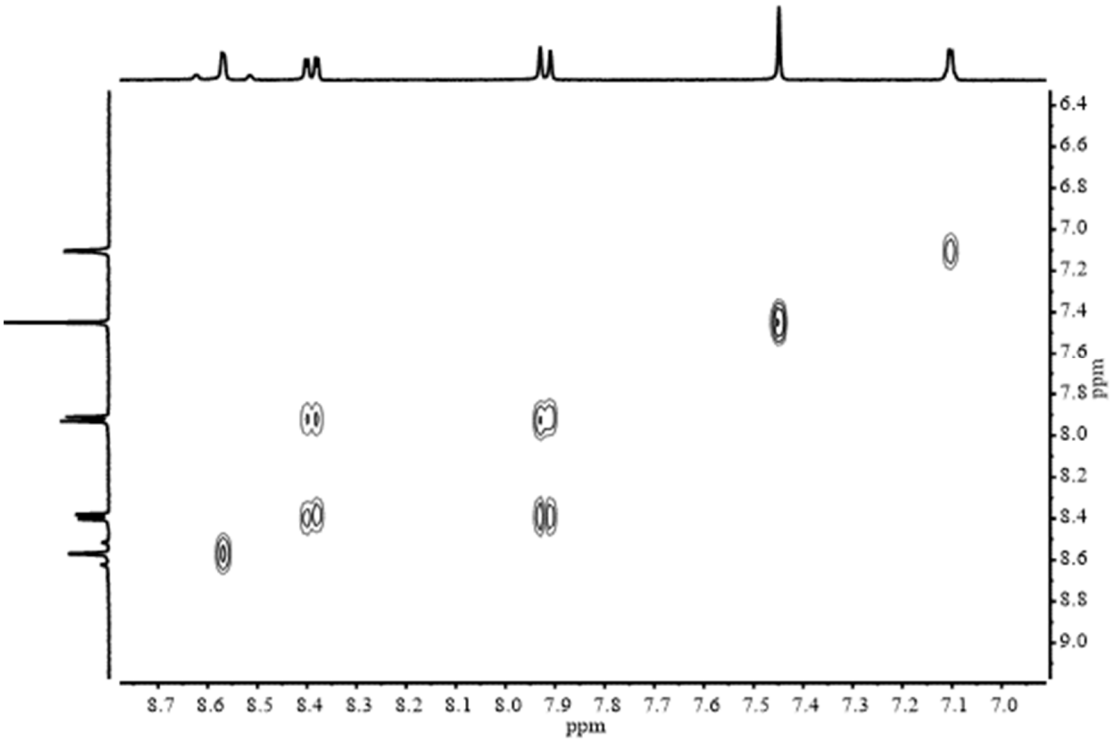

Figure S16. ^{1}H-^{1}H COSY spectrum for *o*-$A^{2}_{2}L_{3}Cd_{2}$ cage (CD_3CN, 25˚C).

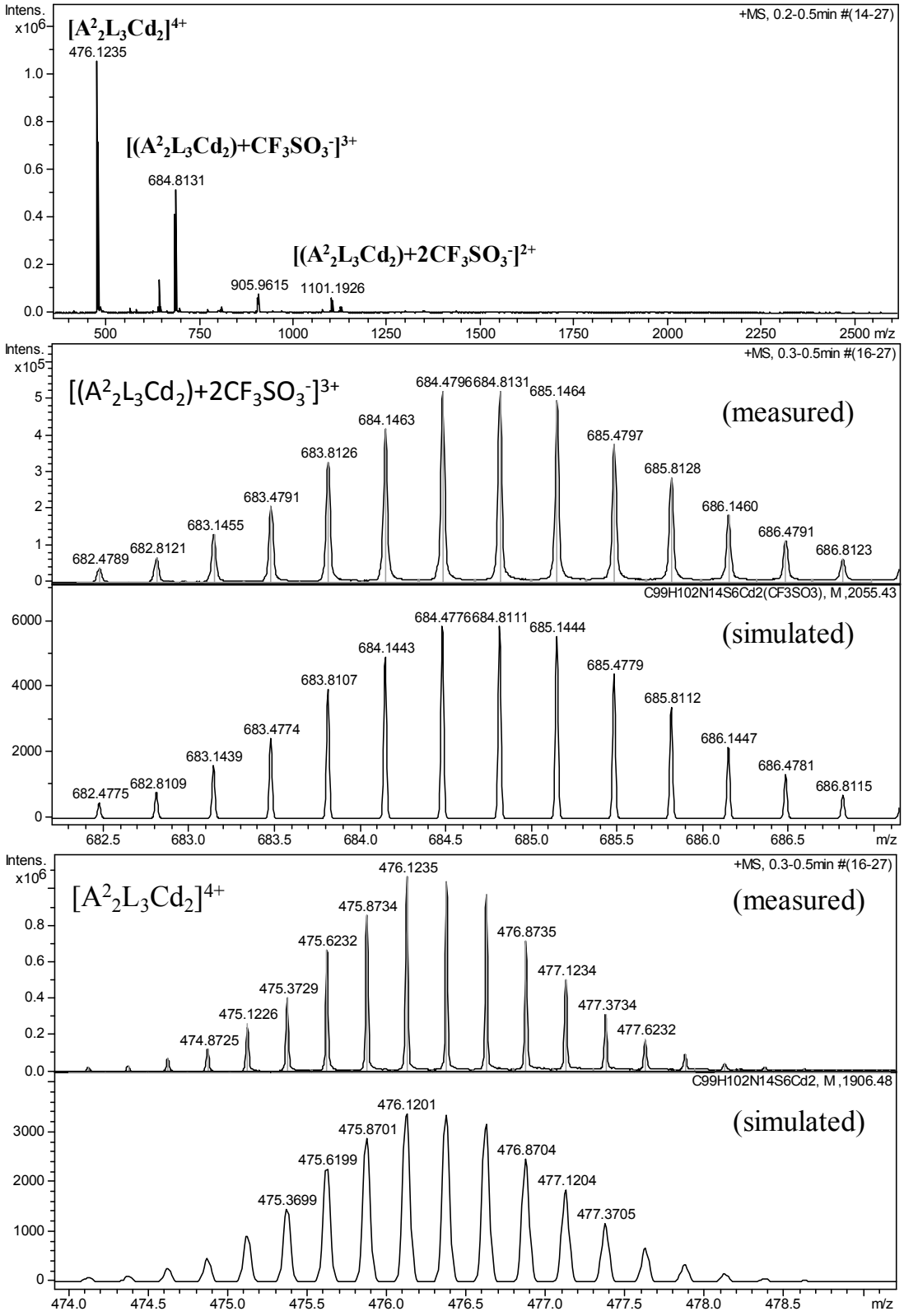

Figure S17. High resolution ESI-MS spectrum for *o*-$A^2_2L_3Cd_2$ cage (CH_3CN, 25˚C).

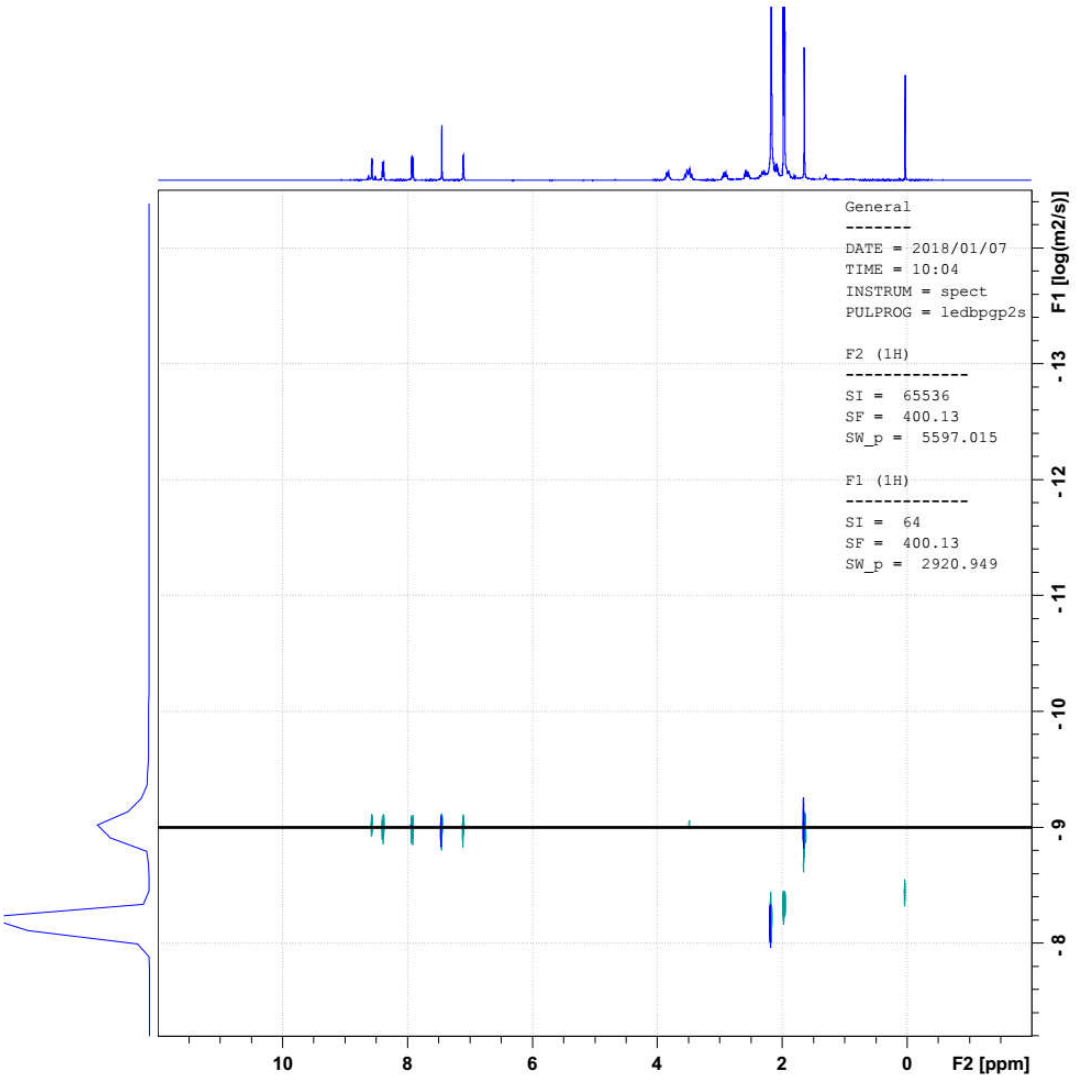

Figure S18. DOSY spectrum for *o*-$A^2_2L_3Cd_2$ cage (CD_3CN, 25˚C).

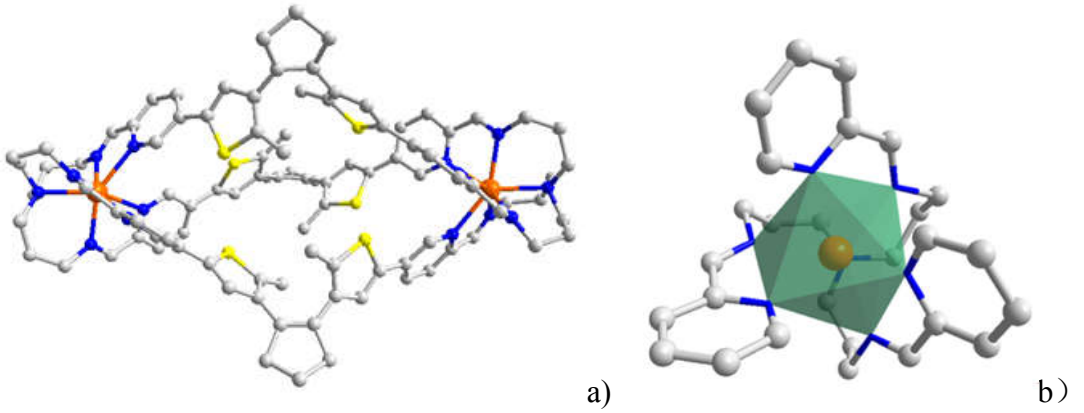

Figure S19. (a) Single-crystal structure of *o*-$A^2_2L_3Cd_2$ cage. (b) Coordination geometry of Cd^{II} (grey for C, blue for N, yellow for S, orange for Cd, H atoms, solvents and counter anions are omitted for clarity).

2.4 *o*-$A^2_2L_3Zn_2$ cage

PADTE (4.7 mg, 0.01 mmol, 3 equiv) and zinc triflate (2.4 mg, 2 equiv) was added into 0.5 mL CH_3CN and stirred for 10 minutes. Addition of tris(3-aminopropyl)amine (1.3 μl, 0.0067 mmol, 2 equiv) resulted in large quantity of precipitates. Further addition of 1 mL $CHCl_3$ and heating at 50 °C for 12 hours resulted in clear yellow solution. Yellow crude product of *o*-$A^1_2L_3Zn_2$ cage was obtained by rotary evaporation of the solvent, which was washed with $CHCl_3$ and water successively, and then dissolved again in CH_3CN. Pure powder product of the cage was obtained by evaporation of the filtrate. For single crystal suitable for X-ray diffraction, 10 mg powder product of the R-$A^1_2L_3$ cage was dissolved in $CHCl_3$ and natural evaporation under room temperature for three months led to block colorless single crystals. High resolution ESI-MS (m/z) data: calc. (measured): 1054.2167 (1054.1936) for $[A^2_2L_3Zn_2 + 2CF_3SO_3]^{2+}$; 653.1603 (653.1422) for $[A^2_2L_3Zn_2 + CF_3SO_3]^{3+}$; 452.6321 (452.6233) for $[A^2_2L_3Zn_2]^{4+}$. ^{1}H NMR (400 MHz, CD_3CN) δ 8.54 – 8.46 (m, 2H), 7.97 (d, *J* = 8.2 Hz, 1H), 7.61 (d, *J* = 3.4 Hz, 1H), 7.39 (d, *J* = 2.2 Hz, 1H), 3.61 (dd, *J* = 11.3, 6.4 Hz, 1H), 3.30 (t, *J* = 10.7 Hz, 1H), 2.94 (dq, *J* = 18.8, 12.1, 9.8 Hz, 3H), 2.59 (dt, *J* = 14.5, 7.2 Hz, 2H), 2.15 – 2.03 (m, 3H), 1.73 (s, 3H).

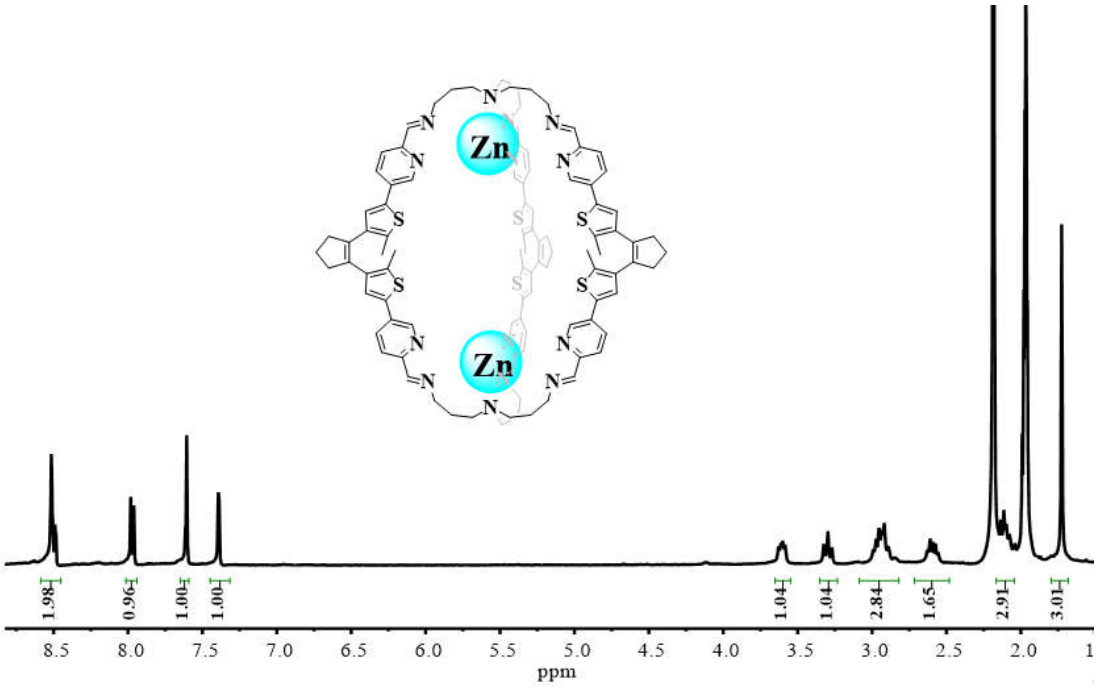

Figure S20. ^{1}H NMR spectrum for *o*-$A^2_2L_3Zn_2$ cage (CD_3CN, 25°C).

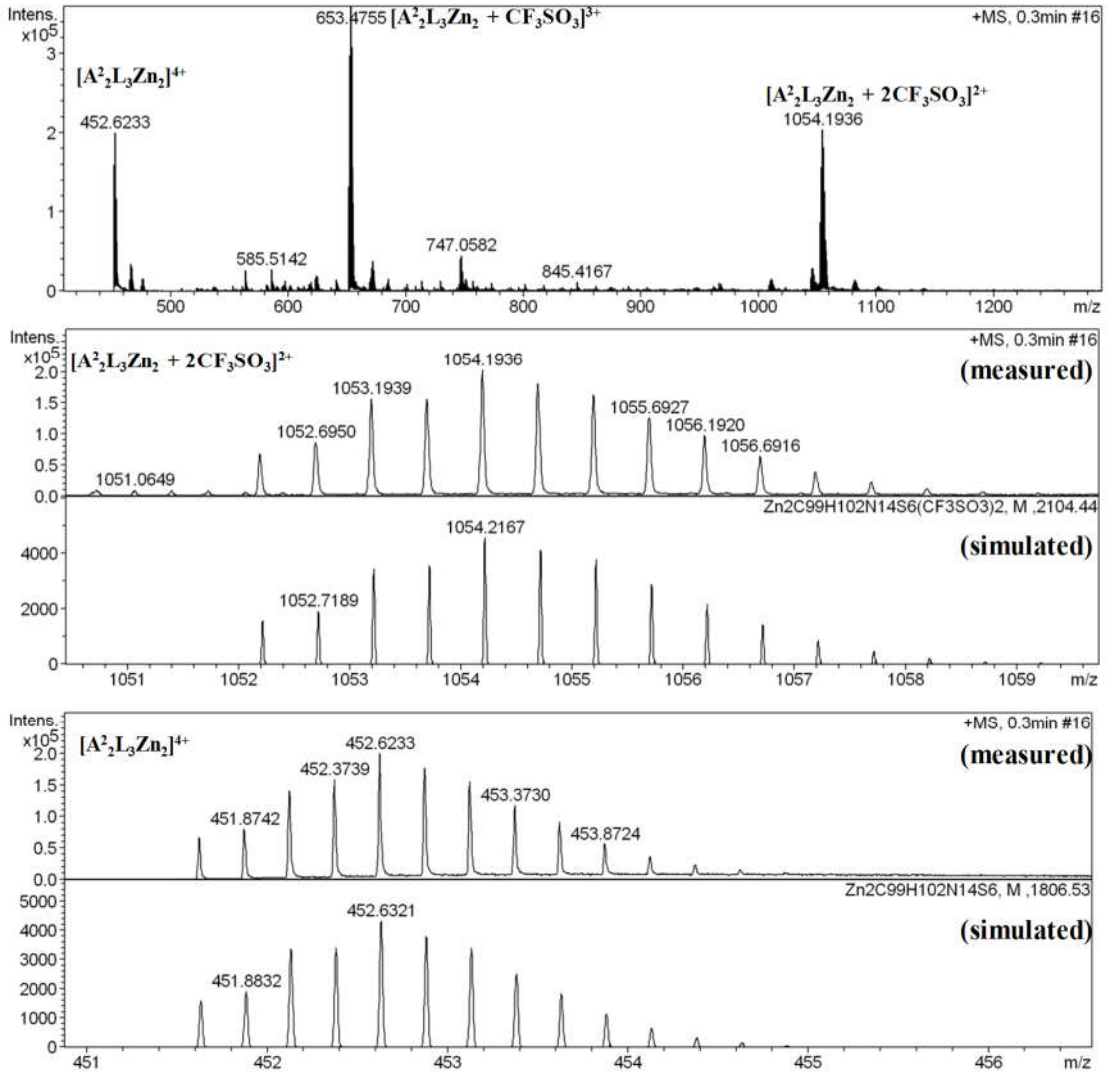

Figure S21. High resolution ESI-MS spectrum for *o*-$A^2_2L_3Zn_2$ cage (CH_3CN, 25˚C).

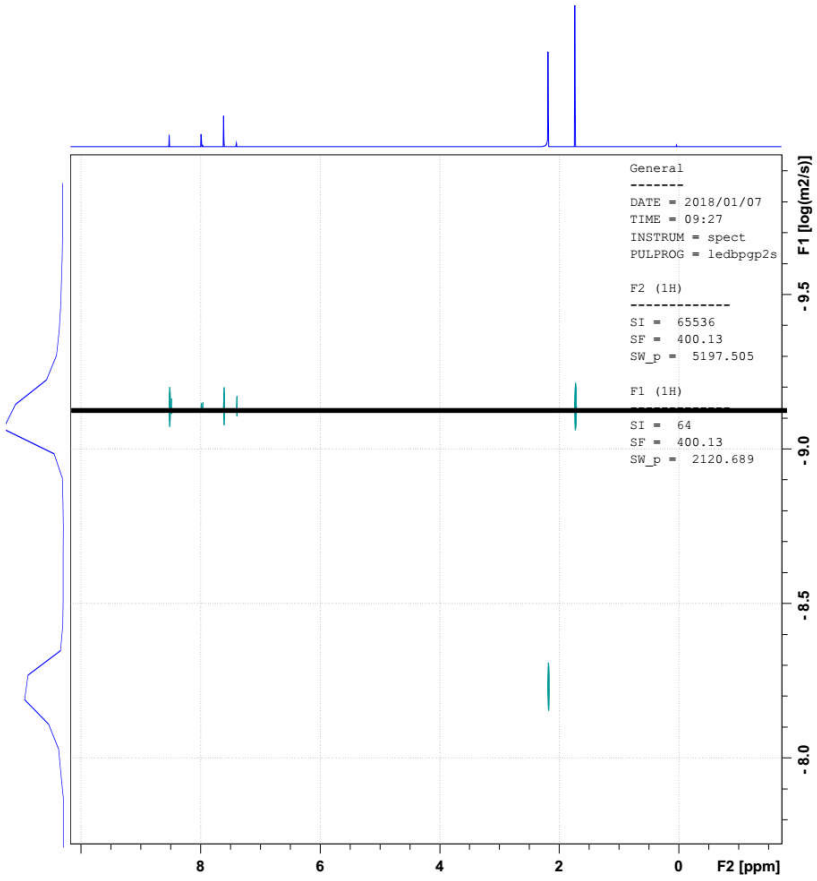

Figure S22. DOSY spectrum for *o*-$A^2{}_2L_3Zn_2$ cage (CD_3CN, 25˚C).

2.5 *o*-R-$A^1{}_2L_3$ cage

To a 50 mL flask was added *o*-$A^1{}_2L_3Zn_2$ cage (110 mg, 0.05 mmol, 1 equiv), sodium borohydride (60 mg, 1.6 mmol, 32 equiv) and dry MeOH (15 mL). The solution was stirred overnight under a nitrogen atmosphere at room temperature. Then 37% hydrochloric acid was added to bring the pH to 2, and a pale green solid precipitated out. This precipitate was washed by water, dissolved by CH_3OH and then 2M NaOH aqueous solution was added, giving a light purple precipitatate. The precipitate was isolated by centrifugation, washed by water, and then dissolved by CH_3OH, concentrated in vacuo. The product was obtained as a pale purple solid (50 mg, 62%). High resolution ESI-MS (m/z) data: calc. (measured): 804.8455 (804.8512) for $[R\text{-}A^1{}_2L_3 + 2H]^{2+}$; 536.8995 (536.9033) for $[R\text{-}A^1{}_2L_3 + 3H]^{3+}$; 402.9264 (402.9289) for $[R\text{-}A^1{}_2L_3 + 4H]^{4+}$. ^{1}H NMR (400 MHz, CD_3OD) δ 8.41 (s, 2H), 7.66 (d, 2H), 7.31 (d, 2H), 7.22 (s, 2H), 3.89 (s, 4H), 2.88 (s, 4H), 2.82 (t, 4H), 2.75 (s, 4H), 2.08 (t, 2H), 1.75 (s, 6H). ^{13}C NMR (100 MHz, CD_3OD) δ 156.61, 144.95, 137.12, 135.61, 135.06, 134.46, 132.68, 129.03, 124.82, 122.00, 53.50, 53.12, 38.48, 22.40, 13.63. IR (KBr pellets, cm^{-1}): 3248, 2918, 2836, 1658, 1598, 1564, 1498, 1436, 1384, 1292, 1254, 1200, 1122, 1028, 948, 824, 752, 642, 564, 498.

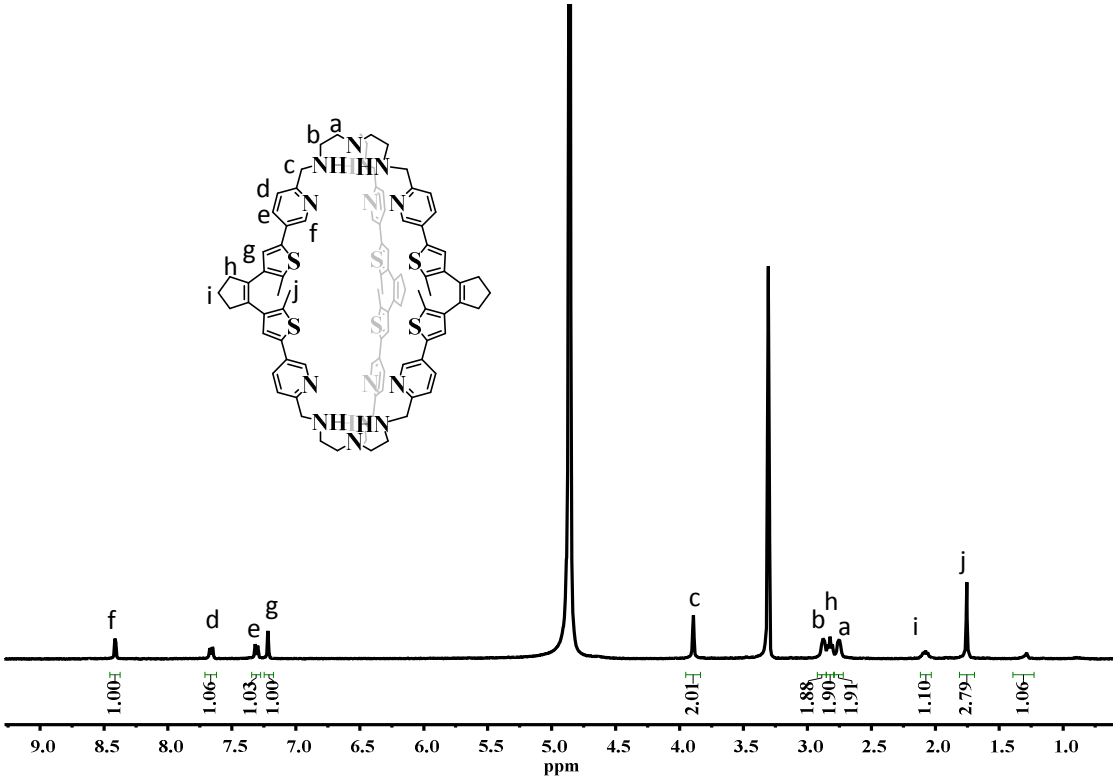

Figure S23. ^{1}H NMR spectrum for *o*-R-A$^{1}_{2}$L$_{3}$ cage (CD$_{3}$OD, 25˚C).

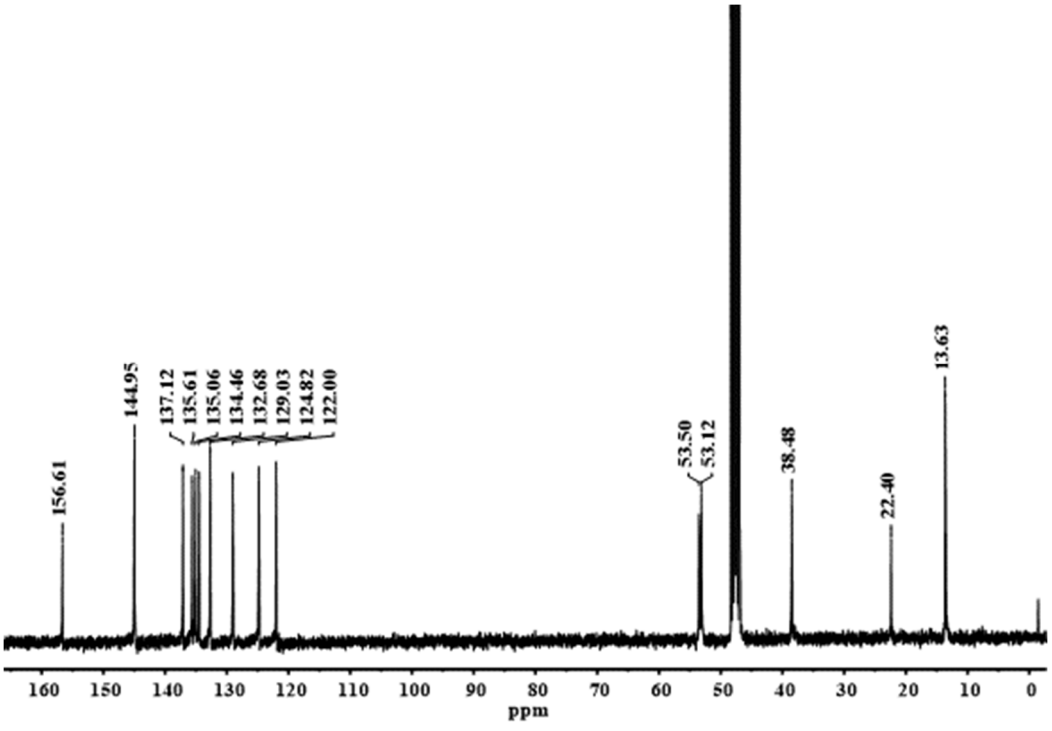

Figure S24. ^{13}C NMR spectrum for *o*-R-A$^{1}_{2}$L$_{3}$ cage (CD$_{3}$OD, 25˚C).

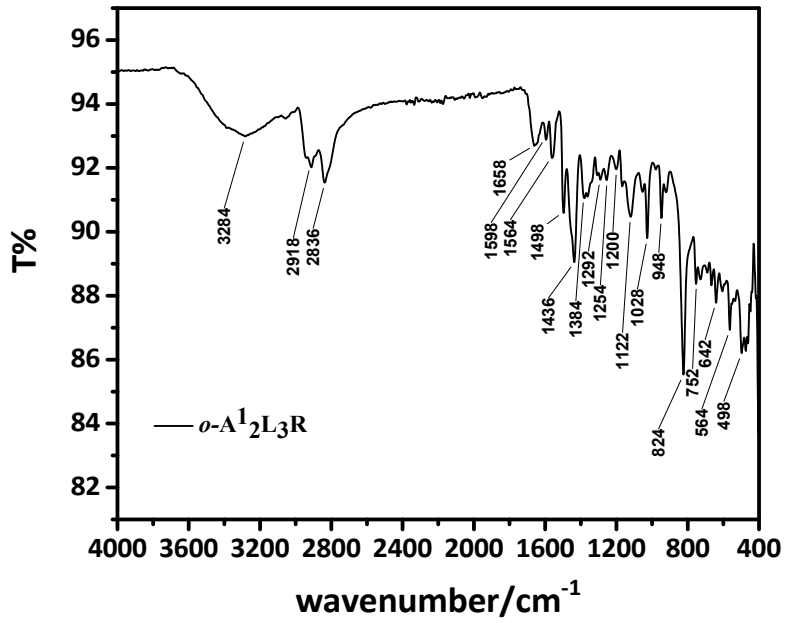

Figure S25. FT-IR spectrum for *o*-R-$A^1_2L_3$ cage.

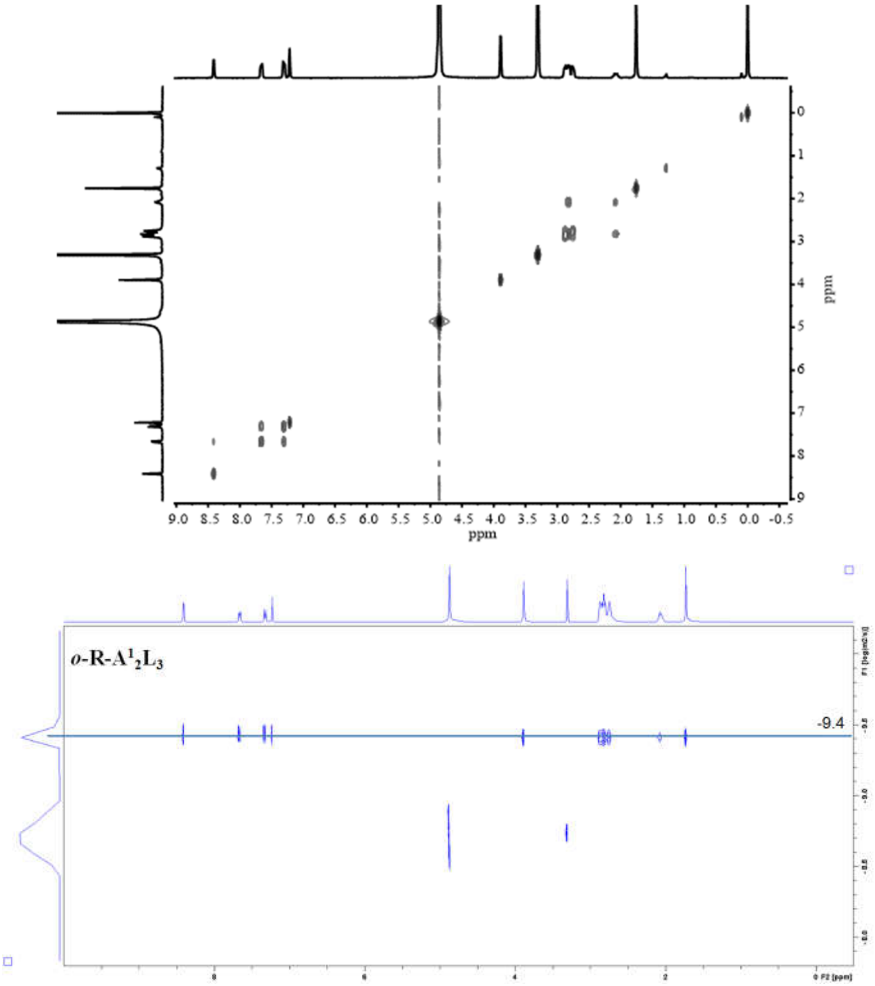

Figure S26. ^{1}H-^{1}H COSY spectrum (upper) and DOSY spectrum (lower) for *o*-R-$A^1_2L_3$ cage (CD_3OD, 25˚C).

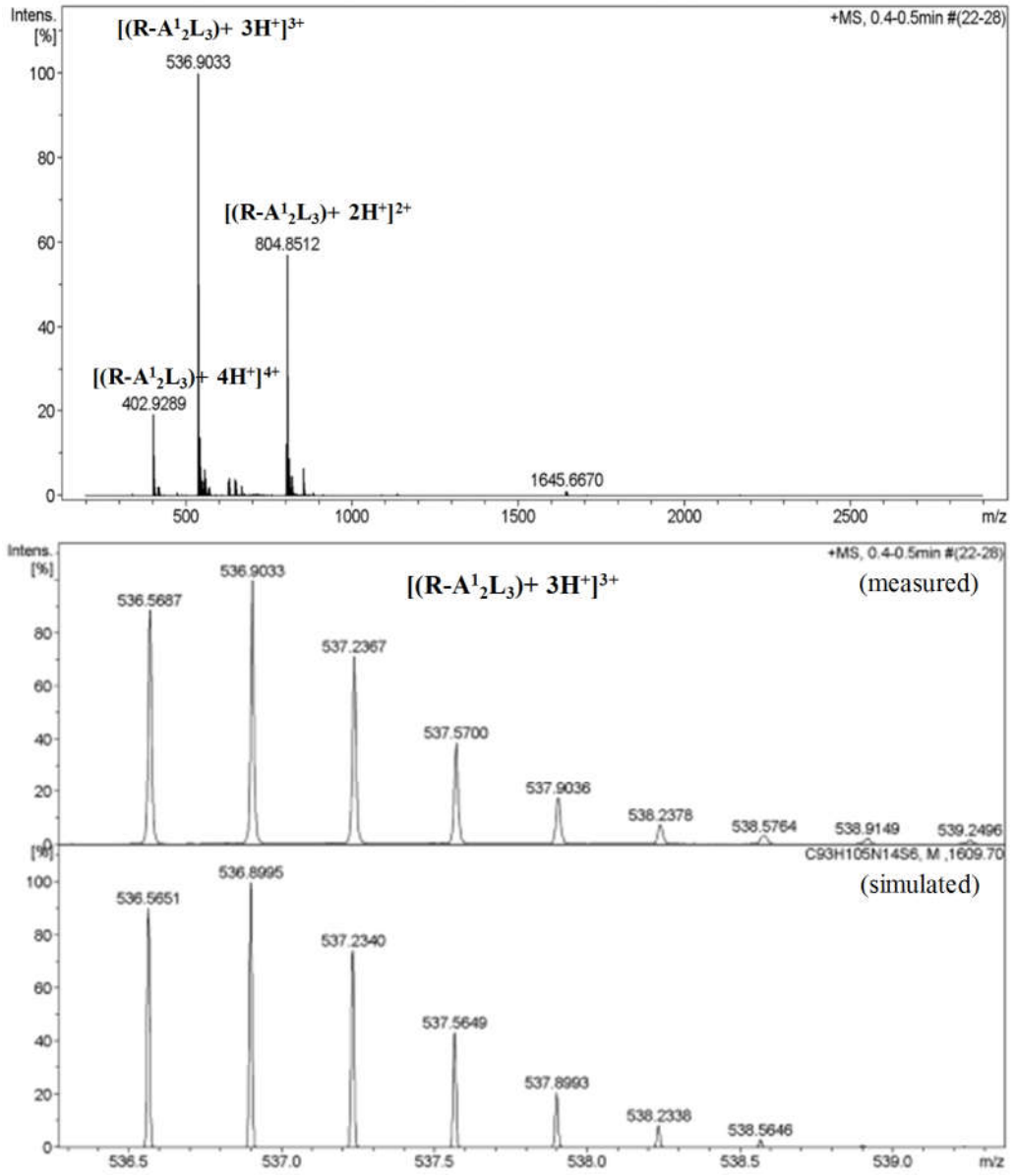

Figure S27. High resolution ESI-MS spectrum for *o*-R-A$^1_2$L$_3$ cage (CH$_3$OH, 25˚C).

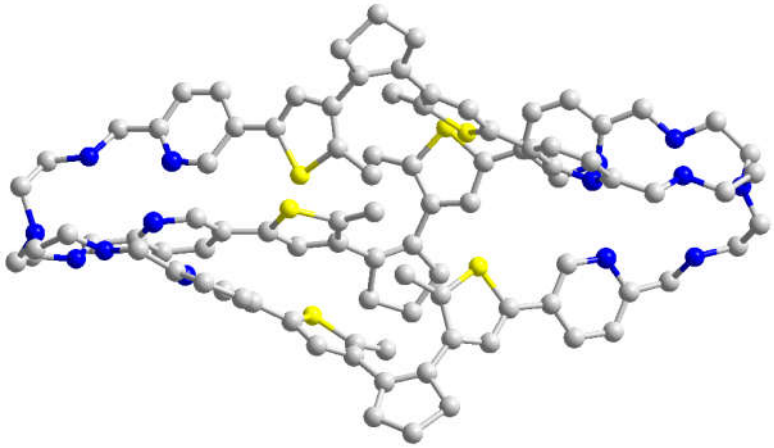

Figure S28. Single-crystal structure of *o*-R-A$^1_2$L$_3$ cage (grey for C, blue for N, yellow for S, H atoms and solvents are omitted for clarity).

2.6 *o*-R-$A^2_2L_3$ cage

To a 25 mL flask was added *o*-$A^2_2L_3Cd_2$ cage (50.0 mg, 18.7 μmol, 1 equiv), sodium borohydride (60 mg, 1.6 mmol, 86 equiv) and dry MeOH (8 mL). The solution was stirred overnight under a nitrogen atmosphere at 50 °C. Then 37% hydrochloric acid was added to bring the pH to 2, and a pale green solid precipitated out. This precipitate was washed by water, dissolved by CH_3OH and then 2M NaOH aqueous solution was added, giving a solid precipitatate. The precipitate was isolated by centrifugation, washed by water twice, and then dissolved by CH_3OH, concentrated in vacuo. The product was obtained as a pale purple solid (22 mg, 68%). High resolution ESI-MS (m/z) data: calc. (measured): 1692.7777 (1692.7493) [R-$A^2_2L_3$ + H^+]$^+$, 846.8925 (846.8807) [R-$A^2_2L_3$ + $2H^+$]$^{2+}$, 564.9308 (564.9236) [R-$A^2_2L_3$ + $3H^+$]$^{3+}$. ^{1}H NMR (400 MHz, CD_3OD) δ 8.65 (d, *J* = 2.4 Hz, 1H), 7.80 (dd, *J* = 8.1, 2.4 Hz, 1H), 7.28 (d, *J* = 8.1 Hz, 1H), 7.25 (s, 1H), 3.74 (s, 2H), 2.82 (t, *J* = 7.4 Hz, 2H), 2.66 (t, *J* = 7.0 Hz, 2H), 2.40 (d, *J* = 6.5 Hz, 3H), 2.06 (q, *J* = 7.6 Hz, 1H), 1.79 – 1.68 (m, 2H), 1.64 (s, 3H), 1.29 (s, 1H). ^{13}C NMR (100 MHz, CD_3OD) δ 158.11, 145.71, 137.77, 136.43, 135.86, 135.02, 133.55, 129.70, 125.52, 123.29, 54.74, 52.94, 39.27, 27.31, 23.24, 14.22. IR (KBr, cm^{-1}): 3450, 2915, 2852, 1654, 1589, 1562, 1495, 1459, 1380, 1258, 1223, 1162, 1031, 899, 875, 639.

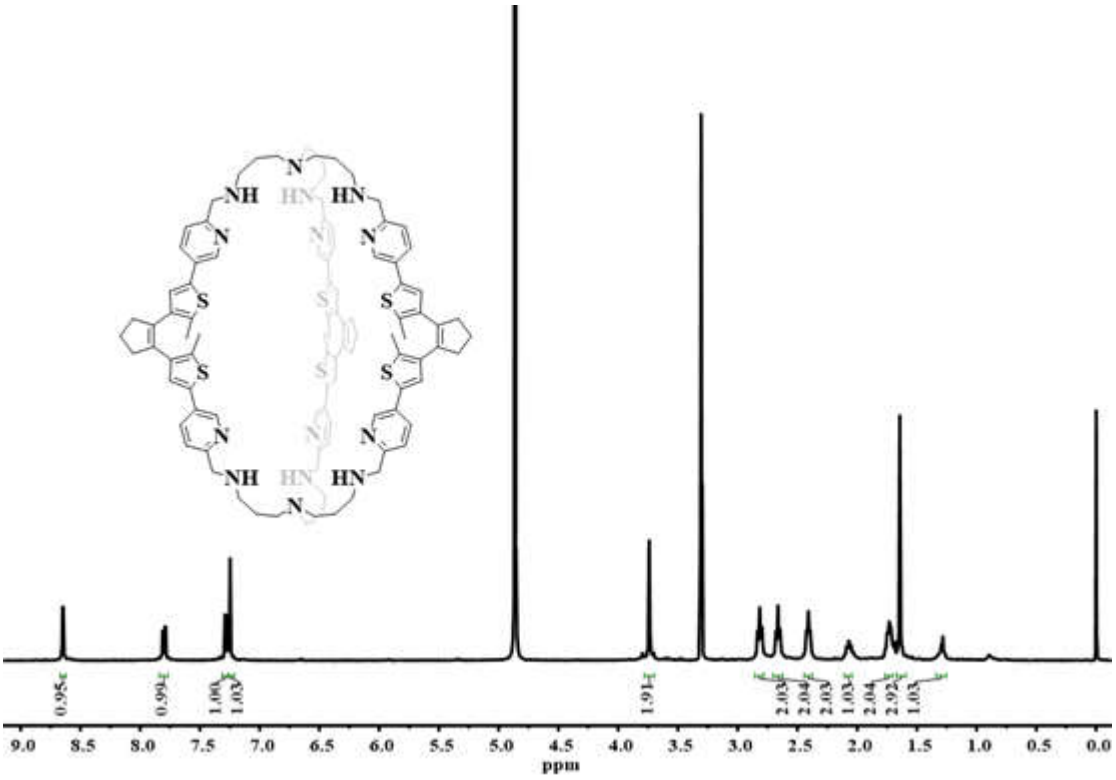

Figure S29. ^{1}H NMR spectrum for *o*-R-$A^2_2L_3$ cage (CD_3OD, 25˚C).

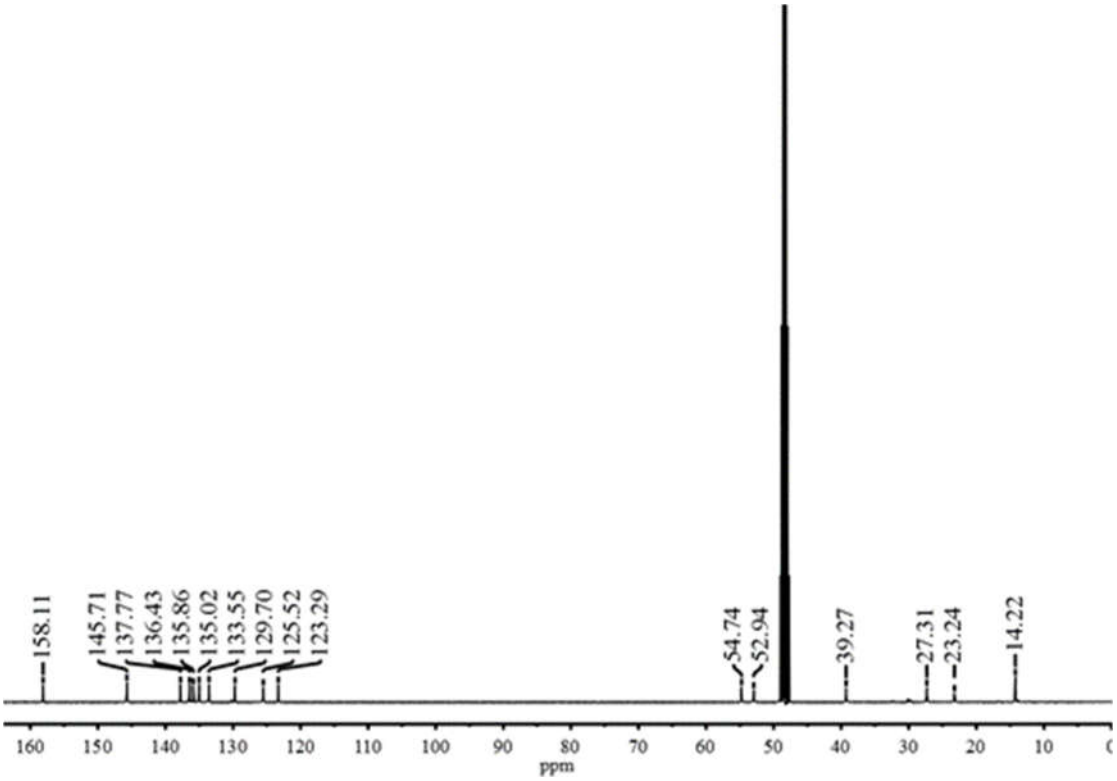

Figure S30. ^{13}C NMR spectrum for *o*-R-$A^2_2L_3$ cage (CD_3OD, 25˚C).

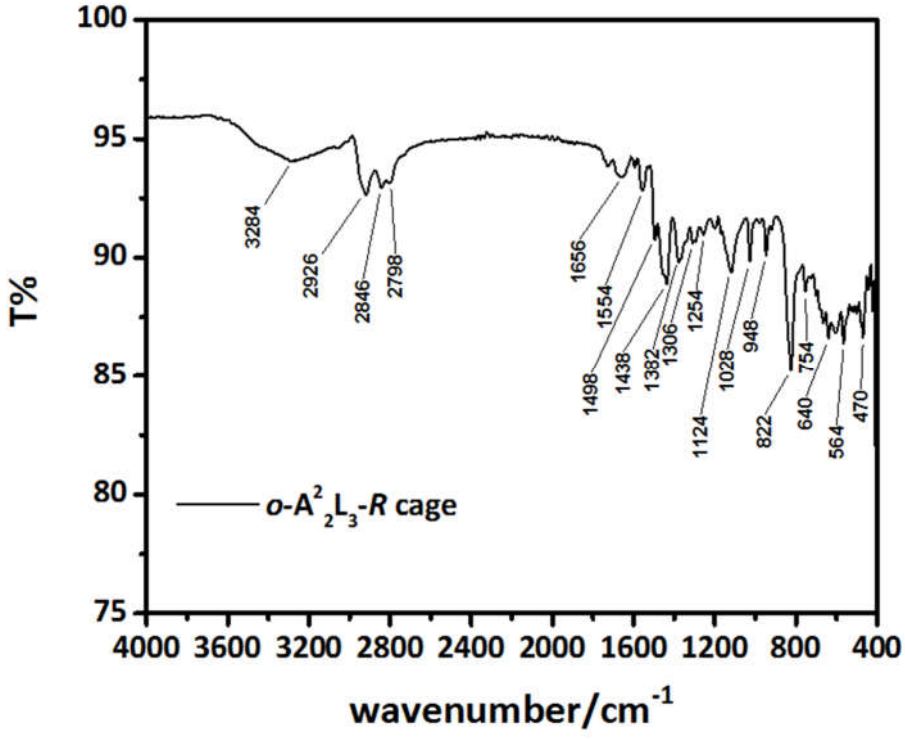

Figure S31. FT-IR spectrum for *o*-R-$A^2_2L_3$ cage.

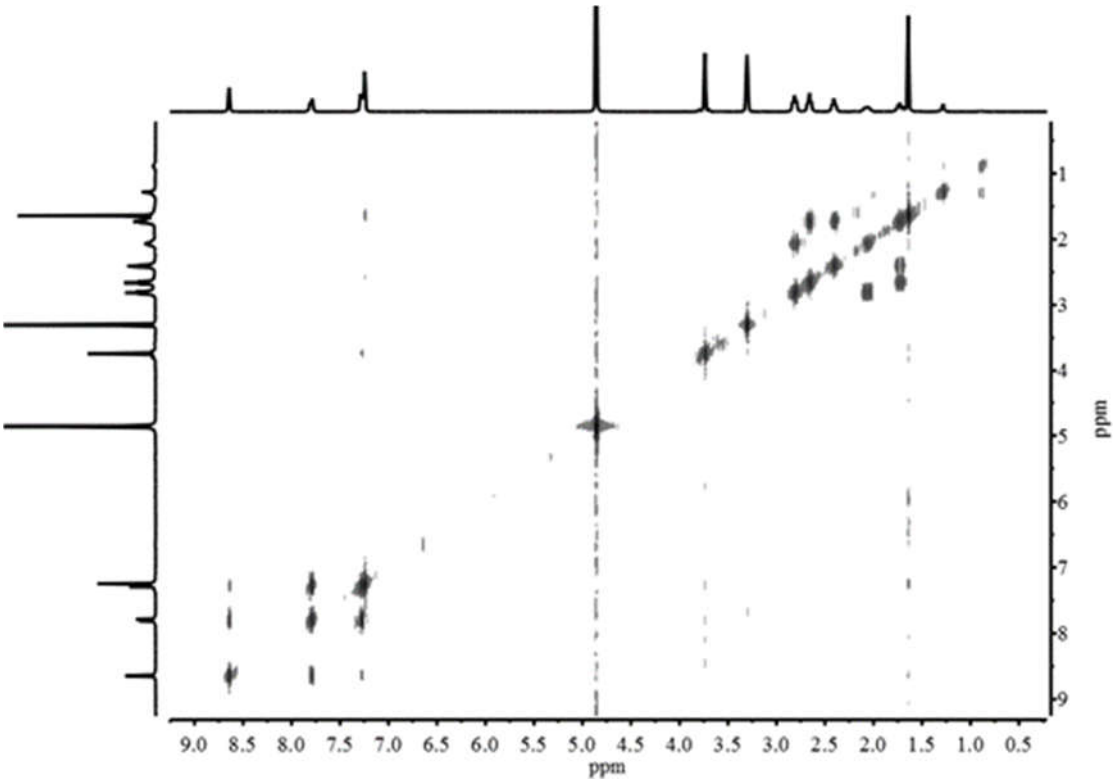

Figure S32. ^{1}H-^{1}H COSY spectrum for *o*-R-A$^{2}_{2}$L$_{3}$ cage (CD$_{3}$OD, 25˚C).

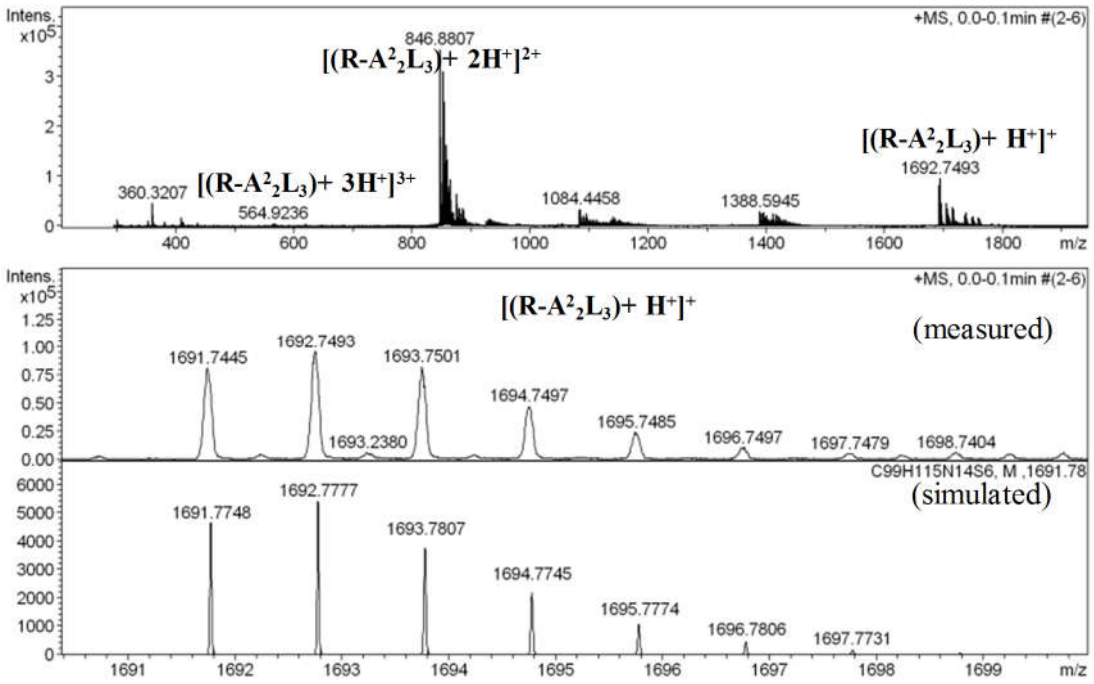

Figure S33. High resolution ESI-MS spectrum for *o*-R-A$^{2}_{2}$L$_{3}$ cage (CH$_{3}$OH, 25˚C).

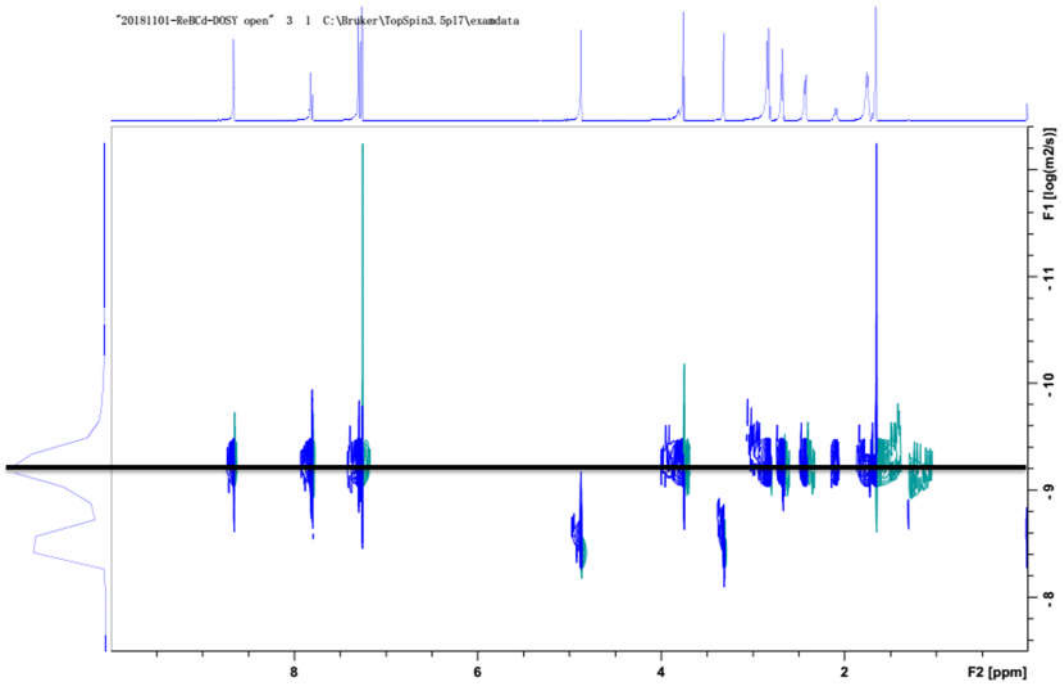

Figure S34. DOSY spectrum for *o*-R-$A^2_2L_3$ cage (CD_3OD, 25˚C).

2.7 Crystal structures

Table S1. Crystallographic data summary for *o*-PADTE (CCDC 1917233), *c*-PADTE (CCDC 1919654).

	***o*-PADTE**	***c*-PADTE**
Empirical Formula	$C_{27}H_{22}N_2O_2S_2$	$C_{27}H_{22}N_2O_2S_2$
Formula weight	470.58	470.58
Temperature/K	161(17)	150.00(10)
Crystal system	monoclinic	monoclinic
Space group	*C*2/c	*C*2/c
a (Å)	24.6968(7)	22.3150(13)
b (Å)	9.9776(3)	12.4269(5)
c (Å)	9.3115(2)	8.2043(5)
α (˚)	90	90
β (˚)	93.975(2)	92.884(5)
γ (˚)	90	90
V (Å^3)	2288.97(11)	2272.2(2)
Z	4	4
ρ_{calc}g/cm^3	1.366	1.376
μ/mm^{-1}	2.330	2.348
F(000)	984.0	984.0
2θ range for data collection/°	7.176 to 133.022	7.934 to 145.482
Reflections collected	3471	3604
Independent reflections	1995 R_{int} = 0.0154, R_{sigma} = 0.0200	2171 R_{int} = 0.0245, R_{sigma} = 0.0399
Data/restraints/parameters	1995/0/151	2171/19/151
Goodness-of-fit on F^2	1.056	1.034
Final *R* indexes [*I*> = 2σ (*I*)]	R_1 = 0.0345, wR_2 = 0.0928	R_1 = 0.0624, wR_2 = 0.1505
Final *R* indexes [all data]	R_1 = 0.0367, wR_2 = 0.0946	R_1 = 0.0819, wR_2 = 0.1658
Largest diff. peak/hole / e Å^{-3}	0.38/-0.28	1.04/-0.42

Table S2. Bond lengths (Å) for PADTE (**L**).

o-**PADTE**	Bond lengths(Å)	*c*-**PADTE**	Bond lengths(Å)
S1-C7	1.7330(16)	S1-C7	1.773(3)
S1-C10	1.7261(17)	S1-C10	1.844(4)
O1-C1	1.208(2)	O1-C1	1.205(5)
N1-C2	1.343(2)	N1-C2	1.350(5)
N1-C6	1.328(2)	N1-C6	1.329(5)
C1-C2	1.483(2)	C1-C2	1.481(5)
C2-C3	1.378(3)	C2-C3	1.379(5)
C3-C4	1.384(3)	C3-C4	1.386(5)
C4-C5	1.386(2)	C4-C5	1.389(5)
C5-C6	1.399(3)	C5-C7	1.463(4)
C5-C7	1.462(2)	C5-C6	1.408(5)
C7-C8	1.364(2)	C7-C8	1.353(5)
C8-C9	1.425(2)	C8-C9	1.422(5)
C9-C10	1.374(2)	C9-C10	1.529(5)
C9-C12	1.475(2)	C9-C12	1.353(5)
C10-C11	1.497(2)	C10-C10[1]	1.450(9)
C12-C12[1]	1.344(3)	C10-C11	1.652(7)
C12-C13	1.516(2)	C12-C121	1.429(6)
C13-C14	1.504(2)	C12-C13	1.505(4)
C14-C13[1]	1.504(2)	C13-C14	1.537(4)
		C14-C13[1]	1.536(4)

[1] 1-X, +Y,1/2-Z

Table S3. Bond angles (°) for PADTE (**L**).

o-**PADTE**	Bond angles (°)	*c*-**PADTE**	Bond angles (°)
C10-S1-C7	92.60(8)	C7-S1-C10	92.37(17)
C6-N1-C2	117.33(15)	C6-N1-C2	116.8(3)
O1-C1-C2	124.27(18)	O1-C1-C2	124.5(4)
N1-C2-C1	114.74(15)	N1-C2-C1	113.8(3)
N1-C2-C3	123.06(16)	N1-C2-C3	123.3(3)
C3-C2-C1	122.19(16)	C3-C2-C1	122.9(3)
C2-C3-C4	118.69(16)	C2-C3-C4	119.0(3)
C3-C4-C5	119.75(17)	C3-C4-C5	119.4(3)
C4-C5-C6	116.80(15)	C4-C5-C7	123.6(3)
C4-C5-C7	123.12(16)	C4-C5-C6	116.9(3)
C6-C5-C7	120.05(15)	C6-C5-C7	119.5(3)
N1-C6-C5	124.32(16)	C5-C7-S1	121.4(3)
C5-C7-S1	121.89(13)	C8-C7-S1	112.9(2)
C8-C7-S1	109.78(12)	C8-C7-C5	125.6(3)
C8-C7-C5	128.17(15)	C7-C8-C9	115.1(3)
C7-C8-C9	114.66(15)	C8-C9-C10	112.6(3)
C8-C9-C12	121.06(15)	C12-C9-C8	127.4(3)
C10-C9-C8	111.62(15)	C12-C9-C10	120.0(3)
C10-C9-C12	126.98(15)	C9-C10-S1	104.2(3)
C9-C10-S1	111.33(12)	C9-C10-C11	107.8(4)
C9-C10-C11	129.67(16)	C101-C10-S1	120.0(4)
C11-C10-S1	118.88(13)	C101-C10-C9	112.5(3)
C9-C12-C13	117.80(14)	C101-C10-C11	104.5(5)
C12[1]-C12-C9	131.20(9)	C11-C10-S1	107.3(3)
C12[1]-C12-C13	110.96(9)	C9-C12-C12[1]	120.68(19)
C14-C13-C12	105.04(15)	C9-C12-C13	128.6(3)
C13[1]-C14-C13	107.8(2)	C12[1]-C12-C13	110.69(17)
		C12-C13-C14	105.1(3)
		C13[1]-C14-C13	108.4(4)
		N1-C6-C5	124.5(3)

[1] 1-X, +Y,1/2-Z

Table S4. Crystallographic data summary for *o*-$A^1{}_2L_3Zn_2$ cage, CCDC 1917232), *c*-$A^1{}_2L_3Zn_2$ cage, CCDC 1917235).

	o-$A^1{}_2L_3Zn_2$	*c*-$A^1{}_2L_3Zn_2$
Empirical Formula	$C_{193}H_{180}F_{21}N_{28}O_{21}S_{19}Zn_4$	$C_{97}H_{90}F_{12}N_{14}O_{12}S_{10}Zn_2$
Formula weight	4497.26	2323.16
Temperature/K	173(2)	173(2)
Crystal system	triclinic	monoclinic
Space group	*P*-1	$P2_1/n$
a (Å)	17.1885(8)	21.3852(6)
b (Å)	18.1907(8)	18.2160(3)
c (Å)	19.2773(8)	28.8807(4)
α (˚)	67.867(4)	90
β (˚)	83.882(4)	91.739(2)
γ (˚)	83.880(4)	90
V (Å^3)	5537.0(5)	11245.4(4)
Z	1	4
ρ_{calc}g/cm^3	1.349	1.372
μ/mm^{-1}	2.867	2.956
F(000)	2315.0	4776.0
2θ range for data collection/°	7.114 to 130.068	7.018 to 148.59
Reflections collected	33920	44414
Independent reflections	18381 R_{int} = 0.0631, R_{sigma} = 0.0744	22259 R_{int} = 0.0368, R_{sigma} = 0.0429
Data/restraints/parameters	18381/249/1361	22259/98/1330
Goodness-of-fit on F^2	1.036	1.048
Final *R* indexes [*I*> = 2σ (*I*)]	R_1 = 0.0951, wR_2 = 0.2656	R_1 = 0.0914, wR_2 = 0.2692
Final *R* indexes [all data]	R_1 = 0.1225, wR_2 = 0.2974	R_1 = 0.1109, wR_2 = 0.3000
Largest diff. peak/hole / e Å^{-3}	2.20/-1.97	1.18/-0.86

Table S5. Selected bond lengths (Å) for $A^1{}_2L_3Zn_2$ cage.

o-$A^1{}_2L_3Zn_2$	Bond lengths(Å)	*c*-$A^1{}_2L_3Zn_2$	Bond lengths(Å)
Zn1-N2	2.095(6)	Zn1-N11	2.093(4)
Zn1-N11	2.122(6)	Zn1-N2	2.118(4)
Zn1-N10	2.124(5)	Zn1-N10	2.125(5)
Zn1-N9	2.219(5)	Zn1-N9	2.203(4)
Zn1-N12	2.294(5)	Zn1-N3	2.267(4)
Zn1-N3	2.321(5)	Zn1-N12	2.398(4)
Zn2-N7	2.104(6)	Zn2-N7	2.104(5)
Zn2-N5	2.109(6)	Zn2-N5	2.111(4)
Zn2-N14	2.141(6)	Zn2-N14	2.136(5)
Zn2-N8	2.187(5)	Zn2-N8	2.254(4)
Zn2-N13	2.331(5)	Zn2-N4	2.272(4)
Zn2-N4	2.336(5)	Zn2-N13	2.311(4)

Table S6. Selected bond angles (°) for $A^1{}_2L_3Zn_2$ cage.

o-$A^1{}_2L_3Zn_2$	Bond angles (°)	*c*-$A^1{}_2L_3Zn_2$	Bond angles (°)
N2-Zn1-N11	100.8(2)	N11-Zn1-N2	101.27(16)
N2-Zn1-N10	111.3(2)	N11-Zn1-N10	105.45(19)
N11-Zn1-N10	104.9(2)	N2-Zn1-N10	100.93(17)
N2-Zn1-N9	98.0(2)	N11-Zn1-N9	97.99(16)
N11-Zn1-N9	159.7(2)	N2-Zn1-N9	160.51(14)
N10-Zn1-N9	75.0(2)	N10-Zn1-N9	76.52(17)
N2-Zn1-N12	157.2(2)	N11-Zn1-N3	163.90(18)
N11-Zn1-N12	74.7(2)	N2-Zn1-N3	76.15(15)
N10-Zn1-N12	91.4(2)	N10-Zn1-N3	90.62(16)
N9-Zn1-N12	84.94(18)	N9-Zn1-N3	84.52(14)
N2-Zn1-N3	75.1(2)	N11-Zn1-N12	74.68(17)
N11-Zn1-N3	89.5(2)	N2-Zn1-N12	95.69(15)
N10-Zn1-N3	162.3(2)	N10-Zn1-N12	162.95(16)
N9-Zn1-N3	87.88(18)	N9-Zn1-N12	86.53(15)
N12-Zn1-N3	82.39(19)	N3-Zn1-N12	89.66(14)
N7-Zn2-N5	105.7(2)	N7-Zn2-N5	106.18(17)
N7-Zn2-N14	102.5(2)	N7-Zn2-N14	109.29(19)
N5-Zn2-N14	100.7(2)	N5-Zn2-N14	100.50(17)
N7-Zn2-N8	76.4(2)	N7-Zn2-N8	75.73(17)
N5-Zn2-N8	161.3(2)	N5-Zn2-N8	97.06(16)
N14-Zn2-N8	96.83(19)	N14-Zn2-N8	159.33(15)
N7-Zn2-N13	163.2(2)	N7-Zn2-N4	161.42(17)
N5-Zn2-N13	91.2(2)	N5-Zn2-N4	74.82(15)
N14-Zn2-N13	74.5(2)	N14-Zn2-N4	88.44(17)
N8-Zn2-N13	87.42(18)	N8-Zn2-N4	85.71(15)
N7-Zn2-N4	99.4(2)	N7-Zn2-N13	94.88(16)
N5-Zn2-N4	75.5(2)	N5-Zn2-N13	158.85(17)
N14-Zn2-N4	158.03(19)	N14-Zn2-N13	73.75(16)
N8-Zn2-N4	85.8(2)	N8-Zn2-N13	85.96(15)
N13-Zn2-N4	83.89(19)	N4-Zn2-N13	84.58(14)

Symmetry code: 'x, y, z'; '-x, -y, -z'

Table S7. Crystallographic data summary for *o*-$A^2_2L_3Cd_2$ cage, CCDC 1917234 and *c*-$A^2_2L_3Cd_2$ cage, CCDC 1917798.

	o-$A^2_2L_3Cd_2$	*c*-$A^2_2L_3Cd_2$
Empirical Formula	$C_{109}H_{111}Cd_2F_{12}N_{17}O_{12}S_{10}$	$C_{105}H_{105}Cd_2F_{12}N_{15}O_{12}S_{10}$
Formula weight	2624.54	2542.43
Temperature/K	150.00(10)	150(2)
Crystal system	tetragonal	triclinic
Space group	$P4_32_12$	P-1
a (Å)	13.54180(10)	17.6556(11)
b (Å)	13.54180(10)	18.0529(12)
c (Å)	66.0707(8)	19.857(2)
α (˚)	90	78.743(8)
β (˚)	90	75.912(8)
γ (˚)	90	79.512(5)
V (Å^3)	12116.1(2)	5960.2(9)
Z	4	2
ρ_{calc}g/cm^3	1.439	1.417
μ/mm^{-1}	5.122	5.182
F(000)	5376.0	2600.0
2θ range for data collection/°	6.662 to 146.892	6.994 to 117.868
Reflections collected	33381	17052
Independent reflections	11878 R_{int} = 0.0435, R_{sigma} = 0.0407	17052 R_{int} = 0.1188, R_{sigma} = 0.1296
Data/restraints/parameters	11878/302/756	17052/1537/1412
Goodness-of-fit on F^2	1.024	1.034
Final R indexes [$I >= 2\sigma$ (I)]	R_1 = 0.0978, wR_2 = 0.2610	R_1 = 0.1205, wR_2 = 0.0.2045
Final R indexes [all data]	R_1 = 0.1046, wR_2 = 0.2706	R_1 = 0.2064, wR_2 = 0.2296
Largest diff. peak/hole / e Å^{-3}	4.61/-1.94	0.97/-1.00

Table S8. Selected bond lengths (Å) for $A^2_2L_3Cd_2$ cage.

o-$A^2_2L_3Cd_2$	Bond lengths(Å)	*c*-$A^2_2L_3Cd_2$	Bond lengths(Å)
Cd1-N1	2.464(9)	Cd1-N1	2.338(13)
Cd1-N2	2.329(10)	Cd1-N9	2.366(14)
Cd1-N3	2.502(9)	Cd1-N7	2.424(14)
Cd1-N4	2.352(9)	Cd1-N10	2.438(13)
Cd1-N5	2.462(10)	Cd1-N14	2.536(13)
Cd1-N6	2.334(10)	Cd1-N2	2.547(10)
Cd1-N7	2.456(11)	Cd1-N1	2.338(13)
		Cd2-N4	2.339(15)
		Cd2-N12	2.345(12)
		Cd2-N5	2.351(16)
		Cd2-N6	2.430(15)
		Cd2-N3	2.444(13)
		Cd2-N13	2.454(17)
		Cd2-N11	2.513(17)

Table S9. Selected bond angles (°) for $A^2_2L_3Cd_2$ cage.

o-$A^2_2L_3Cd_2$	Bond angles (°)	*c*-$A^2_2L_3Cd_2$	Bond angles (°)
N1-Cd1-N3	130.7(3)	N8-Cd1-N1	118.8(5)
N2-Cd1-N1	80.2(3)	N8-Cd1-N9	119.7(5)
N2-Cd1-N3	68.6(3)	N1-Cd1-N9	111.0(6)
N2-Cd1-N4	117.6(3)	N8-Cd1-N7	70.4(5)
N2-Cd1-N5	81.9(3)	N1-Cd1-N7	151.4(4)
N2-Cd1-N6	114.1(4)	N9-Cd1-N7	82.0(5)
N2-Cd1-N7	148.4(4)	N8-Cd1-N10	147.9(5)
N4-Cd1-N1	79.3(3)	N1-Cd1-N10	80.1(5)
N4-Cd1-N3	149.0(3)	N9-Cd1-N10	69.1(4)
N4-Cd1-N5	68.6(3)	N7-Cd1-N10	81.3(5)
N4-Cd1-N7	82.1(3)	N8-Cd1-N14	77.9(5)
N5-Cd1-N1	129.9(3)	N1-Cd1-N14	79.0(5)
N5-Cd1-N3	83.3(3)	N9-Cd1-N14	80.4(5)
N6-Cd1-N1	80.1(4)	N7-Cd1-N14	129.2(5)
N6-Cd1-N3	79.2(3)	N10-Cd1-N14	133.4(5)
N6-Cd1-N4	119.3(4)	N8-Cd1-N2	82.6(4)
N6-Cd1-N5	149.3(4)	N1-Cd1-N2	69.8(5)
N6-Cd1-N7	69.4(4)	N9-Cd1-N2	148.5(4)
N7-Cd1-N1	129.9(4)	N7-Cd1-N2	85.9(4)
N7-Cd1-N3	82.0(3)	N10-Cd1-N2	80.5(4)
N7-Cd1-N5	83.4(4)	N14-Cd1-N2	128.6(5)
		N4-Cd2-N12	125.3(6)
		N4-Cd2-N5	117.9(5)
		N12-Cd2-N5	106.6(5)
		N4-Cd2-N6	80.6(6)
		N12-Cd2-N6	148.0(6)
		N5-Cd2-N6	69.0(5)
		N4-Cd2-N3	69.0(5)
		N12-Cd2-N3	87.0(4)
		N5-Cd2-N3	151.5(6)
		N6-Cd2-N3	86.1(5)
		N4-Cd2-N13	79.3(5)

	N12-Cd2-N13	79.7(5)
	N5-Cd2-N13	79.0(6)
	N6-Cd2-N13	127.7(5)
	N3-Cd2-N13	128.8(6)
	N4-Cd2-N11	145.1(5)
	N12-Cd2-N11	69.2(6)
	N5-Cd2-N11	80.1(5)
	N6-Cd2-N11	79.0(5)
	N3-Cd2-N11	81.7(4)
	N13-Cd2-N11	135.3(4)

Symmetry code: 'x, y, z'; '-x, -y, -z'

Table S10. DOSY data and calculated solvodynamic radii for cages.

Cages	**log D**	**D[$\times 10^{-10}$ m^2 s^{-1}]**	**r[Å]**
o-$A^1_2L_3Zn_2$	-9.20	6.31	9.4
c-$A^1_2L_3Zn_2$	-9.09	8.13	7.3
o-$A^2_2L_3Zn_2$	-9.13	7.41	8.0
c-$A^2_2L_3Zn_2$	-9.15	7.08	8.3
o-$A^2_2L_3Cd_2$	-9.05	8.91	6.6
c-$A^2_2L_3Cd_2$	-9.07	8.51	6.9
o-R-$A^1_2L_3$	-9.42	3.80	9.6
c-R-$A^1_2L_3$	-9.45	3.55	10.2
o-R-$A^2_2L_3$	-9.20	6.31	5.8
c-R-$A^2_2L_3$	-9.18	6.61	5.5

Note: Stokes-Einstein equation

$$D = \frac{k_B T}{6\pi\eta \mathrm{r}},$$

was applied to estimate the dynamic radius for the cages. In which, D is diffusion coefficient obtained from DOSY spectra, k_B is Boltzmann constant, T is temperature 298 K, η is dynamic viscosity of CD_3CN (3.7×10^{-4} Pa s^{-1}) or CD_3OD (6.0×10^{-4} Pa s^{-1}), and r is the estimated dynamic radius.

Table S11. Crystallographic data summary for *o*-R-$A^1{}_2L_3$ (CCDC 1922928).

	o-R-$A^1{}_2L_3$
Empirical Formula	$C_{93}H_{102}N_{14}S_6$
Formula weight	1608.24
Temperature/K	149.99(10)
Crystal system	monoclinic
Space group	$P2_1/c$
a (Å)	21.0570(9)
b (Å)	15.0503(3)
c (Å)	34.322(3)
α (˚)	90
β (˚)	90.522(6)
γ (˚)	90
V (Å^3)	10876.7(11)
Z	4
ρ_{calc}g/cm^3	0.982
μ/mm^{-1}	1.496
F(000)	3416.0
2θ range for data collection/°	5.15 to 122.336
Reflections collected	83143
Independent reflections	16130 R_{int} = 0.1042, R_{sigma} = 0.0543
Data/restraints/parameters	16130/1097/989
Goodness-of-fit on F^2	0.906
Final *R* indexes [I> = 2σ (I)]	R_1 = 0.2016, wR_2 = 0.4995
Final *R* indexes [all data]	R_1 = 0.2304, wR_2 = 0.5148
Largest diff. peak/hole / e Å^{-3}	1.50/-0.65

Table S12. Bond lengths (Å) for *o*-R-$A^1{}_2L_3$.

o-R-$A^1{}_2L_3$	Bond lengths(Å)	*o*-R-$A^1{}_2L_3$	Bond lengths(Å)
S1-C9	1.724(15)	N6-C31	1.53(3)
S1-C12	1.774(16)	N6-C62	1.454(9)
S2-C20	1.769(18)	N6-C93	1.464(9)
S2-C23	1.762(17)	N7-C33	1.49(2)
S3-C40	1.686(15)	N7-C34	1.51(2)
S3-C43	1.664(18)	N9-C57	1.39
S4-C51	1.718(16)	N9-C56	1.39
S4-C54	1.781(16)	N10-C60	1.385(10)
S5-C71	1.725(11)	N10-C61	1.437(9)
S5-C74	1.751(11)	N11-C64	1.477(16)
S6-C82	1.689(13)	N11-C65	1.437(16)
S6-C85	1.719(13)	N12-C66	1.413(16)
N1-C1	1.40(2)	N12-C67	1.415(17)
N1-C32	1.39(2)	N14-C91	1.50(2)
N1-C63	1.500(19)	N14-C92	1.45(2)
N2-C2	1.455(18)	N3-C5	1.39
N2-C3	1.381(19)	C35-N8	1.29(2)
N4-C25	1.32(2)	N8-C39	1.39(2)
N4-C26	1.302(19)	C88-N13	1.39
N5-C29	1.50(2)	N13-C87	1.39
N5-C30	1.46(2)		

Table S13. Bond angles (°) for *o*-R-$A^1{}_2L_3$.

o-R-$A^1{}_2L_3$	Bond angles (°)	*o*-R-$A^1{}_2L_3$	Bond angles (°)
C9-S1-C12	91.5(7)	N4-C26-C27	121.8(16)
C23-S2-C20	88.7(9)	N4-C26-C29	118.2(16)
C43-S3-C40	94.1(8)	C26-C29-N5	110.9(15)
C51-S4-C54	92.6(8)	C31-C30-N5	113.2(19)
C71-S5-C74	94.4(6)	C30-C31-N6	116.2(18)
C82-S6-C85	91.6(6)	N1-C32-C33	112.0(15)
C1-N1-C63	110.8(14)	C32-C33-N7	109.6(16)
C32-N1-C1	109.5(13)	C35-C34-N7	112.9(18)
C32-N1-C63	114.1(14)	N8-C35-C34	114.3(18)
C3-N2-C2	113.0(13)	N8-C35-C36	120(2)
C26-N4-C25	119.5(16)	C35-N8-C39	119.3(16)
C30-N5-C29	114.5(15)	C50-C51-S4	108.4(12)
C62-N6-C31	114.4(17)	C52-C51-S4	121.3(13)
C62-N6-C93	112.5(9)	C55-C54-S4	118.8(11)
C93-N6-C31	115.5(17)	C53-C54-S4	106.1(12)
C33-N7-C34	113.8(16)	N10-C60-C57	111.6(16)
C57-N9-C56	120	N10-C61-C62	101.8(15)
N9-C57-C58	120	N6-C62-C61	118.0(16)
N9-C57-C60	127.2(11)	N1-C63-C64	108.8(13)
C55-C56-N9	120	N11-C64-C63	111.3(12)
C60-N10-C61	112.1(16)	N11-C65-C66	113.5(11)
C65-N11-C64	112.2(11)	N12-C66-C65	121.5(11)
C66-N12-C67	119.1(11)	C70-C66-N12	120.0(12)
C92-N14-C91	107.8(15)	N12-C67-C68	118.5(11)
N1-C1-C2	110.7(14)	C68-C71-S5	123.0(8)
N2-C2-C1	108.4(13)	C72-C71-S5	109.6(9)
N2-C3-C4	111.8(12)	C73-C74-S5	107.4(9)
N3-C4-C3	124.4(9)	C75-C74-S5	122.8(9)
N3-C4-C8	120	C81-C82-S6	111.7(9)
C4-N3-C5	120	C83-C82-S6	120.0(9)
N3-C5-C6	120	C84-C85-S6	110.3(10)
C6-C9-S1	120.1(10)	C86-C85-S6	119.5(9)

C10-C9-S1	113.1(11)	N13-C88-C89	120
C11-C12-S1	108.9(11)	N13-C88-C91	117.2(10)
C13-C12-S1	118.1(12)	C88-N13-C87	120
C19-C20-S2	111.9(13)	N13-C87-C86	120
C21-C20-S2	114.1(14)	C88-C91-N14	110.7(13)
C22-C23-S2	111.9(13)	N14-C92-C93	107.4(17)
C24-C23-S2	119.6(14)	N6-C93-C92	113.8(16)
N4-C25-C24	122.6(16)	C38-C39-N8	123.0(16)

2.7 Er-1, Er-5, Er-9

Macroporous ZrO_2:Er(III)-Yb(III) materials with different Er/Yb molar ratios (1:1, 1:5, 1:9 for samples Er-1, Er-5, Er-9, respectively) were prepared by sol-gel method combined with polystyrene (PS) sphere templating technique.[S2] Appropriate amounts of $Er(NO_3)_3$ and $Yb(NO_3)_3$ were added into the methanol solution of Zr(IV)-polyacetylacetone under stirring, and then dripped onto PS templates. The products were dried in air at room temperature for 24 h, then annealed at 900 °C for 5 h.

3. Study of photochromic process of PADTE ligand and cages

3.1 PADTE ligand

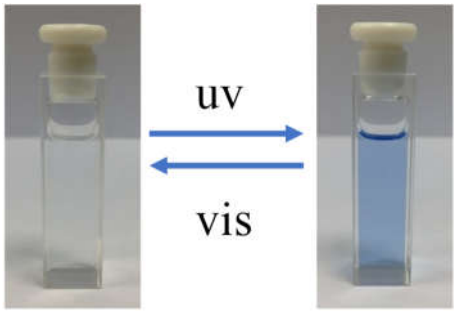

o-PADTE *c*-PADTE

Figure S35. Color change of PADTE ligand in $CH_3CN/CHCl_3$ (v:v = 1:1, 1×10^{-5} mol L^{-1}) solution by UV/Vis irradiation.

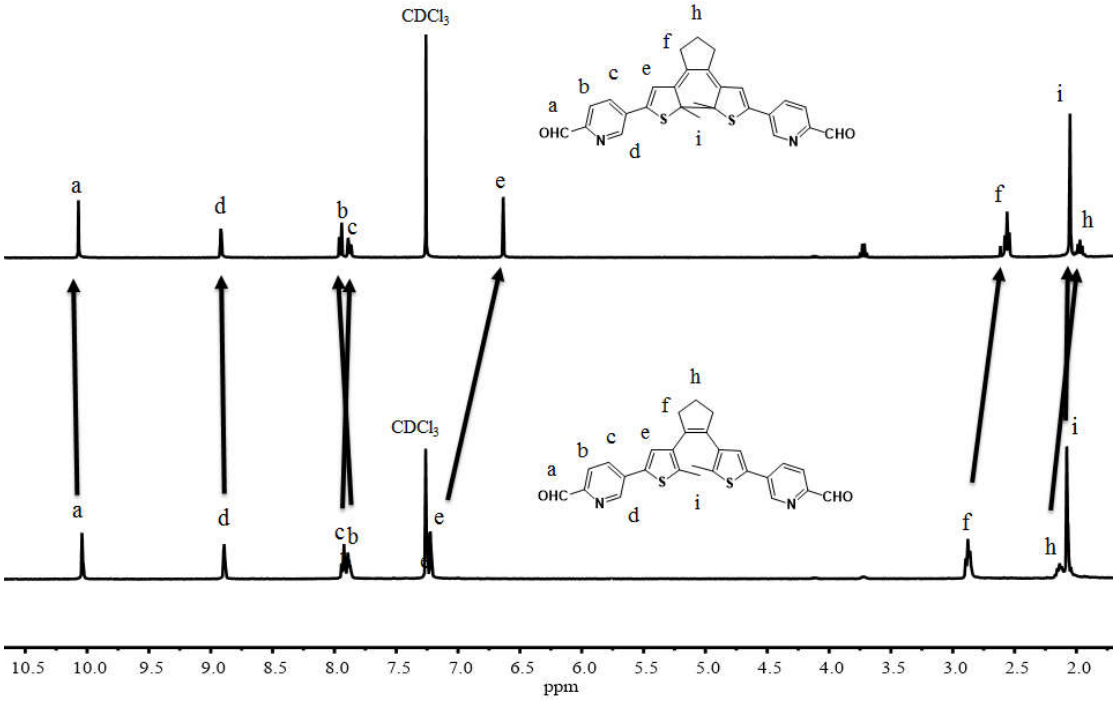

Figure S36. ^{1}H NMR comparison of *o*- and *c*-PADTE ligand ($CDCl_3$, 25 ^{o}C).

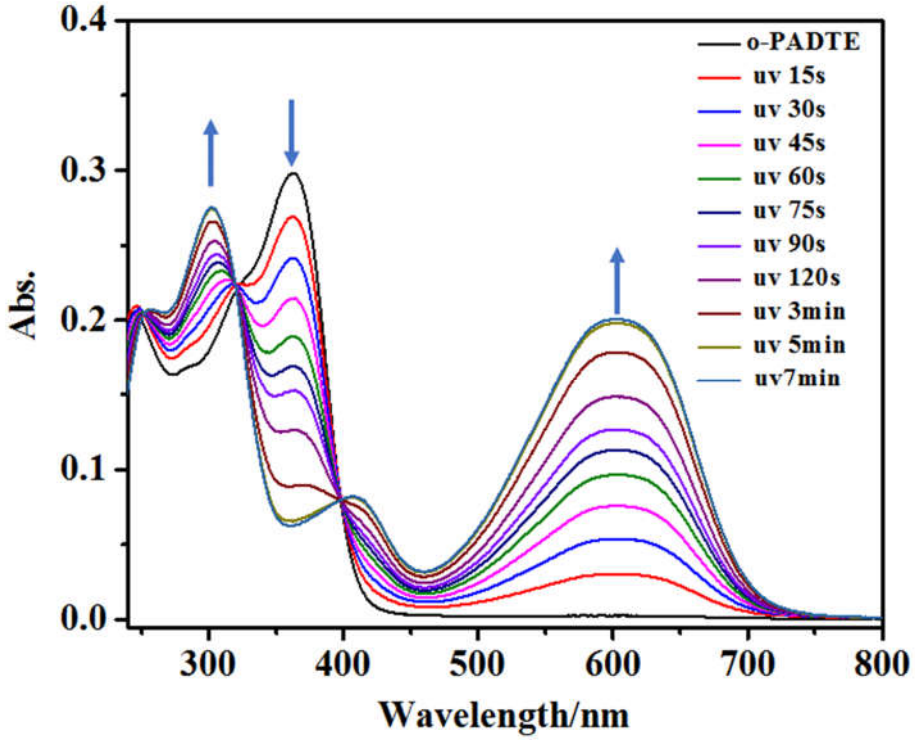

Figure S37. UV-Vis spectra of *o*-PADTE ligand during ring-closing process under UV irradiation for different time ($CH_3CN/CHCl_3$, v:v=1:1, 1×10^{-5} mol L^{-1}, room temperature).

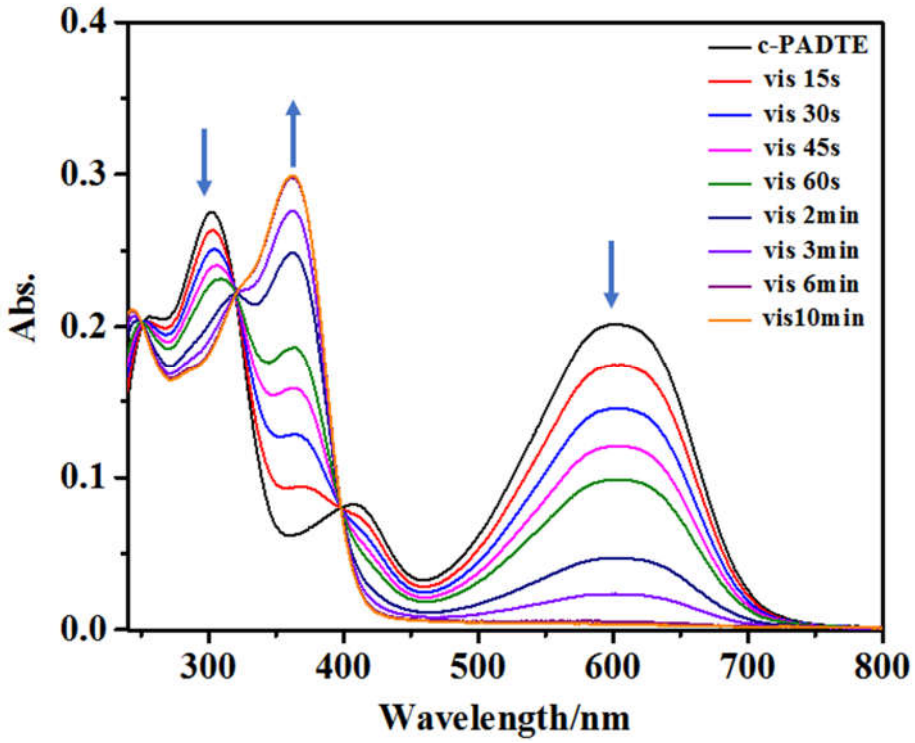

Figure S38. UV-Vis spectra of *c*-PADTE ligand during ring-opening process under visible irradiation for different time ($CH_3CN/CHCl_3$, v:v=1:1, 1×10^{-5} mol L^{-1}, room temperature).

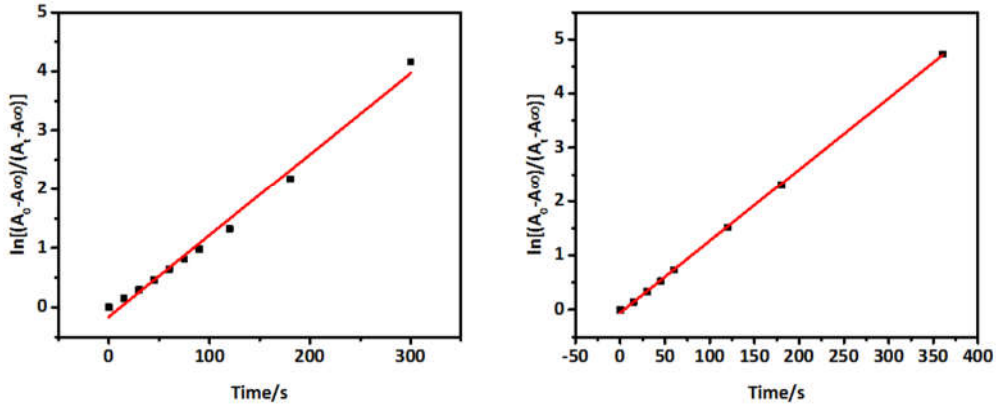

(a) (b)

Figure S39. (a) Plot of $\ln[(A_0-A_\infty)/(A_t-A_\infty)]$ with time for UV-Vis absorption of *o*-PADTE ligand during ring-closing process, and (b) *c*-PADTE ligand during ring-opening process ($CH_3CN/CHCl_3$, v:v = 1:1, 1×10^{-5} mol L^{-1}, room temperature).

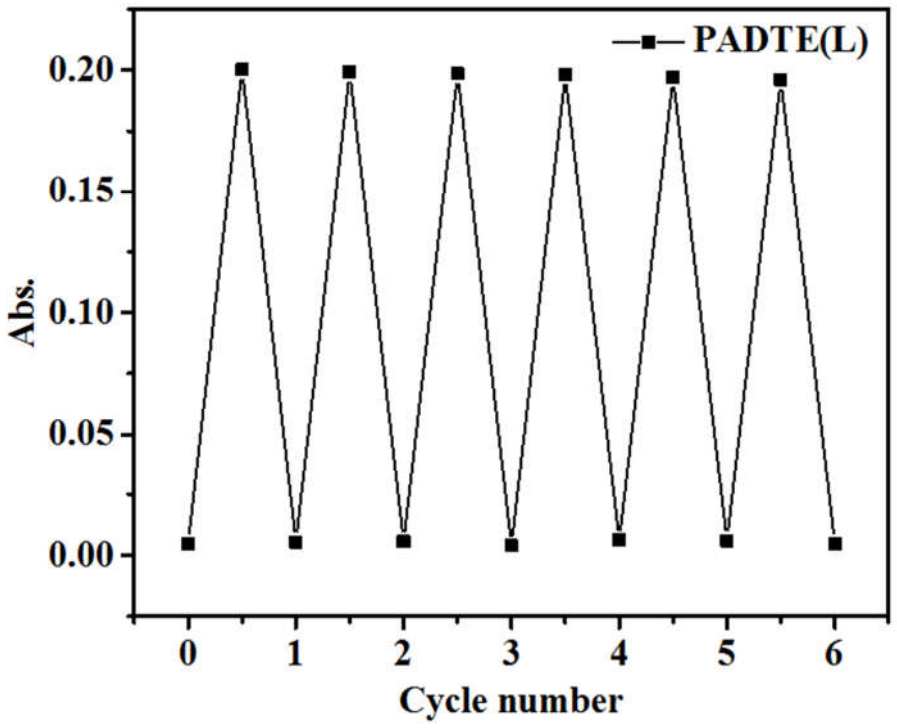

Figure S40. Cycled signals for absorbance at 605 nm of PADTE during alternative ring-closing/ring-opening processes

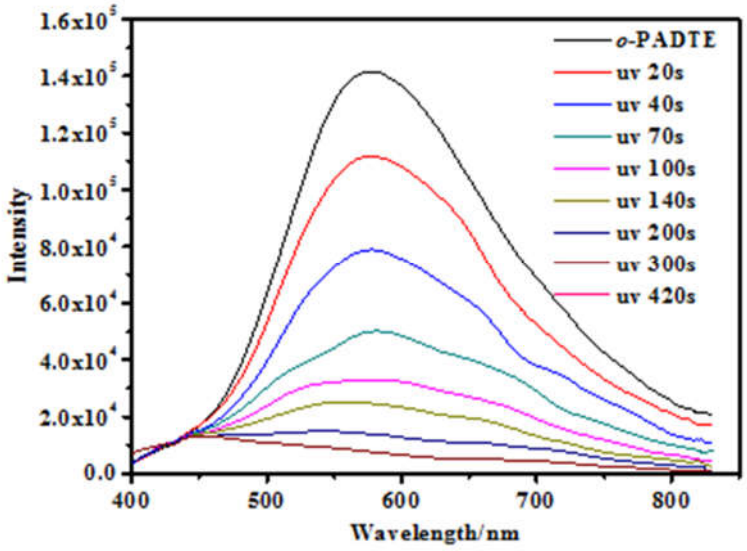

Figure S41. Emission spectra of *o*-PADTE ligand during ring-closing process ($CH_3CN/CHCl_3$, v:v = 1:1, 1×10^{-5} mol L^{-1}, room temperature).

3.2 $A^1_2L_3Zn_2$ cage

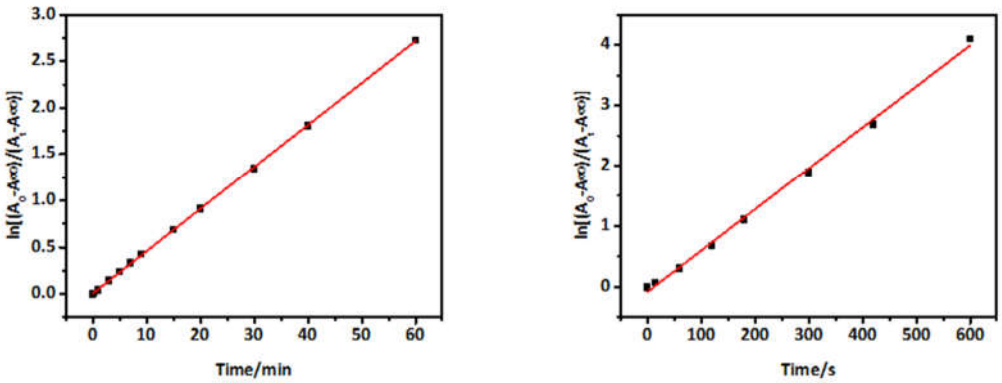

(a) (b)

Figure S42. (a) Plot of $\ln[(A_0-A_\infty)/(A_t-A_\infty)]$ with time for UV-Vis absorption of *o*-$A^1_2L_3Zn_2$ cage during ring-closing process, and (b) *c*-$A^1_2L_3Zn_2$ cage during ring-opening process ($CH_3CN/CHCl_3$, v:v = 1:1, 1×10^{-5} mol L^{-1}, room temperature).

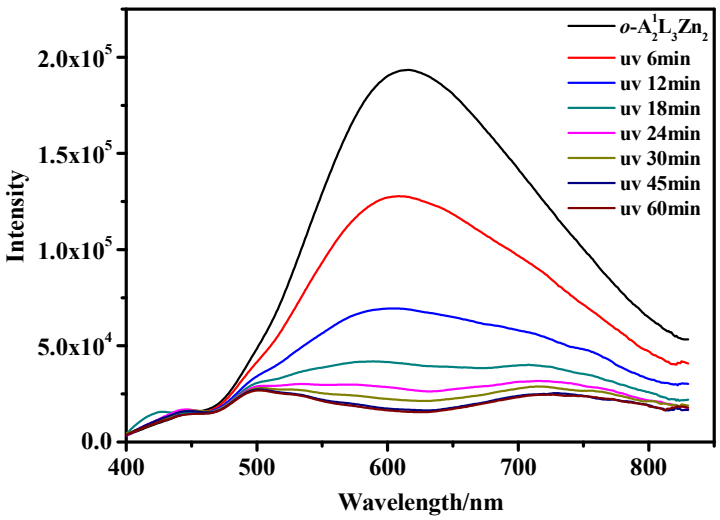

Figure S43. The emission spectra of *o*-$A^1_2L_3Zn_2$ cage during ring-closing process ($CH_3CN/CHCl_3$, v:v = 1:1, 1×10^{-5} mol L^{-1}, room temperature).

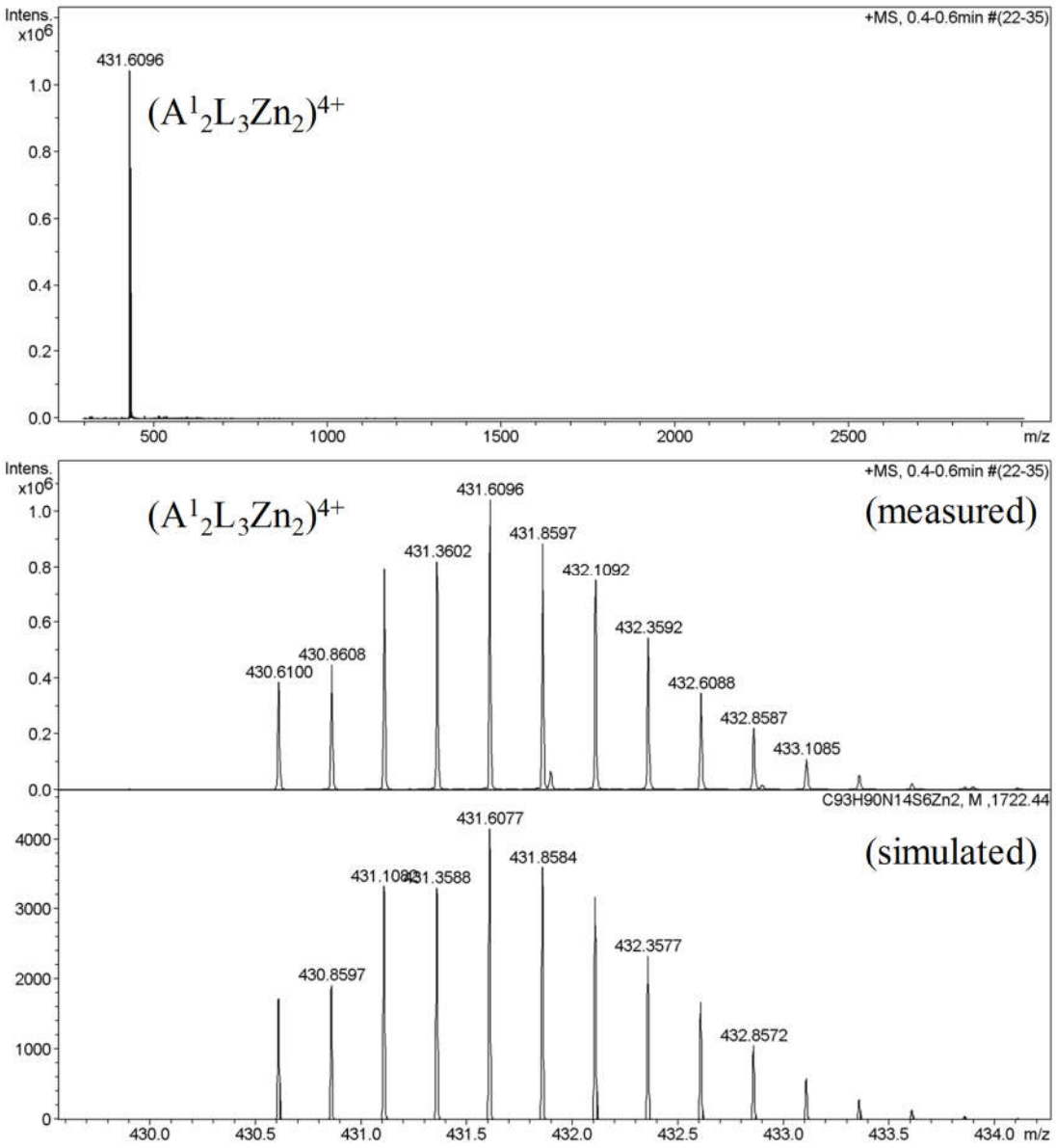

Figure S44. High resolution ESI-MS spectra of *c*-$A^1{}_2L_3Zn_2$ cage (CH_3CN, room temperature).

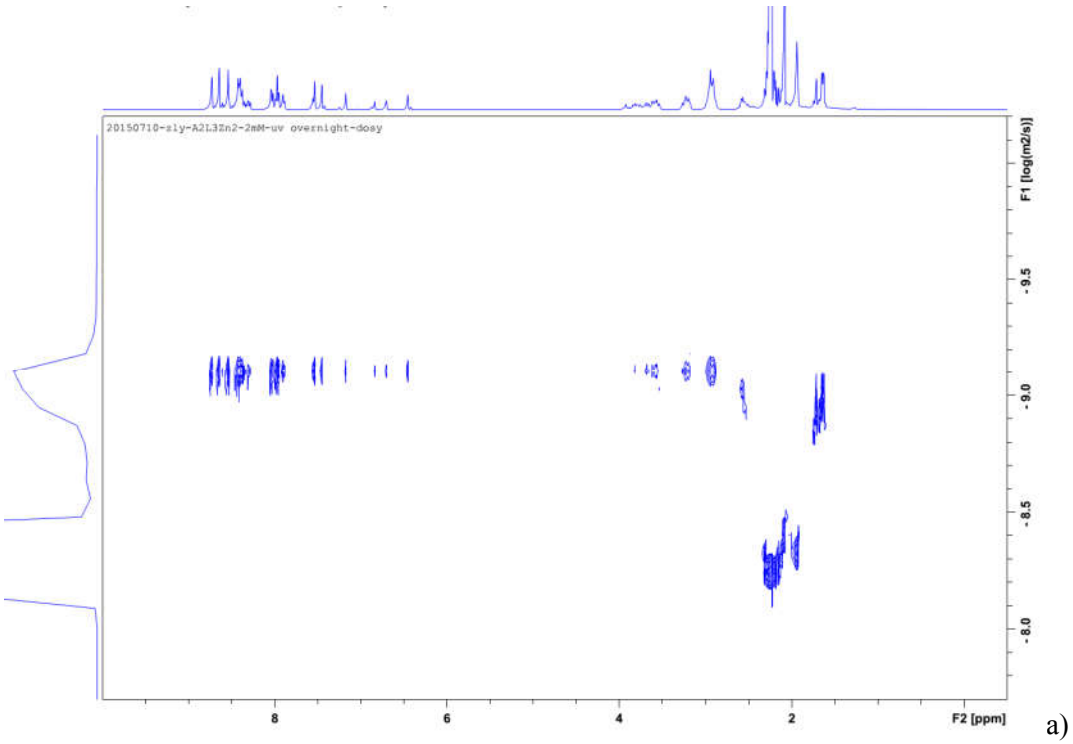

a)

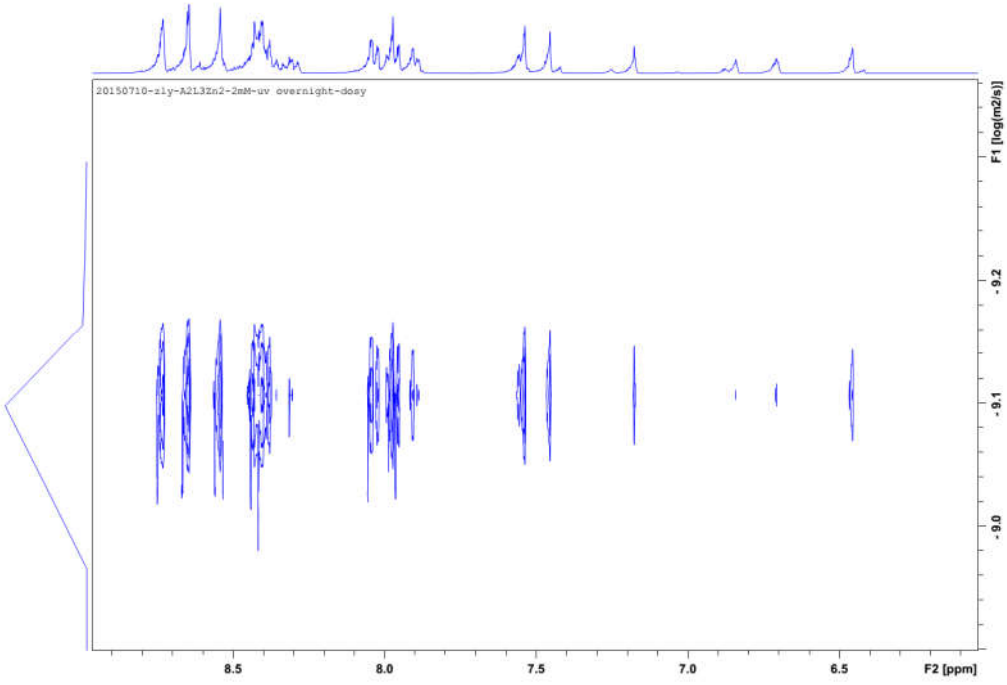

b)

Figure S45. (a) DOSY and (b) its partial enlargement spectra of *c*-$A^1{}_2L_3Zn_2$ cage (CD_3CN, room temperature).

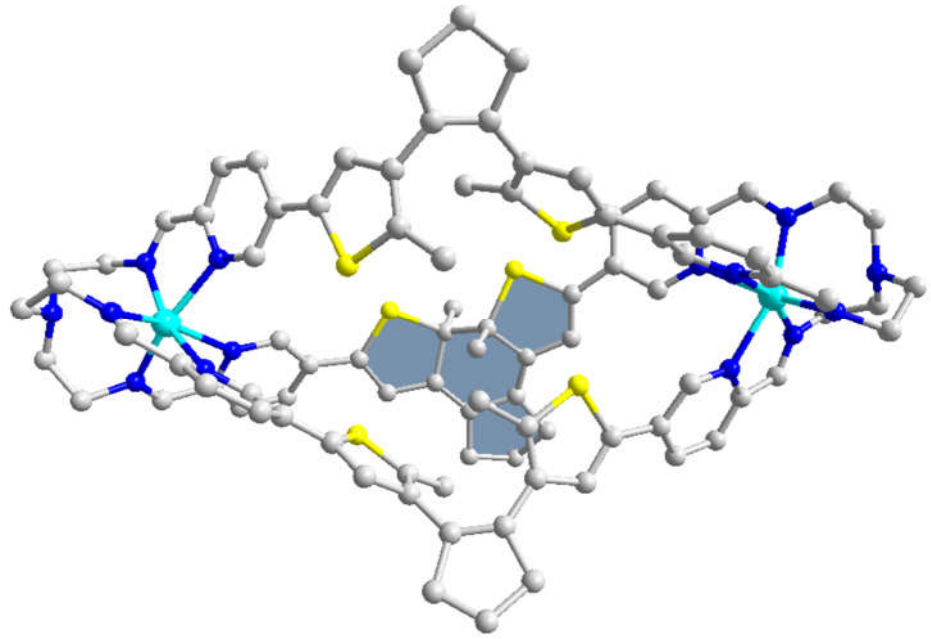

a)

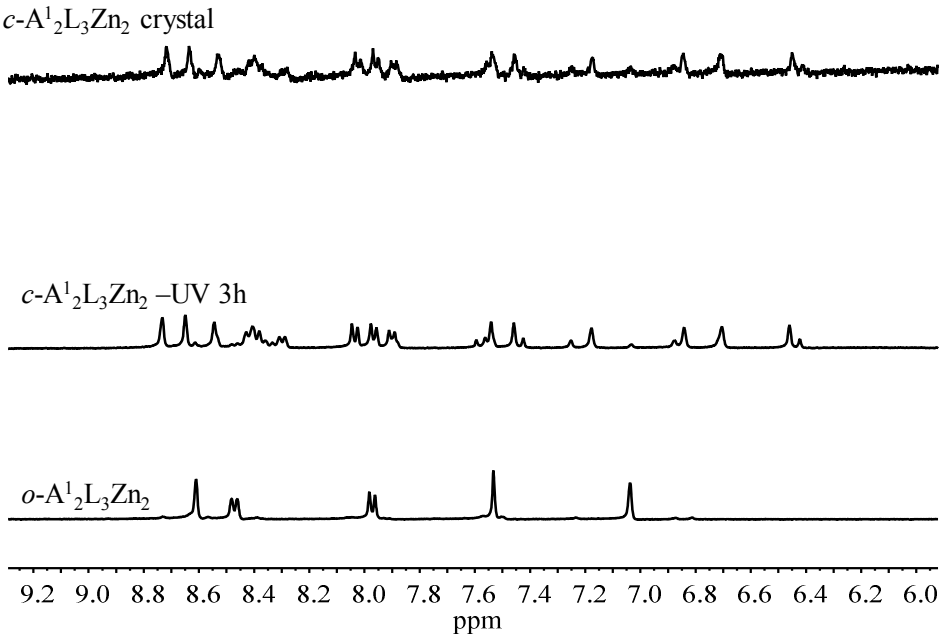

b)

Figure S46. (a) Single-crystal structure of *c*-$A^1_2L_3Zn_2$ cage (grey for C, blue for N, yellow for S, cyan for Zn, the closed PADTE-moiety is shown in shadow, H atoms, solvents and counter anions are omitted for clarity). (b) NMR spectra (CD_3CN, room temperature) for the crystallized sample of *c*-$A^1_2L_3Zn_2$ cage (top), and the solution sample of *o*-$A^1_2L_3Zn_2$ cage before (bottom) and after UV irradiation for 3 hours (middle).

3.3 $A^2_2L_3Cd_2$ cage

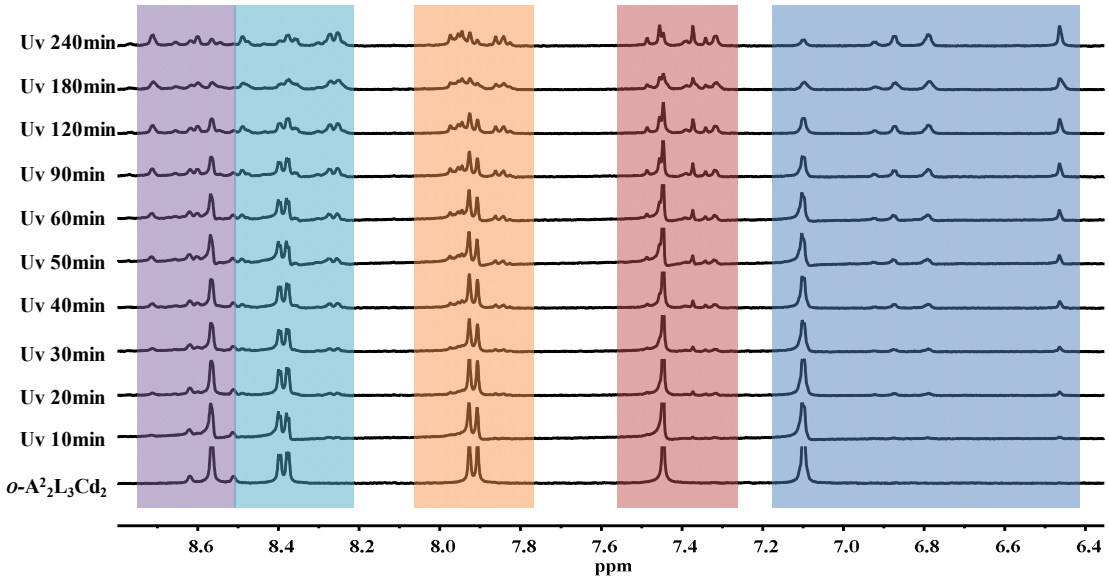

Figure S47. ^{1}H NMR spectra evolution of *o*-$A^2_2L_3Cd_2$ cage under UV irradiation for different time (400 MHz, CD_3CN, 298 K).

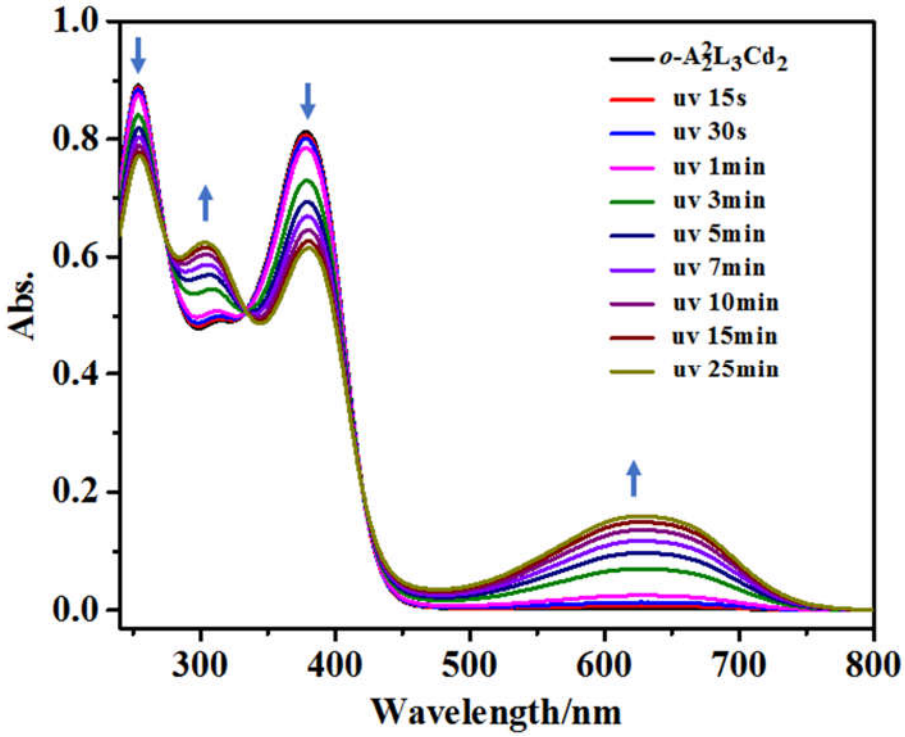

Figure S48. UV-Vis spectra of *o*-$A^2_2L_3Cd_2$ cage during ring-closing process ($CH_3CN/CHCl_3$, v:v = 1:1, 1×10^{-5} mol L^{-1}, room temperature).

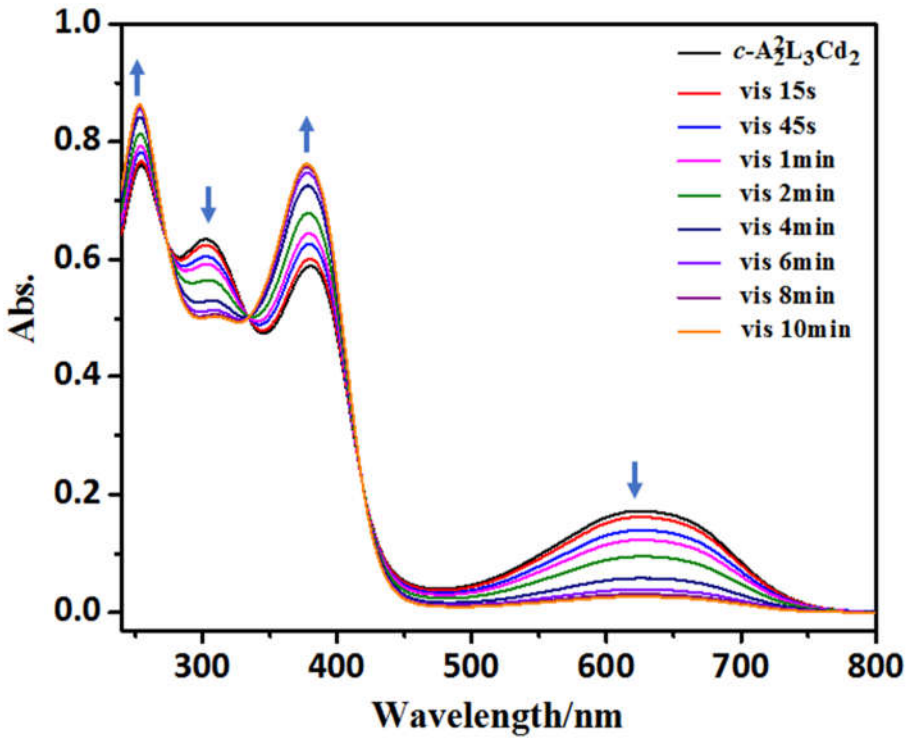

Figure S49. UV-Vis spectra of *c*-$A^2_2L_3Cd_2$ cage during ring-opening process ($CH_3CN/CHCl_3$, v:v = 1:1, 1×10^{-5} mol L^{-1}, room temperature).

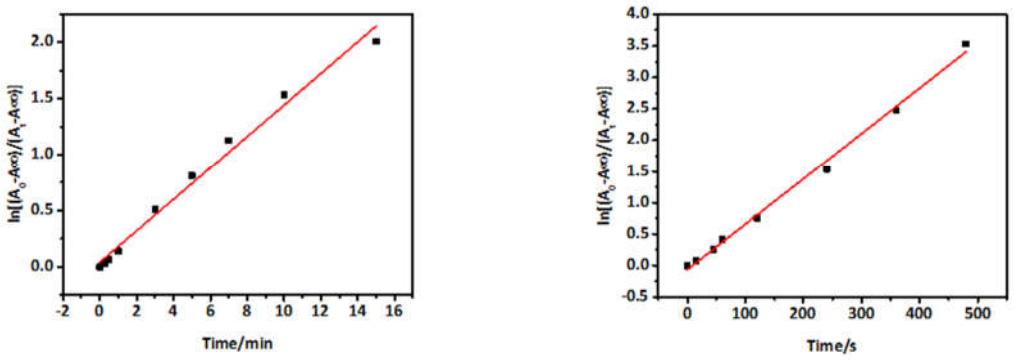

(a) (b)

Figure S50. (a) Plot of $\ln[(A_0-A_\infty)/(A_t-A_\infty)]$ with time for UV-Vis absorption of *o*-$A^2_2L_3Cd_2$ cage during ring-closing process, and (b) *c*-$A^2_2L_3Cd_2$ cage during ring-opening process ($CH_3CN/CHCl_3$, v:v = 1:1, 1×10^{-5} mol L^{-1}, room temperature).

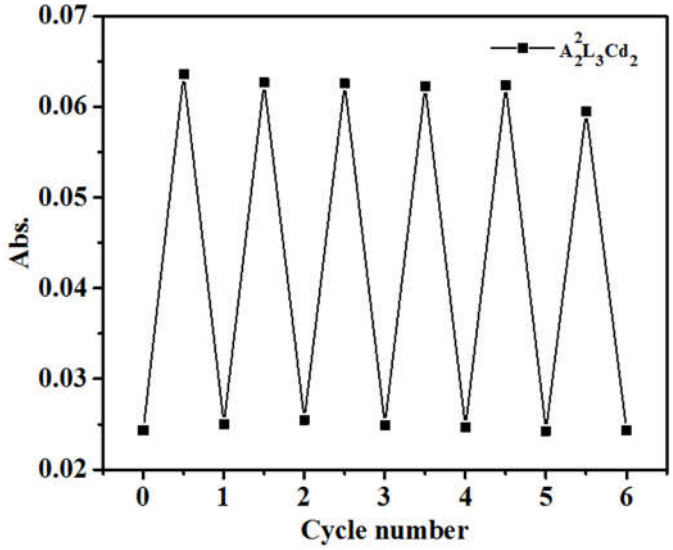

Figure S51. Cycled signals for absorbance at 627 nm of $A^2_2L_3Cd_2$ cage during alternative ring-closing/ring-opening processes.

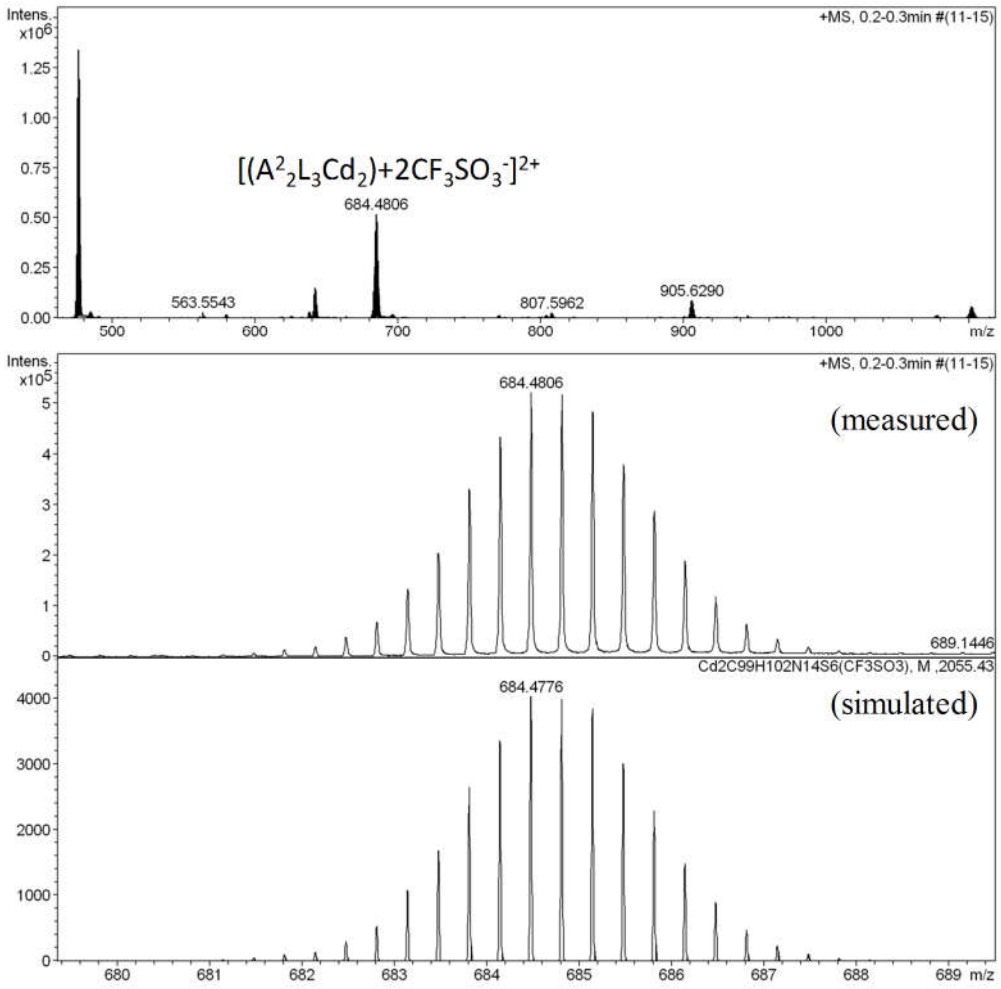

Figure S52. High resolution ESI-MS spectra of *c*-$A^2_2L_3Cd_2$ cage (CH_3CN, room temperature).

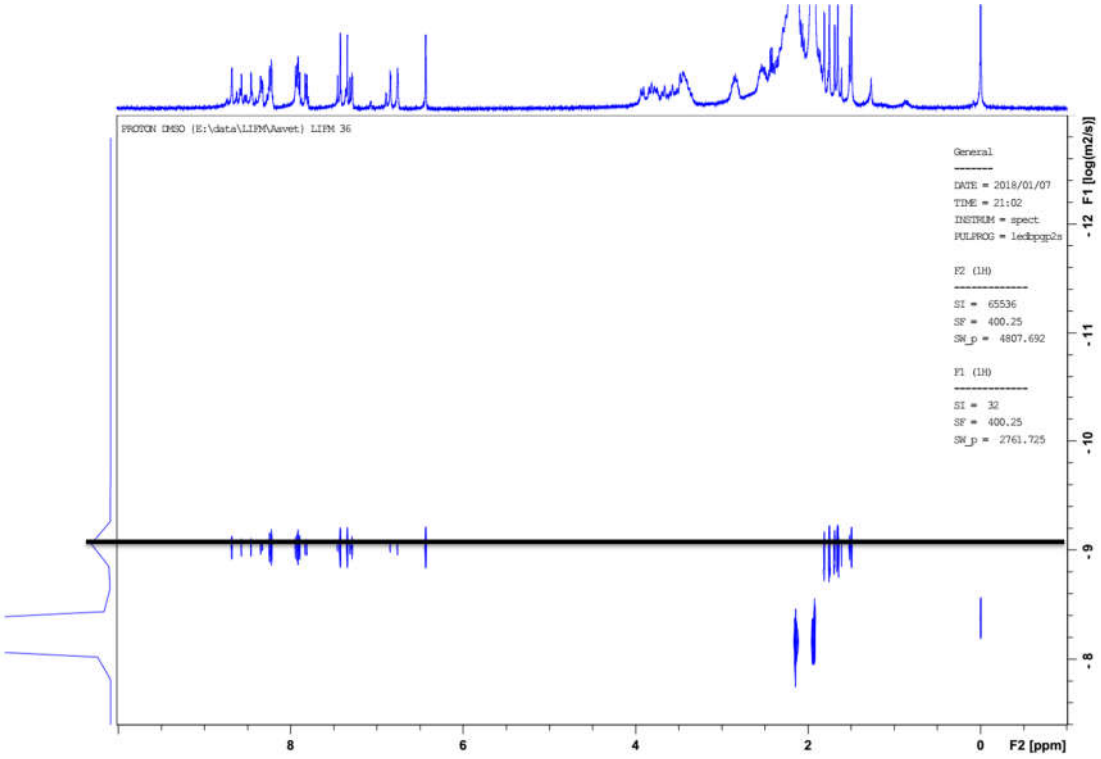

Figure S53. DOSY spectra of *c*-$A^2_2L_3Cd_2$ cage (CD_3CN, room temperature).

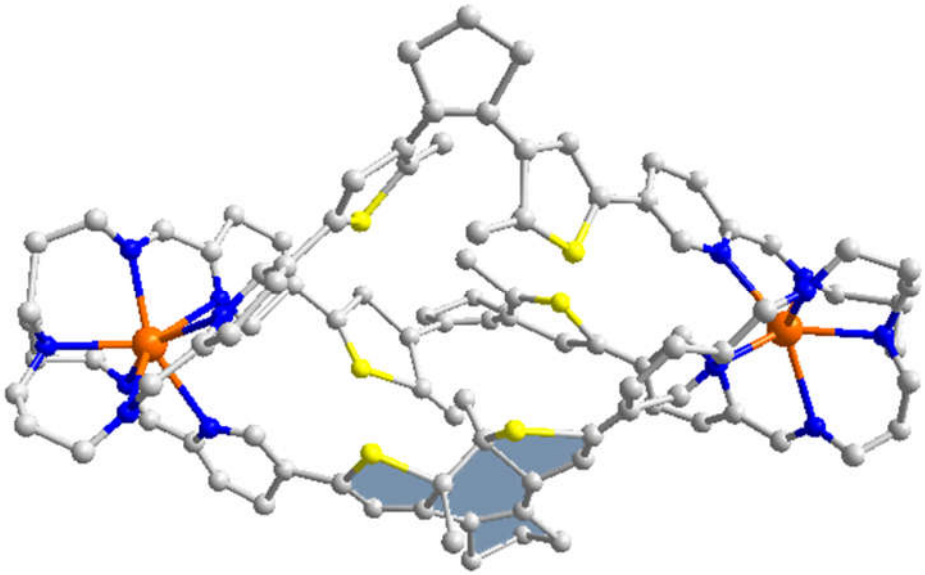

Figure S54. Single-crystal structure of *c*-$A^2_2L_3Cd_2$ cage (grey for C, blue for N, yellow for S, orange for Cd, H atoms, solvents and counter anions are omitted for clarity).

3.4 $A^2_2L_3Zn_2$ cage

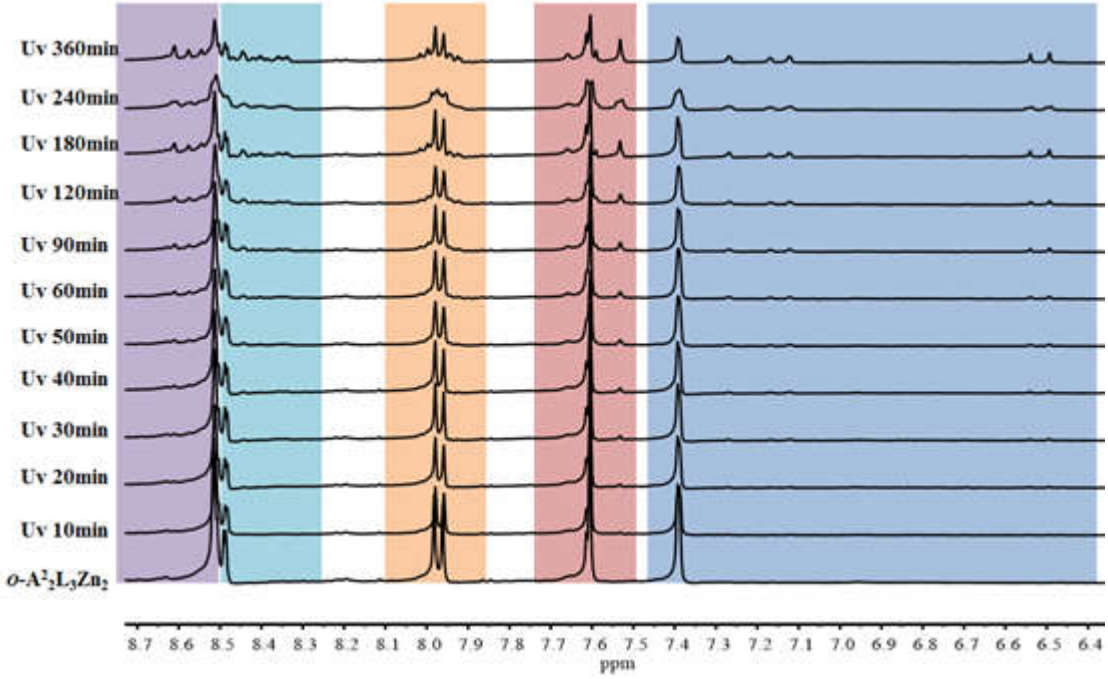

Figure S55. ^{1}H NMR spectra evolution of *o*-$A^2_2L_3Zn_2$ cage under UV irradiation for different time (400 MHz, CD_3CN, 298 K).

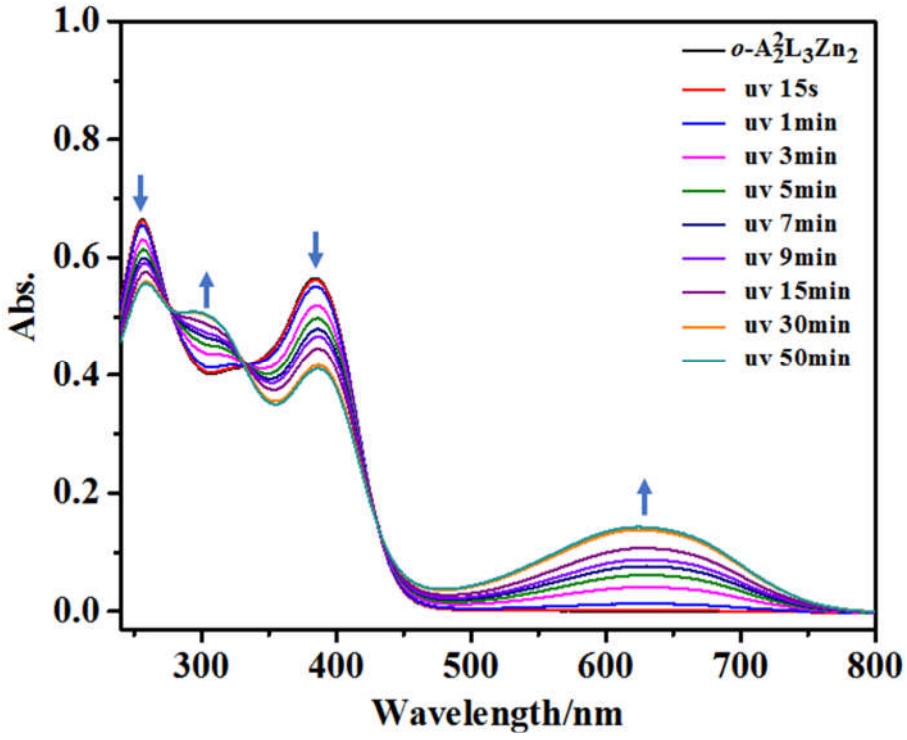

Figure S56. UV-Vis spectra of *o*-$A^2_2L_3Zn_2$ cage during ring-closing process ($CH_3CN/CHCl_3$, v:v = 1:1, 1×10^{-5} mol L^{-1}, room temperature).

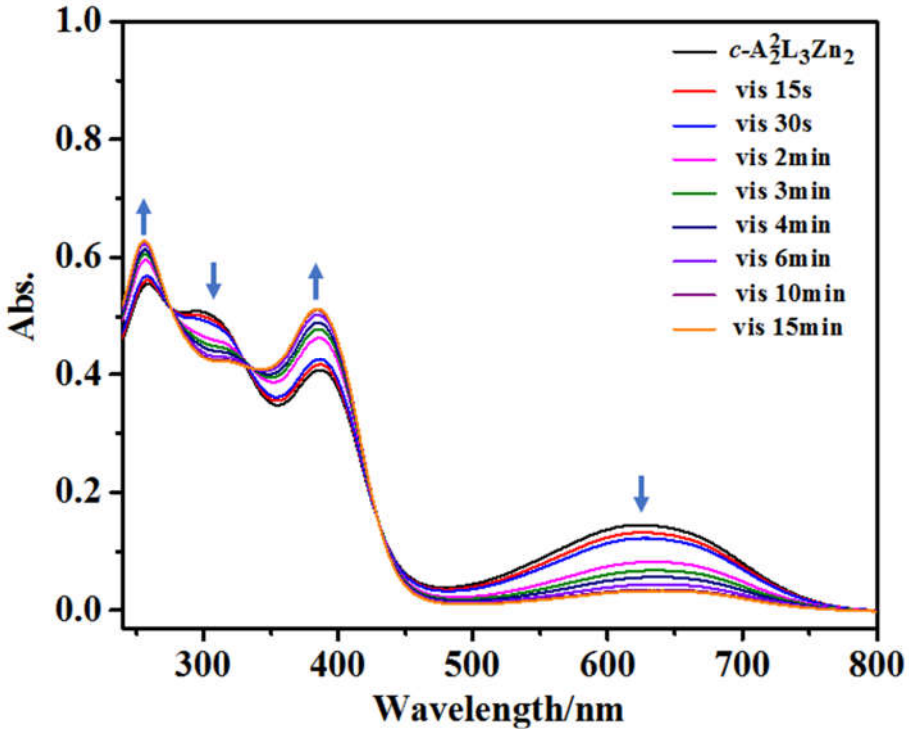

Figure S57. UV-Vis spectra of *c*-$A^2_2L_3Zn_2$ cage during ring-opening process ($CH_3CN/CHCl_3$, v:v=1:1, 1×10^{-5} mol L^{-1}, room temperature).

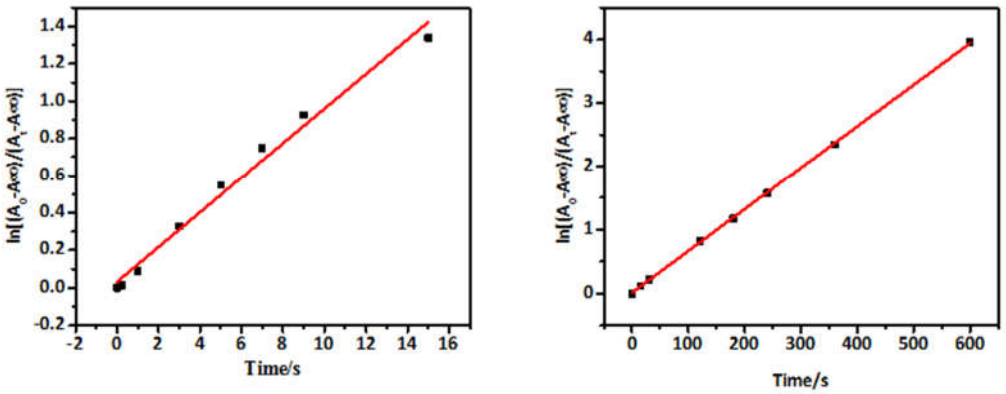

Figure S58. (a) Plot of $\ln[(A_0-A_\infty)/(A_t-A_\infty)]$ with time for UV-Vis absorption of *o*-$A^2_2L_3Zn_2$ cage during ring-closing process, and (b) *c*-$A^2_2L_3Zn_2$ cage during ring-opening process ($CH_3CN/CHCl_3$, v:v = 1:1, 1×10^{-5} mol L^{-1}, room temperature).

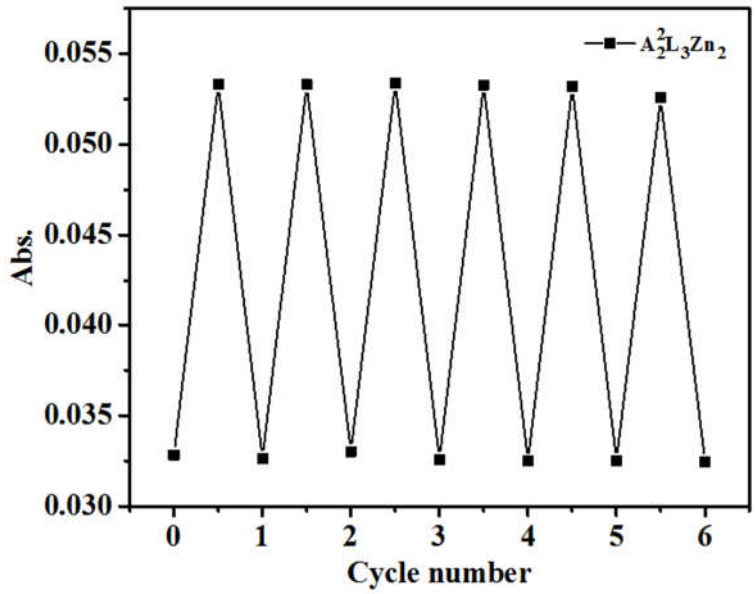

Figure S59. Cycled signals for absorbance at 627 nm of $A^2{}_2L_3Zn_2$ during alternative ring-closing/ring-opening processes.

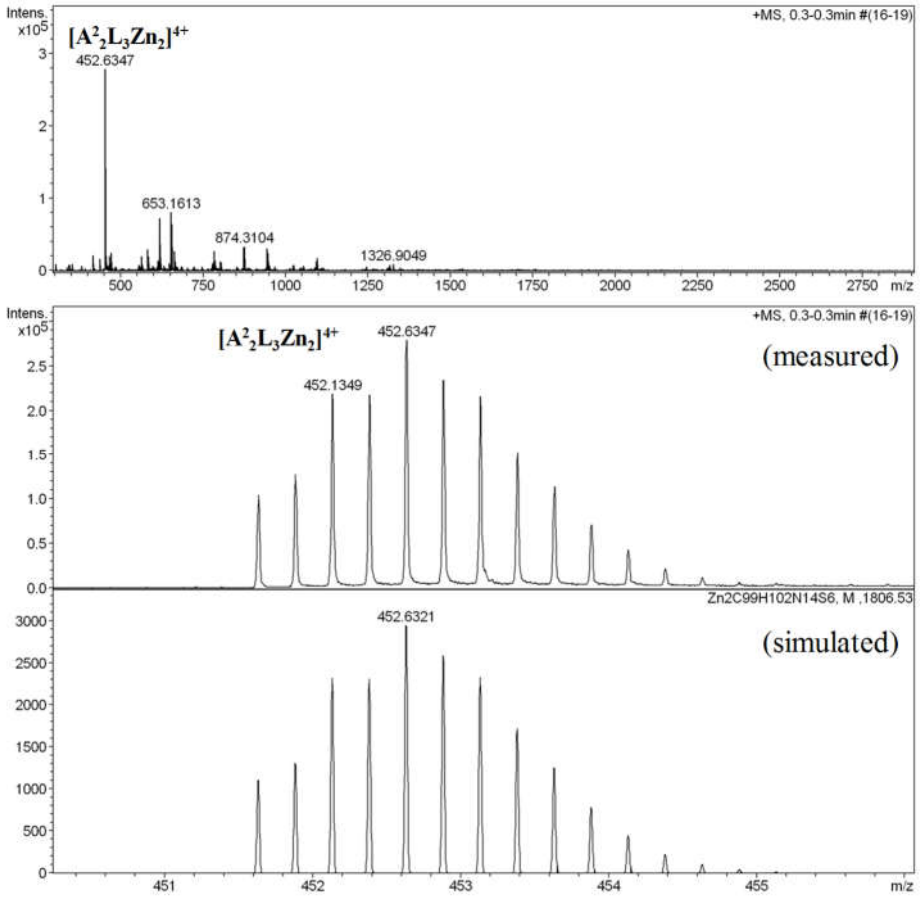

Figure S60. High resolution ESI-MS spectra of *c*-$A^2{}_2L_3Zn_2$ cage (CH_3CN, room temperature).

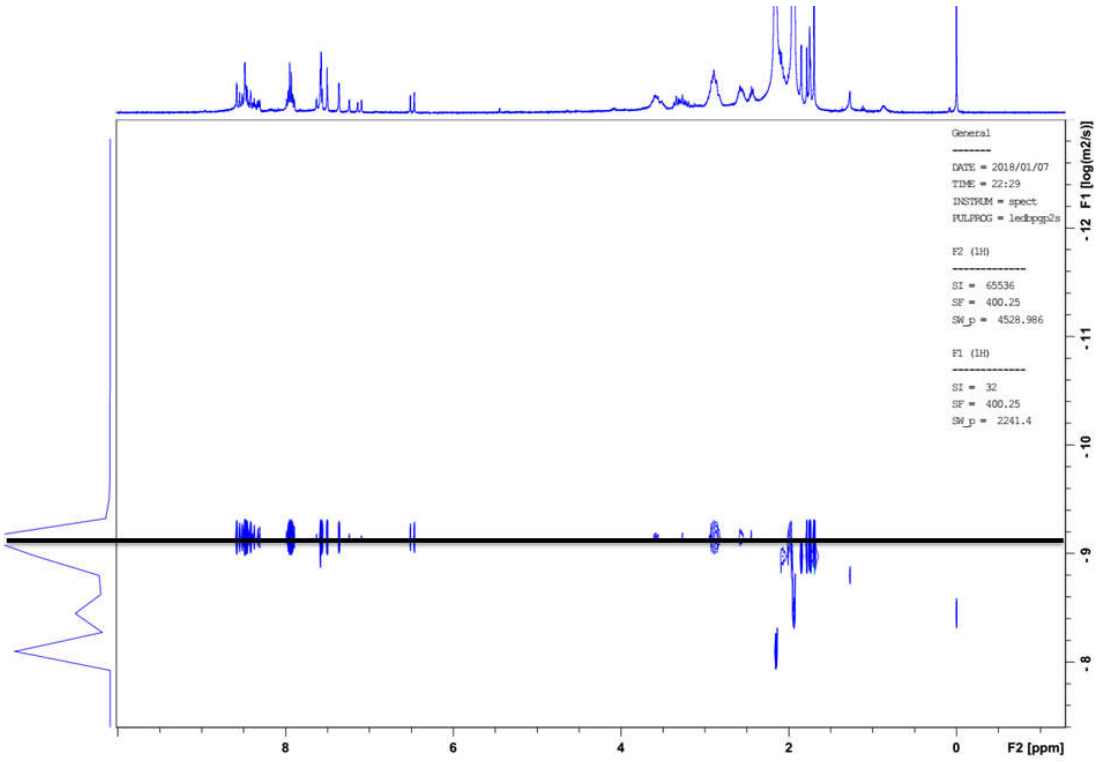

Figure S61. DOSY spectra of *c*-$A^2_2L_3Zn_2$ cage (CD_3CN, room temperature).

3.5 R-$A^1_2L_3$ cage

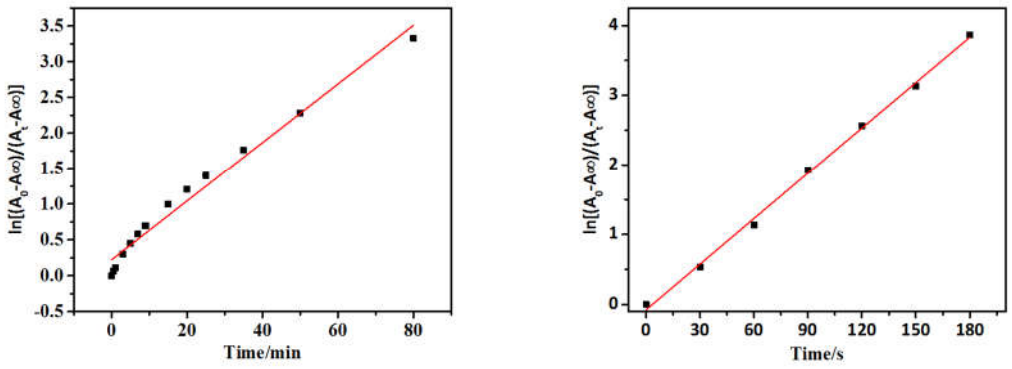

(a) (b)

Figure S62. (a) Plot of $\ln[(A_0-A_\infty)/(A_t-A_\infty)]$ with time for UV-Vis absorption of *o*-R-$A^1_2L_3$ cage during ring-closing process, and (b) *c*-R-$A^1_2L_3$ cage during ring-opening process ($CH_3CN/CHCl_3$, v:v = 1:1, 1×10^{-5} mol L^{-1}, room temperature).

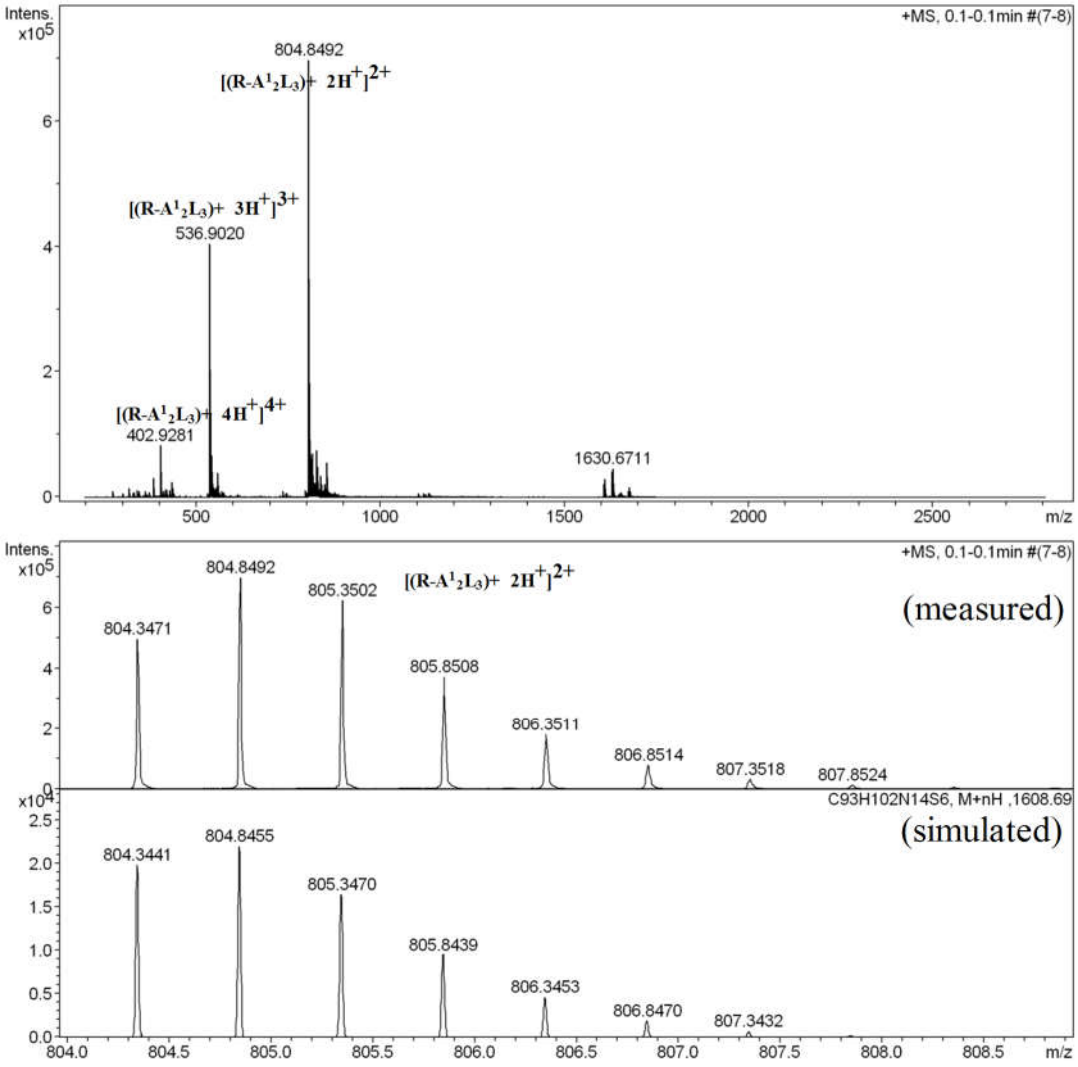

Figure S63. High resolution ESI-MS spectra of *c*-R-A$^1_2$L$_3$ cage (CH_3OH, room temperature).

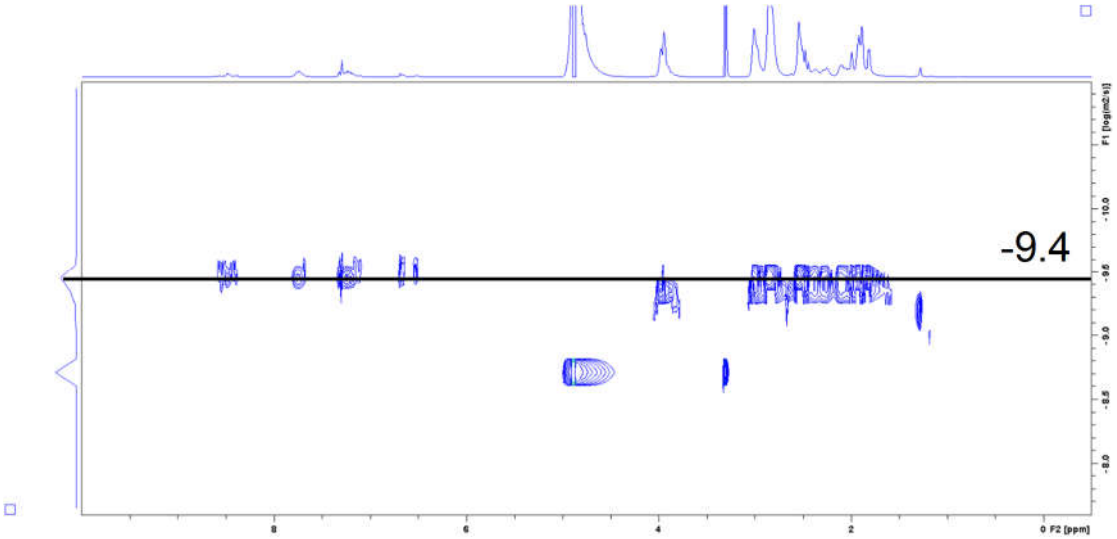

Figure S64. DOSY spectra of *c*-R-A$^1_2$L$_3$ cage (CD_3OD, room temperature).

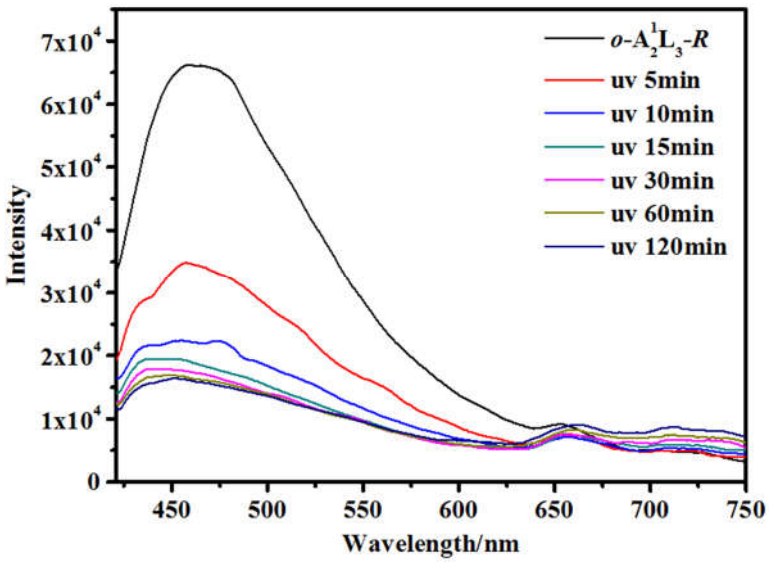

Figure S65. The emission spectra of *o*-R-$A^1{}_2L_3$ cage during ring-closing process ($CH_3CN/CHCl_3$, v:v = 1:1, 1×10^{-5} mol L^{-1}, room temperature).

3.6 R-$A^2{}_2L_3$

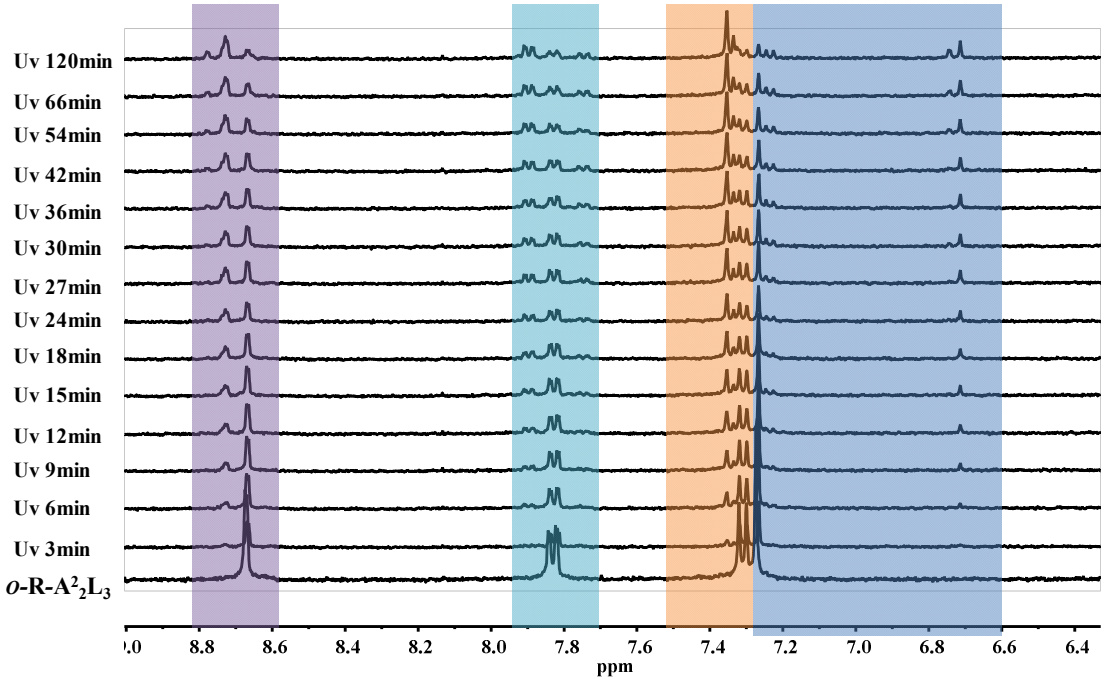

Figure S66. ^1H NMR spectra evolution of *o*-R-$A^2{}_2L_3$ cage under UV irradiation for different time (400 MHz, CD_3OD, 298 K).

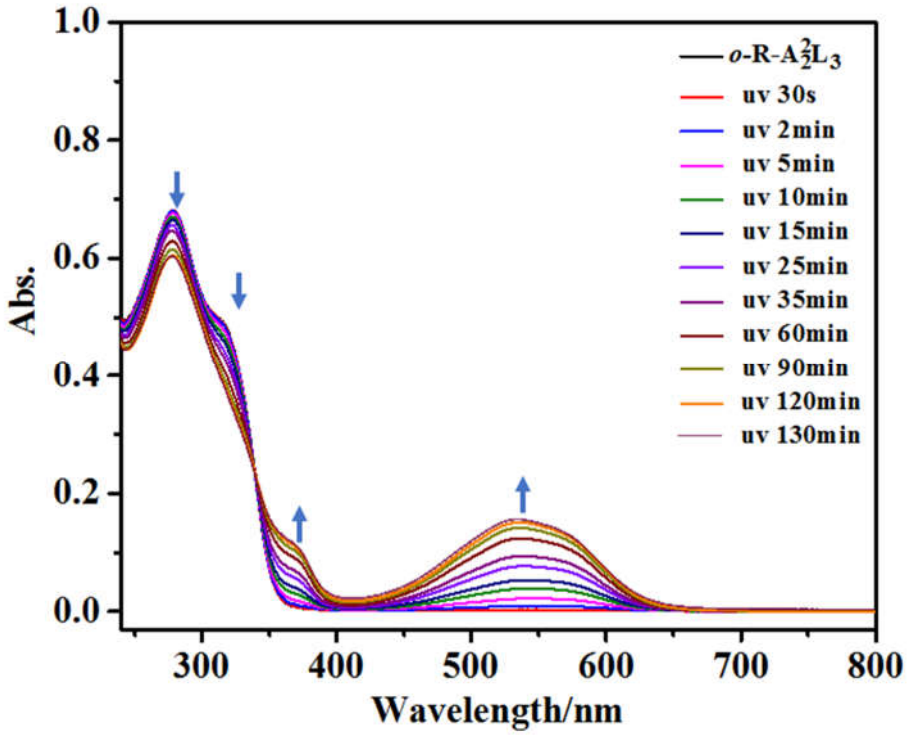

Figure S67. UV-Vis spectra of *o*-R-A$^2_2$L$_3$ cage during ring-closing process ($CH_3CN/CHCl_3$, v:v = 1:1, 1×10^{-5} mol L^{-1}, room temperature).

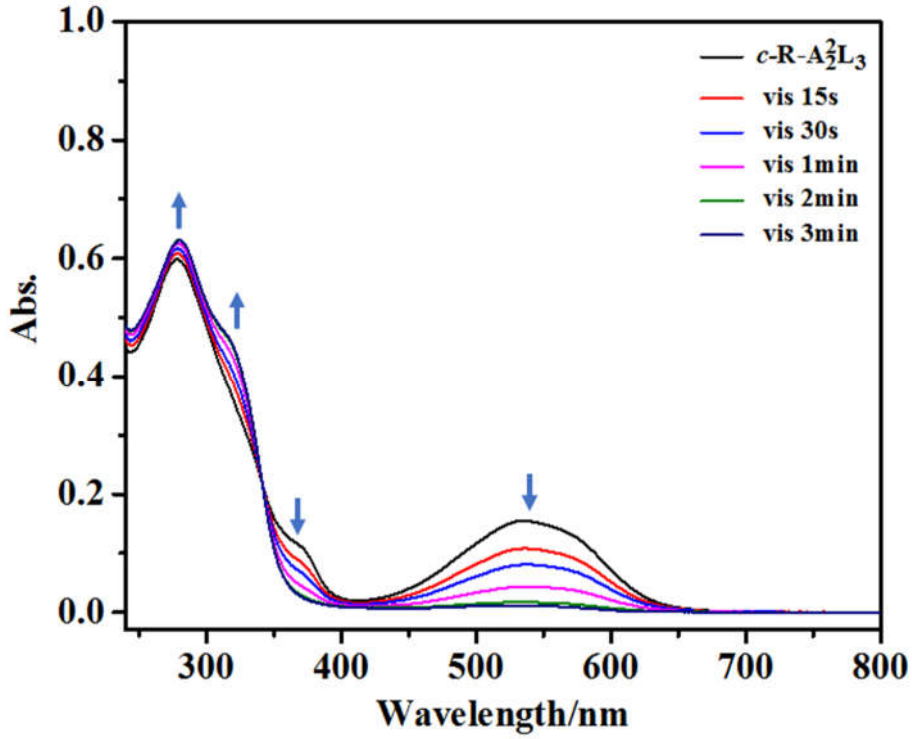

Figure S68. UV-Vis spectra of *c*-R-A$^2_2$L$_3$ cage during ring-opening process ($CH_3CN/CHCl_3$, v:v = 1:1, 1×10^{-5} mol L^{-1}, room temperature).

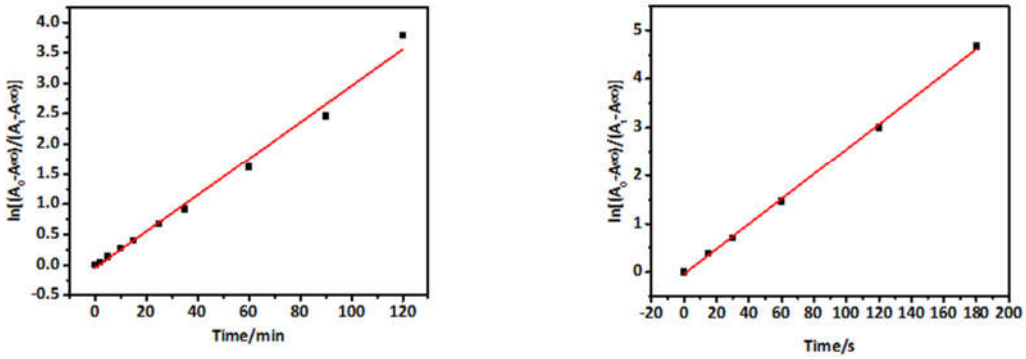

(a) (b)

Figure S69. (a) Plot of $\ln[(A_0-A_\infty)/(A_t-A_\infty)]$ with time for UV-Vis absorption of *o*-R-$A^2_2L_3$ cage during ring-closing process, and (b) *c*-R-$A^2_2L_3$ cage during ring-opening process ($CH_3CN/CHCl_3$, v:v = 1:1, 1×10^{-5} mol L^{-1}, room temperature).

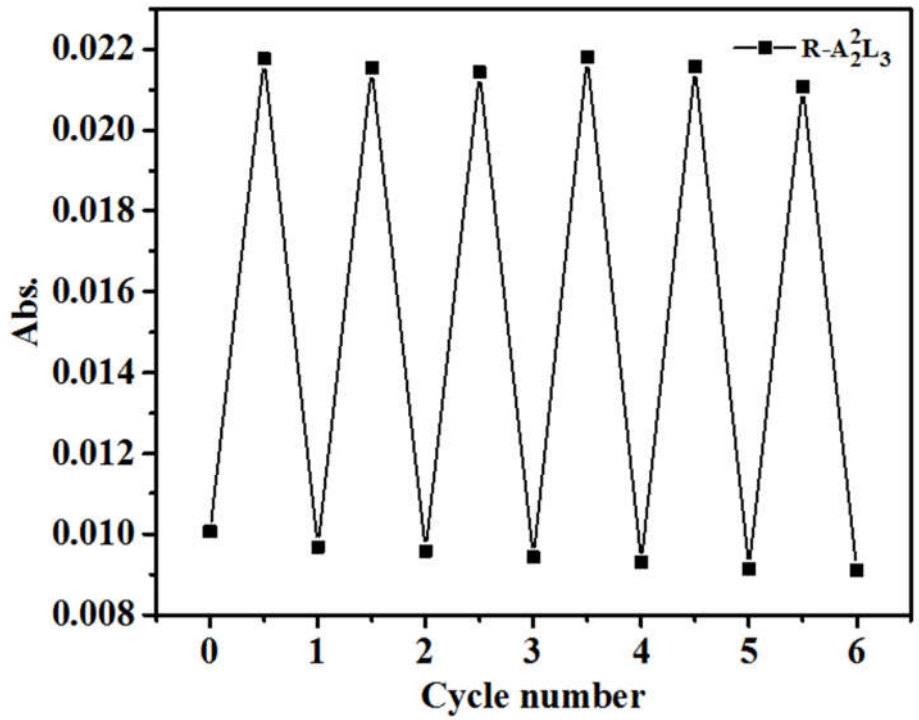

Figure S70. Cycled signals for absorbance at 538 nm of R-$A^2_2L_3$ cage during alternative ring-closing/ring-opening processes.

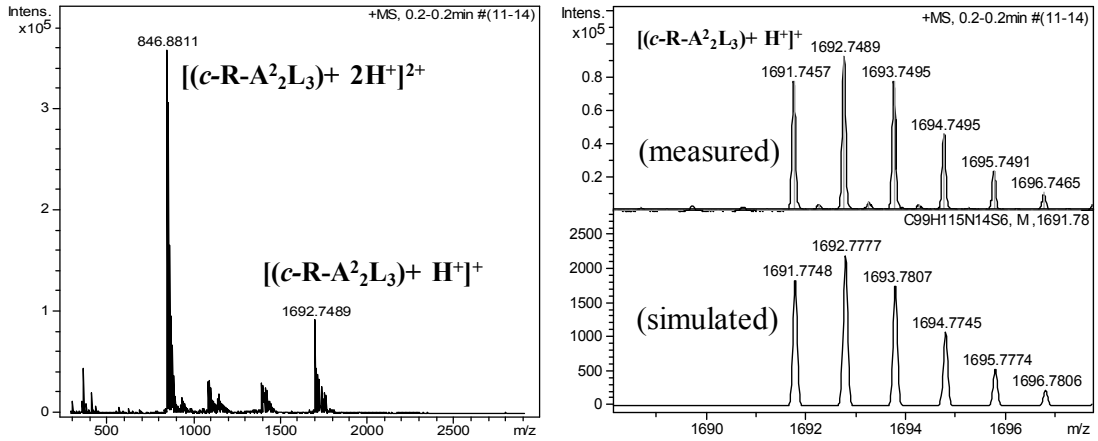

Figure S71. High resolution ESI-MS spectra of *c*-R-A$^2_2$L$_3$ cage (CH_3OH, room temperature).

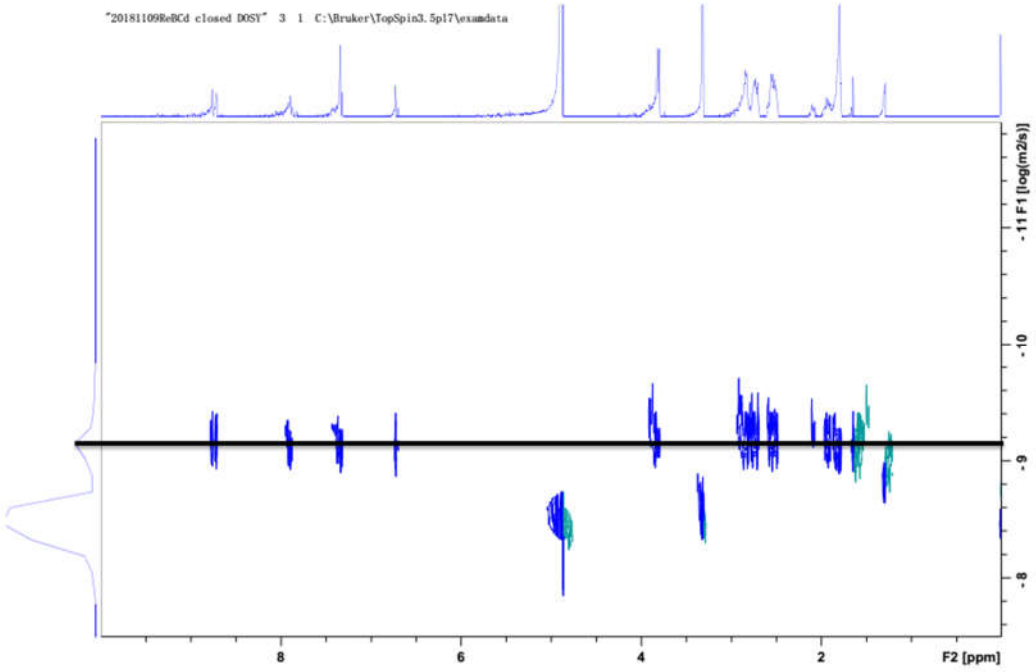

Figure S72. DOSY spectra of *c*-R-A$^2_2$L$_3$ cage (CD_3OD, room temperature).

3.7 Guest effects

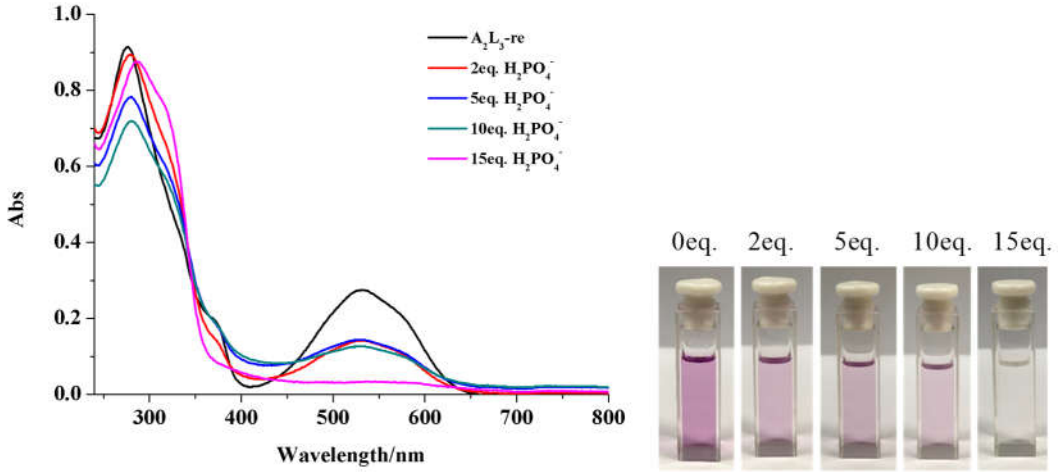

Figure S73. UV-Vis spectra (left) and solution color (right) after adding different amounts of $H_2PO_4^-$ anions into *o*-R-$A^1{}_2L_3$ solution (CH_2Cl_2, 1×10^{-5} mol L^{-1}), and then irradiated under UV light for 90 min.

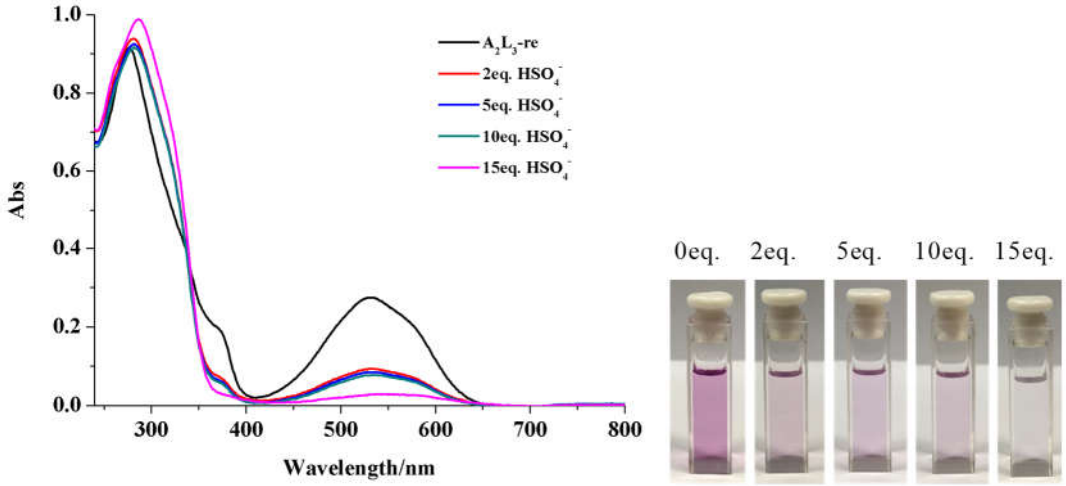

Figure S74. UV-Vis spectra (left) and solution color (right) after adding different amounts of HSO_4^- anions into *o*-R-$A^1{}_2L_3$ solution (CH_2Cl_2, 1×10^{-5} mol L^{-1}), and then irradiated under UV light for 90 min.

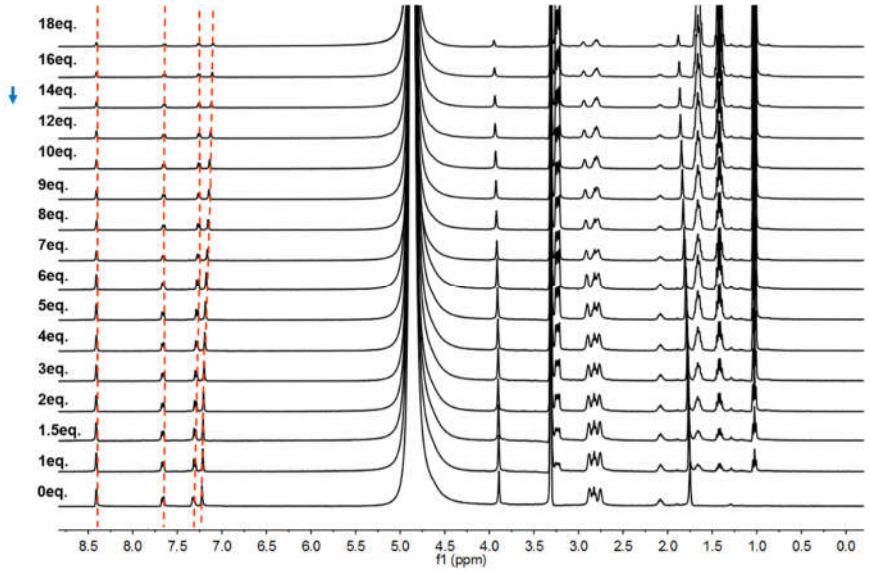

Figure S75. ^{1}H NMR titration spectra of $H_2PO_4^-$ into *o*-R-$A^1{}_2L_3$ solution (CD_3OD, 25˚C).

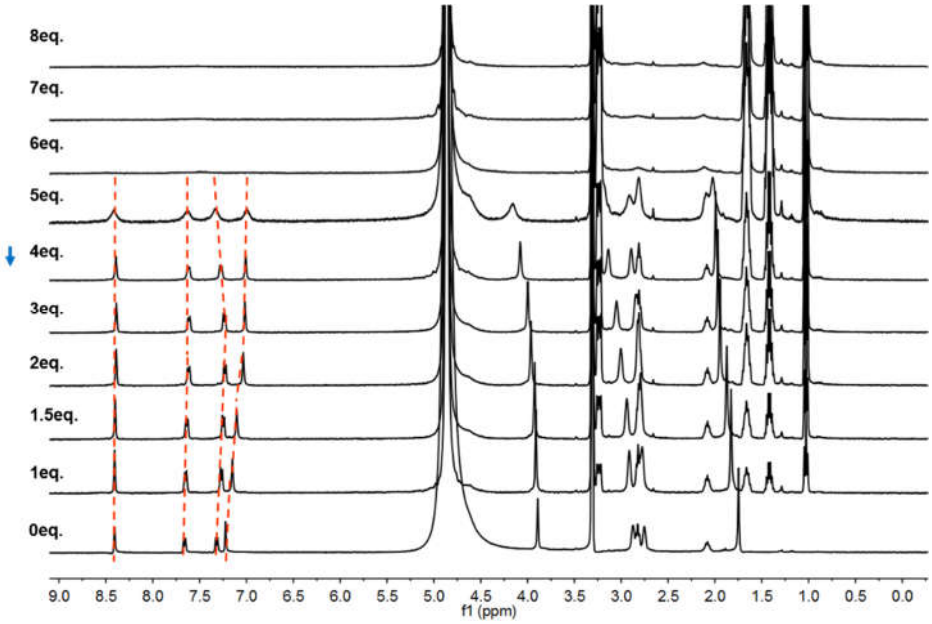

Figure S76. ^{1}H NMR titration spectra of HSO_4^- into *o*-R-$A^1{}_2L_3$ solution (CD_3OD, 25˚C).

4. Up-conversion color tuning applications

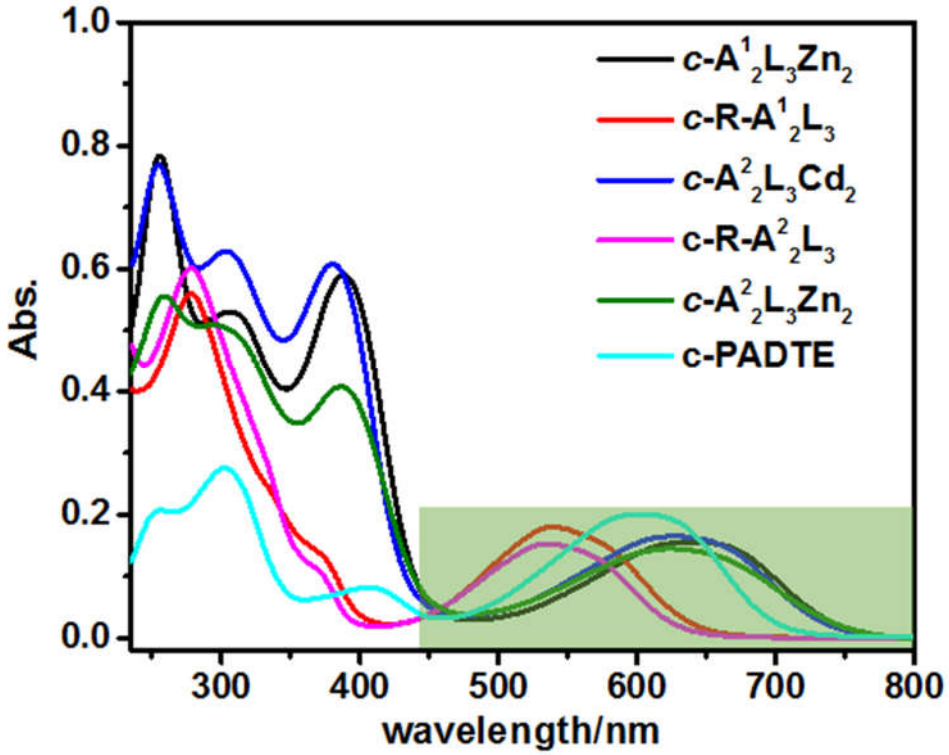

Figure S77. The UV-Vis spectra of *c*-PADTE and *c*-cages.

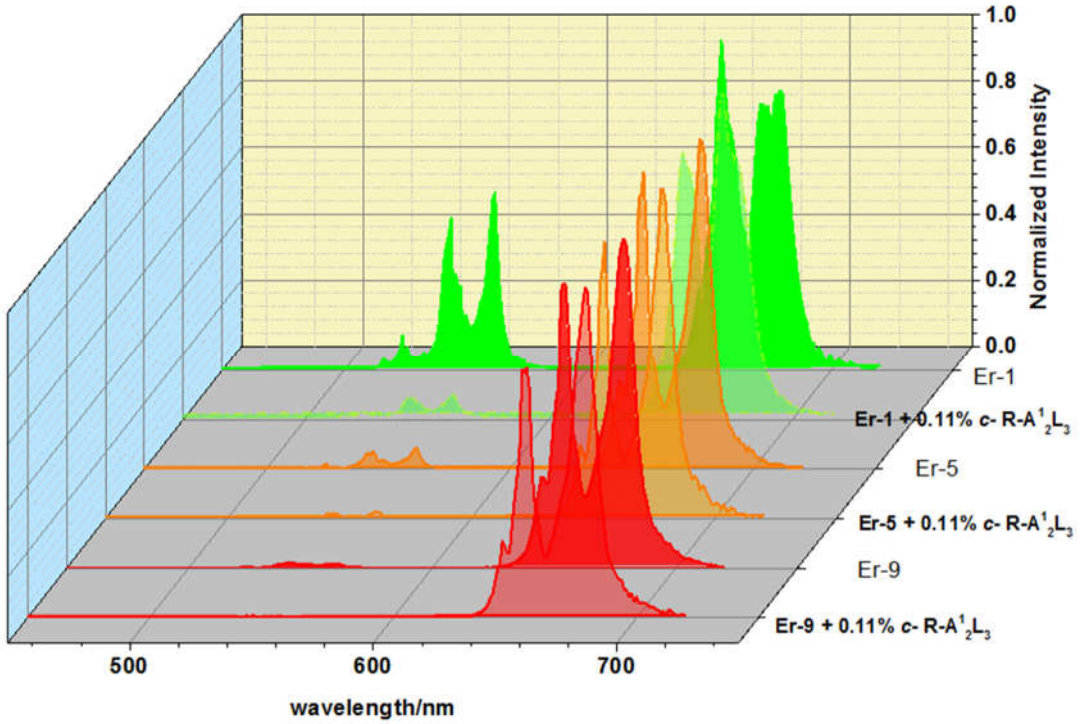

Figure S78. The upconversion luminescence spectra of three kinds of upconversion materials (Er-1, Er-5, Er-9) and their hybrid materials with *c*-R-$A^1_2L_3$ cage.

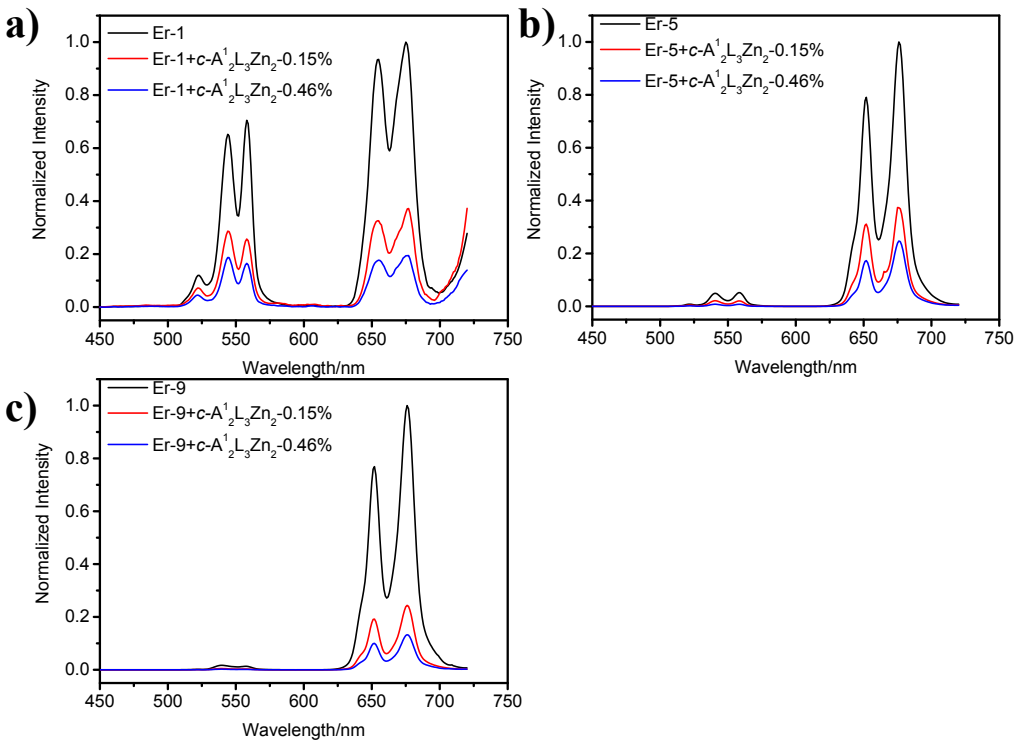

Figure S79. The upconversion emission spectra of nine kinds of hybrid materials.

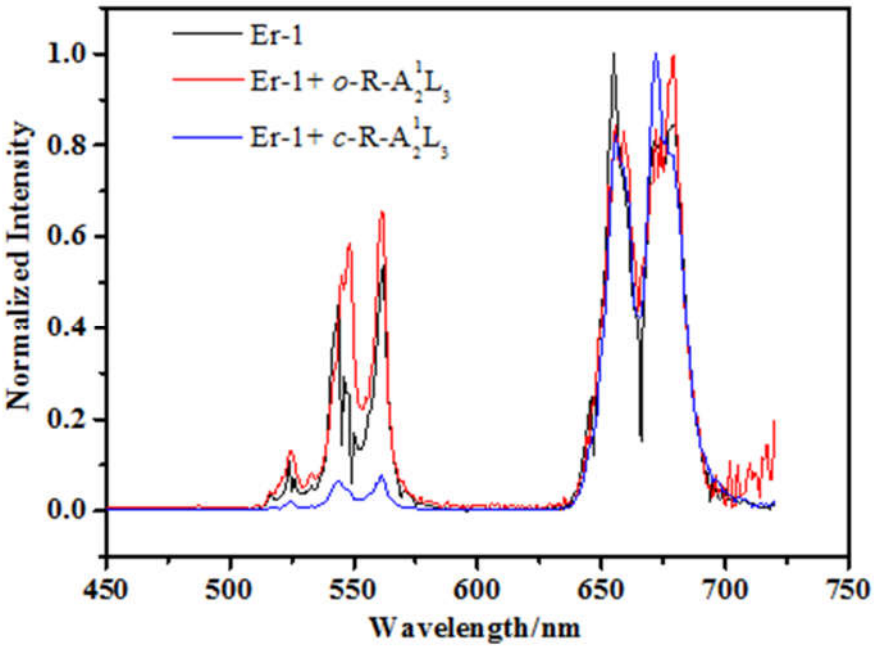

Figure S80. The upconversion emission spectra of Er-1 and its hybrid materials (Er-1 + *o*/*c*-R-$A^1{}_2L_3$).

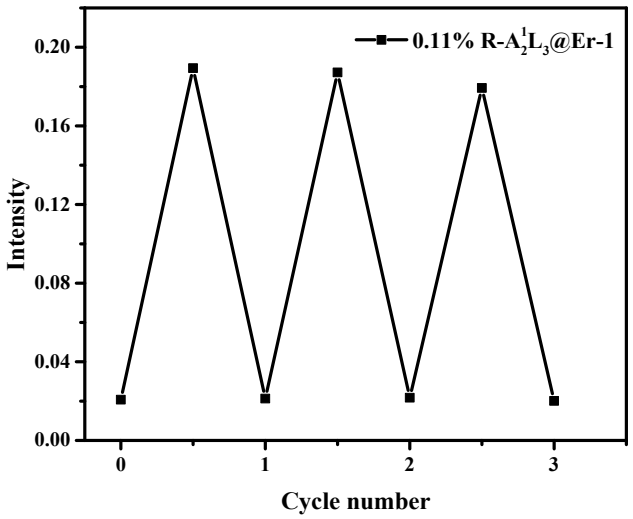

Figure S81. Cycled signals for upconversion PL intensity at 544 nm of 0.11% R-A$^1_2$L$_3$ @ Er-1 hybrid solid state materials during alternative ring-closing/ring-opening processes.

REFERENCES

S1 E. S. Tam, J. J. Parks, W. W. Shum, Y.-W. Zhong, M. E. B. Santiago-Berríos, X. Zheng, W. Yang, G. K.-L. Chan, H. D. Abruna, D. C. Ralph, *ACS Nano*, 2011, **5**, 5115-5123.

S2 S.-Y. Yin, L. Chen, M. Pan, Z. Wang, L.-Y. Zhang, H.-P. Wang, Y.-N. Fan, C.-Y. Su, *ChemistrySelect*, 2016, **1**, 3136-3143.